Structural and Functional Analysis of p26, a Small Heat Shock Protein from *Artemia franciscana*

by

Yu Sun

Submitted in partial fulfillment of the requirements
for the degree of Doctor of Philosophy

at

Dalhousie University
Halifax, Nova Scotia
December, 2004

Your file Votre référence
ISBN: 0-494-00958-6
Our file Notre référence
ISBN: 0-494-00958-6

DALHOUSIE UNIVERSITY

To comply with the Canadian Privacy Act the National Library of Canada has requested that the following pages be removed from this copy of the thesis:

Preliminary Pages
- Examiners Signature Page (pii)
- Dalhousie Library Copyright Agreement (piii)

Appendices
- Copyright Releases (if applicable)

Dedicated to my parents, Maggie, and Rong…

Table of Contents

List of Figures

List of Tables

Abstract

The brine shrimp, *Artemia franciscana,* undergoes encystment and diapause, exhibiting a remarkable resistance to environmental stresses during this time. Encysted *Artemia* embryos contain an abundant small heat shock protein termed p26, a molecular chaperone contributing to development and survival. To investigate the role of p26 during *Artemia* development and upon exposure to stress, the structural and functional characteristics of wild type and modified p26 were determined. Wild type p26 resided predominantly in the cytoplasm of transiently transfected COS-1 cells, however mutated p26 occurred in both cytoplasm and nuclei. Translocation into nuclei was especially evident for variants missing the complete amino-terminal region, a single site mutant R114A, and a multiple-arginine-deleted mutant "R". When produced in either prokaryotic or eukaryotic cells, modified p26 lacking the amino-terminal region occurred mainly as monomers and dimers, indicating the relevance of the amino-terminus for p26 oligomer formation. Assembly of higher order oligomers was strengthened by the carboxy-terminal extension, although removing the ten carboxy-terminal residues had only a marginal effect on oligomerization. A mechanism whereby oligomer disassembly assists translocation of p26 from cytoplasm into nuclei was suggested, this of importance because p26 translocates into *Artemia* embryo nuclei upon exposure to anoxia and thermal shock. However, when examined in *Artemia*, the results suggested a process more complex than just oligomer dissociation for regulation of p26 nuclear translocation. Bacterial thermotolerance and protein chaperoning assays demonstrated that modified p26 had decreased chaperoning capability, with truncated variants, mutant R114A and mutant "R" most dramatically affected. Oligomerization is necessary but not sufficient for full chaperone activity, since mutant R114A formed large oligomers while exhibiting limited chaperone capability. Circular dichroism revealed that secondary structures of most mutants, in comparison with wild type p26, possessed increased α-helices and decreased β-conformations. Intrinsic fluorescence and ANS-binding studies demonstrated altered aromatic residue microenvironments and reduced global hydrophobicity for p26 variants. Comparative modeling indicated the p26 α-crystallin domain is arranged in an immunoglobulin-like fold as a β-sandwich consisting of eight β-strands forming two antiparallel β-sheets. This work, which has important implications for understanding the relationship between p26 structural organization and functional mechanisms during *Artemia* development and stress, provides a model for study of other small heat shock proteins. As such, it may lead to a better appreciation of diseases, including ischemia/reperfusion injury, cataract, desmin-related myopathy and neurodegenerative disorders.

List of Abbreviations and Symbols

ADCC	autosomal dominant congenital cataract
aTc	anhydrotetracycline
ATP	adenosine 5'-triphosphate
BEB	blot electrode buffer
Bis	N', N'-methylenebisacrylamide
ANS	1-anilino-8-naphthalene-sulphonate
bp	base pairs
BSA	bovine serum albumin
cDNA	complementary deoxyribonucleic acid
CoA	coenzyme A
CS	citrate synthase
DAPI	4', 6-diamidino-2-phenylindole, dihydrochloride
DEAE	diethylaminoethyl-Sephadex
DMEM	Dulbecco's modified Eagle's medium
DRM	desmin-related myopathy
DTNB	5, 5'-dithio-bis(2-nitrobenzoic acid)
DTT	dithiothreitol
ddH_2O	double distilled water
ECL	enhanced chemiluminescence
EDTA	ethylene diaminetetraacetic acid
EGTA	ethylene glycol-bis (β-aminoethyl ether)-N, N, N', N'-tetraacetic acid
FBS	fetal bovine serum
FITC	fluorescein isothiocyanate
g	gravity
h	hour
His	histidine
HRP	horse radish peroxidase
HSC	heat shock cognate protein
HSE	heat shock element
HSF	heat shock factor
HSP	heat shock protein
HST	high salt Tween 20
IgG	immunoglobulin G
IMAC	immobilized metal affinity chromatography
IPTG	Isopropyl-1-thio-β-D-galactopyranoside
kDa	kilodaltons
LB	Luria-Bertani
min	minute
PAGE	polyacrylamide gel electrophoresis
PBS	phosphate buffered saline
PCR	polymerase chain reaction
PIPES	piperazine-N, N'-bis (2-ethanesulfonic acid)
PMSF	phenylmethanesulfonyl fluoride
rpm	revolutions per minute

RT	room temperature
S1	cell-free extract of *Artemia*
SDS	sodium dodecyl sulfate
sec	second
TAE	Tris, acetic acid, EDTA
TBS	Tris buffered saline
TEMED	N, N, N', N',-tetramethylethylenediamine
Tris	Tris-(hydroxymethyl)-aminomethane
Tween	polyoxyethylene sorbitan monolaurate
WT	wild type
X-Gal	5-bromo-4-chloro-3-indolyl-β-D-galactopyranoside

Acknowledgements

I am most indebted to my supervisor and mentor Dr. Tom MacRae who made my Ph.D. studies possible and enjoyable. With great guidance, expertise and encouragement, he instructed me on scientific research, English writing and communication. These will be invaluable for my future academic career. I would like to express sincere gratitude to Dr. Jonathan Wright, Dr. William Currie, and Dr. Carmichael Wallace, my supervising committee, for their enthusiastic help, suggestions and assistance. I appreciate Dr. Robert Tanguay, my external examiner, for his time and instructions.

Dr. Stephen Bearne and Dr. Neil Ross provided excellent assistance with biophysics studies. Dr. Ping Li and Mr. Carey Isenor provided expert help with confocal imaging and photo processing.

I thank my lab partners Julie, Ross, Mindy, Gill, Krish, Jagdish, Michelle, Karen, Andrea, Tao, Zhijun, Tania, Paul, John, Katy, Nathan, Svetla and Yan for their laughs, friendship, discussion, and cooperation in efficiently using lab space.

I am grateful to my wife, for her understanding, deepest love and full support of my work, not to mention her delicious dishes and impressive music performances. I owe her so much that I could never make it up! Special, greatest gratitude to my parents for their support, guidance and invariable love that I cherish always.

My sincere appreciation goes to the Nova Scotia Health Research Foundation and Faculty of Graduate Studies, Dalhousie University for generous financial supports.

I. Introduction

1.1 Molecular chaperones

Over 40 years ago, an unusual gene expression profile was observed in the polytene chromosomes of salivary glands in heat shocked *Drosophila melanogaster* larvae (Ritossa, 1962). However, the products of these genes, the heat shock proteins (HSPs), were not identified and named until later, when a rapid and selective increase in the synthesis of specific proteins was demonstrated upon exposure of *Drosophila* larvae to higher than normal temperature (Tissières *et al.*, 1974). According to molecular weight, expression pattern, cell distribution and function, HSPs are categorized as families HSP100, HSP90, HSP70, HSP60, HSP40, and the small HSPs (sHSPs) (Liang and MacRae, 1997; Morimoto and Santoro, 1998; Tsan and Gao, 2004). Many HSPs are expressed constitutively at normal temperature and are indispensable in folding of nascent proteins and stabilizing their structure (Nover and Scharf, 1997; Morrow *et al.*, 2000; Pockley, 2003). Intracellular expression of HSPs is also induced by environmental stresses wherein HSPs function as molecular chaperones, maintaining protein structure and playing a critical role in cell metabolism, growth, differentiation and development (Ohtsuka and Hata, 2000).

The term, molecular chaperone, was first introduced to describe the role of nucleoplasmin, an abundant protein found in *Xenopus* oocytes, in the assembly of nucleosomes *in vitro*. Nucleoplasm binds to purified histones and promotes nucleosome assembly by donating bound histones to assembling chromatin (Laskey *et al.*, 1978). The term was subsequently applied to define a larger family of unrelated proteins that mediate the correct folding of other polypeptides but are not themselves components of the final

functional protein (Hendrick and Hartl, 1993). Molecular chaperones inhibit nonproductive folding by binding specifically and non-covalently to interactive protein surfaces exposed transiently, with many able to refold partially denatured proteins in an ATP-dependent manner (Ellis, 1990; Ohtsuka and Hata, 2000).

1.2 A general view of sHSPs

1.2.1 sHSP Structure

Many, but not all molecular chaperones are HSPs, among which sHSPs compose a distinctive family characterized by a conserved "α-crystallin domain" of 80 to 100 amino acid residues. As a hallmark of the sHSP group, the α-crystallin domain is usually flanked by a nonconserved N-terminal region and a short flexible C-terminal extension (de Jong *et al.*, 1998a; MacRae, 2000; Haslbeck, 2002; Hsu *et al.*, 2003) (Fig. 1). sHSP monomers are usually 12-43 kDa in mass, and assemble into native oligomers of 9 to 40 subunits with mass up to 1 MDa (Muchowski *et al.*, 1999; Fernando *et al.*, 2003). sHSP oligomers undergo dynamic subunit exchange at elevated temperature usually by a rapid process involving ionic and hydrophobic interactions, this of importance in chaperone action (Bova *et al.*, 1997; Friedrich *et al.*, 2004; Haslbeck *et al.*, 2004). sHSPs have a large binding capacity for denatured proteins which are held in a molten-globule folding-competent state until released and refolded by ATP-dependent chaperones such as HSP70/HSP60 upon restoration of physiologically permissive conditions (Fig. 2) (Lee and Vierling, 2000; Diamant *et al.*, 2001; Mogk *et al.*, 2003; Graf *et al.*, 2004; Rekas *et al.*, 2004). Unlike many other chaperones, sHSPs have limited ability to refold nonnative proteins (van Montfort *et al.*, 2001a; Treweek *et al.*, 2003).

Information on the quaternary structure of sHSPs is limited due to oligomer

Figure 1. Multiple sHSP sequence alignment

The amino acid sequences of selected sHSPs were analyzed by CLUSTAL W (1.82). HCRYAA, *Homo sapiens* αA-crystallin, P04289; HCRYAB, *H. sapiens* αB-crystallin, P02511; HHsp27, *H. sapiens* Hsp27, NP_001532; Ap26, *Artemia franciscana* p26, AAB87967; WHsp16.9, *Triticum aestivum* Hsp16.9, 1GME_A. (-) no amino acid residue; (*) identical residues; (:) conserved substitution; (.) semi-conserved substitution. sHSP domains are indicated above the alignment, while the secondary structure of *Triticum aestivum* Hsp16.9 is depicted under the alignment (van Montfort *et al.*, 2001b). Amino acid residues in red, small and hydrophobic; blue, acidic; magenta, basic; green, residues containing a hydroxyl or amine group. Residue number is indicated on the right.

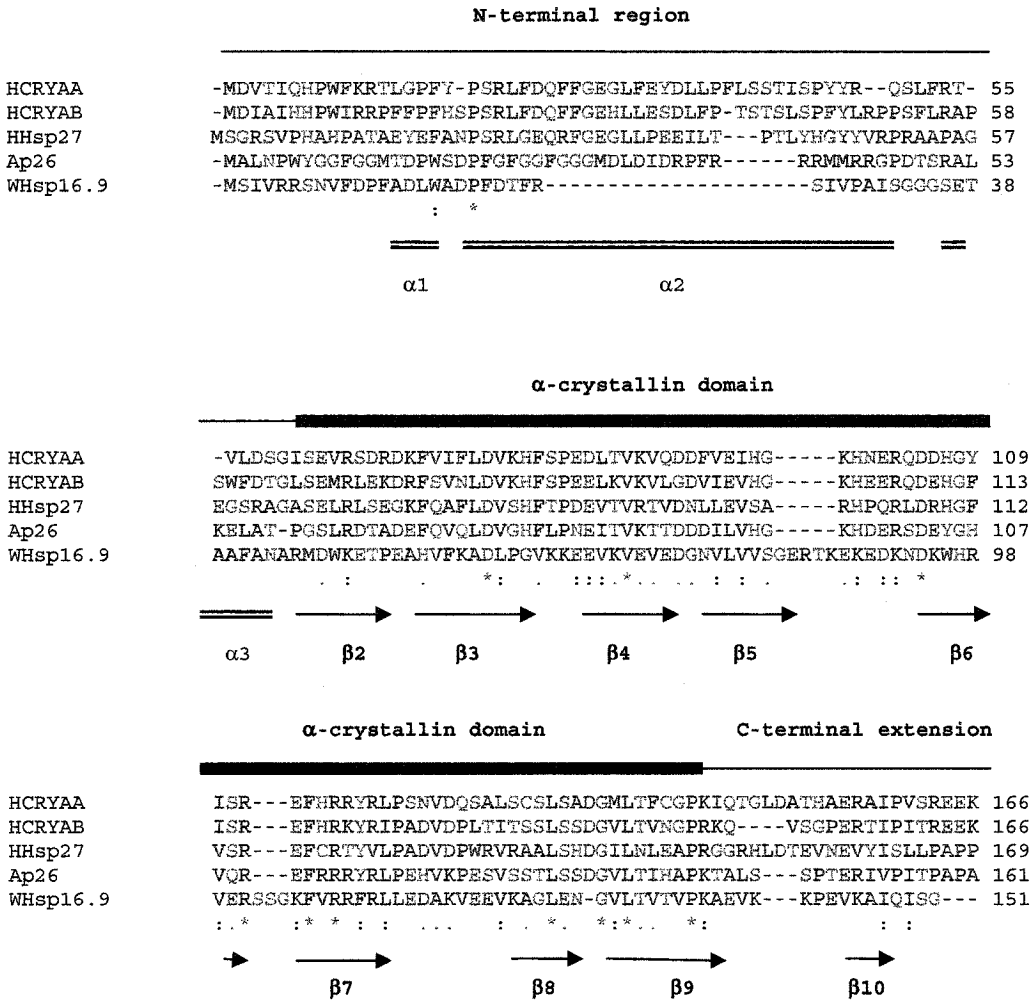
N-terminal region
HCRYAA -MDVTIQHPWFKRTLGPFY-PSRLFDQFFGEGLFEYDLLPFLSSTISPYYR--QSLFRT- 55
HCRYAB -MDIAIHHPWIRRPFFPFHSPSRLFDQFFGEHLLESDLFP-TSTSLSPFYLRPPSFLRAP 58
HHsp27 MSGRSVPHAHPATAEYEFANPSRLGEQRFGEGLLPEEILT---PTLYHGYYVRPRAAPAG 57
Ap26 -MALNPWYGGFGGMTDPWSDPFGFGGFGGGMDLDIDRPFR------RRMMRRGPDTSRAL 53
WHsp16.9 -MSIVRRSNVFDPFADLWADPFDTFR--------------------SIVPAISGGGSET 38
α1
α2
α-crystallin domain
HCRYAA -VLDSGISEVRSDRDKFVIFLDVKHFSPEDLTVKVQDDFVEIHG-----KHNERQDDHGY 109
HCRYAB SWFDTGLSEMRLEKDRFSVNLDVKHFSPEELKVKVLGDVIEVHG-----KHEERQDEHGF 113
HHsp27 EGSRAGASELRLSEGKFQAFLDVSHFTPDEVTVRTVDNLLEVSA-----RHPQRLDRHGF 112
Ap26 KELAT-PGSLRDTADEFQVQLDVGHFLPNEITVKTTDDDILVHG-----KHDERSDEYGH 107
WHsp16.9 AAFANARMDWKETPEAHVFKADLPGVKKEEVKVEVEDGNVLVVSGERTKEKEDKNDKWHR 98
α3
β2
β3
β4
β5
β6
α-crystallin domain
C-terminal extension
HCRYAA ISR---EFHRRYRLPSNVDQSALSCSLSADGMLTFCGPKIQTGLDATHAERAIPVSREEK 166
HCRYAB ISR---EFHRKYRIPADVDPLTITSSLSSDGVLTVNGPRKQ----VSGPERTIPITREEK 166
HHsp27 VSR---EFCRTYVLPADVDPWRVRAALSHDGILNLEAPRGGRHLDTEVNEVYISLLPAPP 169
Ap26 VQR---EFRRRYRLPEHVKPESVSSTLSSDGVLTIHAPKTALS---SPTERIVPITPAPA 161
WHsp16.9 VERSSGKFVRRFRLLEDAKVEEVKAGLEN-GVLTVTVPKAEVK---KPEVKAIQISG--- 151
β7
β8
β9
β10
C-terminal extension
HCRYAA P--TSAPSS---------- 173
HCRYAB PAVTAAPKK---------- 175
HHsp27 DPEEEEEAAIVEP------- 182
Ap26 VGRIEGGTTGTTTGSTASSTPARTTRSGGAA 192
WHsp16.9 ----------

Figure 1

Figure 2. sHSP oligomerization and chaperoning

Denaturation of native proteins upon exposure to stress leads to the formation of nonnative intermediates. Large oligomers of some sHSPs dissociate into smaller oligomers such as dimers (or trimers) which bind tightly to nonnative intermediates, thereby preventing irreversible aggregation. In some species, the large sHSP oligomers may bind to the intermediate proteins directly, without dissociation. Once physiologically permissive conditions are resumed, a limited number of bound intermediates may be released and refold spontaneously. The release of other nonnative intermediates and their reactivation, however, occur in the presence of ATP-dependent molecular chaperones such as HSP70 and HSP60. After release of substrate proteins, sHSP dimers (or trimers) reassociate into oligomers, perhaps as inactive storage forms (Treweek *et al.*, 2003; Haslbeck *et al.*, 2004; Stromer *et al.*, 2004).

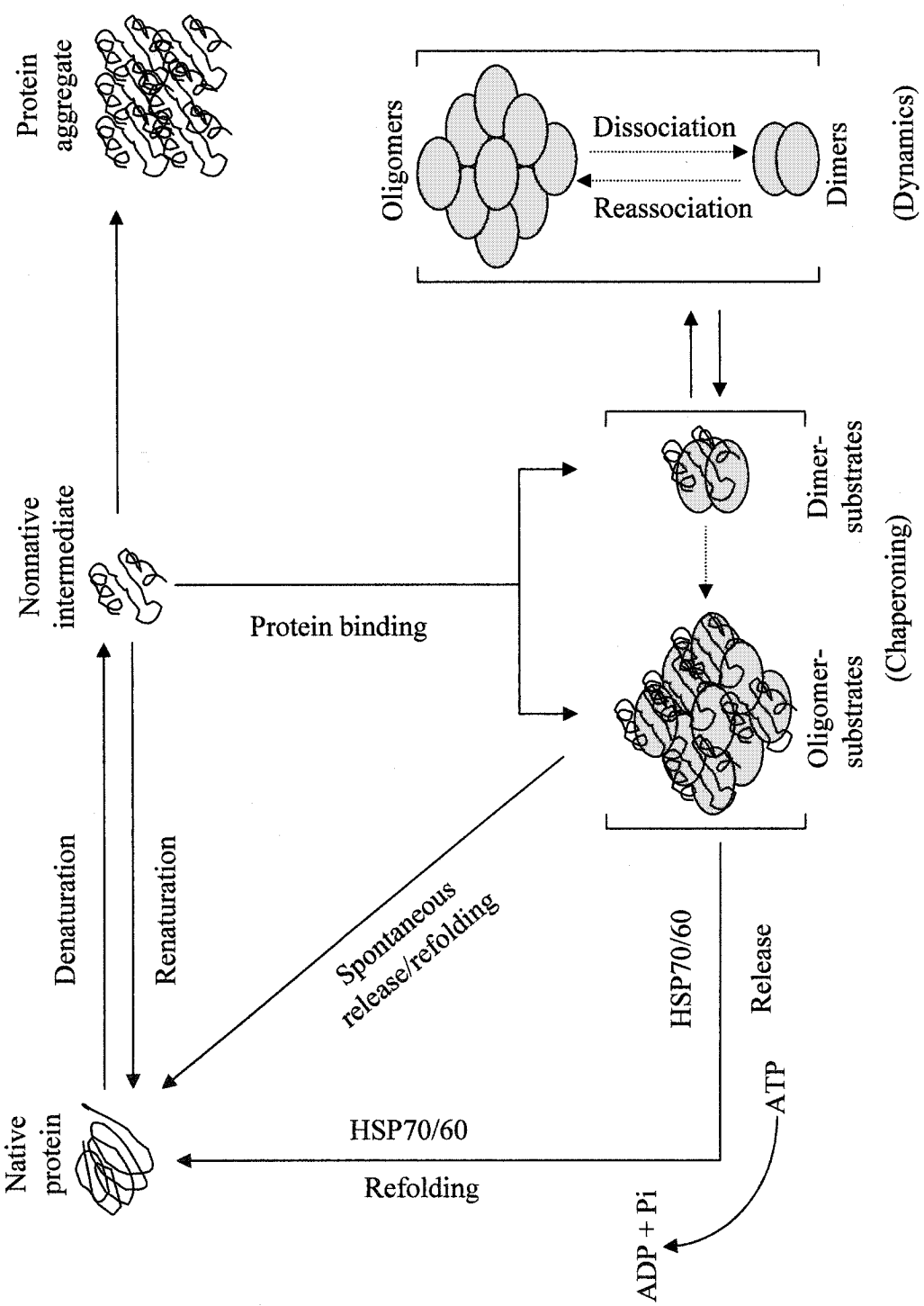
Protein aggregate
Oligomers
Dissociation
Reassociation
Dimers
(Dynamics)
Nonnative intermediate
Protein binding
Dimer-substrates
Oligomer-substrates
(Chaperoning)
Denaturation
Renaturation
Spontaneous release/refolding
HSP70/60
Release
ATP
Native protein
HSP70/60
Refolding
ADP + Pi

Figure 2

polydispersity, with many sHSPs forming a continuum of structures composed of variable numbers of subunits (Haley *et al.*, 2000). sHSPs form globular complexes as occurs for *Methanococcus jannaschii* (*Mj*) Hsp16.5 (Kim *et al.*, 1998), mouse Hsp25 and human Hsp27 (Ehrnsperger *et al.*, 1999; Rogalla *et al.*, 1999), however, *Mycobacterium tuberculosis* (*Mt*) Hsp16.3 exists as nonameric triangles (Chang *et al.*, 1996). Oligomer formation is usually a prerequisite for chaperone activity of most sHSPs, and the complexes may undergo distinct structural changes upon stress. For example, *Saccharomyces cerevisiae* Hsp42 functions as an active chaperone composed of large dynamic oligomers under either physiological or stressful conditions, while Hsp26 from the same organism disassembles reversibly into dimers for efficient interaction with unfolding proteins upon elevated temperatures (Haslbeck *et al.*, 2004; Stromer *et al.*, 2004).

Although the oligomers of most sHSPs show structural variability and are polydisperse, a few sHSPs have monodisperse oligomerization that is well characterized. Reported examples are the X-ray crystallographic structures of archaeal *Mj* Hsp16.5, a 24-subunit oligomer (Kim *et al.*, 1998) (Fig. 3a), and wheat *Triticum aestivum* (*Ta*) Hsp16.9, a 12-subunit oligomer (van Montfort *et al.*, 2001a) (Fig. 3b), which reveal common features although structurally different. Despite limited sequence identity, the α-crystallin domain in monomers of each crystallized sHSP oligomer exhibits a β-sandwich composed of two anti-parallel β-sheets (van Montfort *et al.*, 2001b). The most extensive interface for both oligomers is between dimer subunits and the oligomers are stabilized by the interaction of hydrophobic residues in the C-terminal extension with a hydrophobic groove on the α-crystallin domain of a neighboring subunit dimer (Friedrich *et al.*, 2004). The resolution

Figure 3. X-ray crystallographic structures of sHSPs

a. X-ray crystallographic structure of archaeal *Mj* Hsp16.5. The spherical 24-mer has an outer diameter of 12 nm and inner diameter of 6.5 nm; image resolution is 0.29 nm; b. X-ray crystallographic structure of wheat *Ta* Hsp16.9 arranged as dodecameric double disks which are approximately 9.5 nm wide and 5.5 nm high with a central cavity of about 2.5 nm wide; image resolution is 0.27 nm (Adapted from (Haley *et al.*, 1998; Kim *et al.*, 1998; van Montfort *et al.*, 2001b).

a

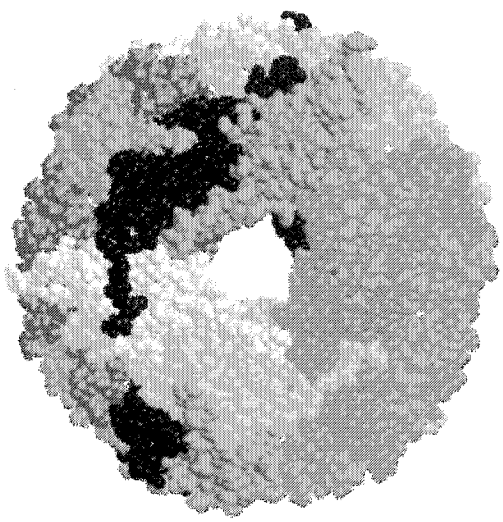

b

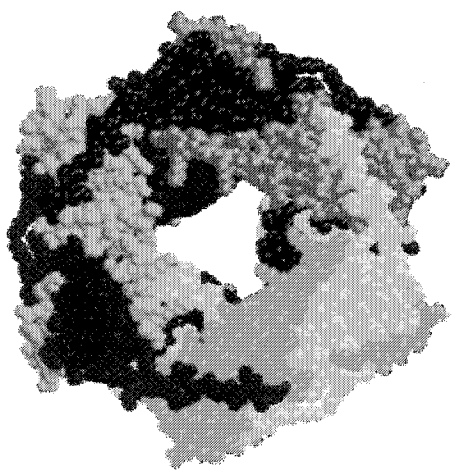

Figure 3

of the N-terminal arms from six subunits indicates wheat *Ta* Hsp16.9 oligomers are further stabilized by extensive N-terminal arm interactions, where essential contacts between dimers are formed by the first 40 N-terminal residues which generate pairs of interwining α-helical domains located inside the dodecamer (van Montfort *et al.*, 2001b; Wintrode *et al.*, 2003).

The dodecameric *Ta* Hsp16.9 consists of two disks, each comprising six α-crystallin domains organized in a trimer of dimers (Fig. 4a). The monomer folding and oligomer assembly are mutually interdependent processes wherein strand exchange, helix swapping, loose knots and hinged extension are involved (van Montfort *et al.*, 2001b). The α-crystallin domain of each monomer consists of a β-sandwich composed of two antiparallel β-sheets encompassing a long loop, followed by a short C-terminal extension (Fig. 4d). Within a dimer, one monomer has a disordered N-terminal arm, while the other has a fully resolved N-terminal arm which is composed of helices connected by random coil. Residue R108 represents one of the most conserved sites among diverse sHSPs, and strengthens the dimer of *Ta* Hsp16.9 by forming an intermolecular salt bridge with E100 in the dimerization loop extending from the β-sandwich which engages in strand exchange to stabilize the partner monomer (Fig. 4c). The dimers of *Ta* Hsp16.9 form "eclipsed" tetramers whose bottom dimers appear hidden when viewed down the crystallographic three-fold axis, with β7 strands and part of the dimerization loops from the two monomers with ordered N-terminal arms, while the dimer interface is strengthened by two C-terminal extensions from monomers with disordered N-terminal arms (Fig. 4b). Residues I147 and I149 from β10 strand of a monomer are associated in a hydrophobic groove between strands β4 and β8 of the interacting monomer, forming a

Figure 4. *Ta* Hsp16.9 structure

a, An overview looking down the crystallographic three-fold axis of *Ta* Hsp16.9, which is perpendicular to three crystallographic two-fold axes. Dimers in the top disk are displayed in red, green and blue, dimers in the bottom disk in pink, sage and turquoise. The dimer-dimer interface that forms an "eclipsed" tetramer whose bottom dimers appear hidden when viewed down the crystallographic three-fold axis, is located between red-pink, blue-turquoise, and green-sage dimers; b, An outside view of one side of the *Ta* Hsp16.9 dodecamer, showing how dimers from the top and bottom disks are related by a two-fold axis to form an "eclipsed" tetramer. In the top dimer, the monomer with a disordered N-terminal arm is shown as a pink ribbon, while the monomer with an ordered arm appears as a solid molecular surface, with surface hydrophobic patches shown in blue. Monomers of the bottom dimer are represented by yellow and red ribbons. Residues I147 and I149 of the I/VXI/V motif in the C-terminal extension from the bottom monomer (yellow) extending from one dimer to another cover hydrophobic grooves which are putative substrate binding sites in the α-crystallin domain of an adjacent dimer; c, The dimer of *Ta* Hsp16.9, composed of a complete monomer (red) and an N-terminal-arm-disordered monomer (pink). N- and C-terminals are labeled, as are E100 and R108, oppositely charged amino acid residues which form an intermolecular salt bridge in the dimerization loop; d, Ribbon diagram of *Ta* Hsp16.9 monomer with the ordered N-terminal arm shown in green, while the α-crystallin domain and the C-terminal extensions are in red (adapted from van Montfort *et al.*, 2001b).

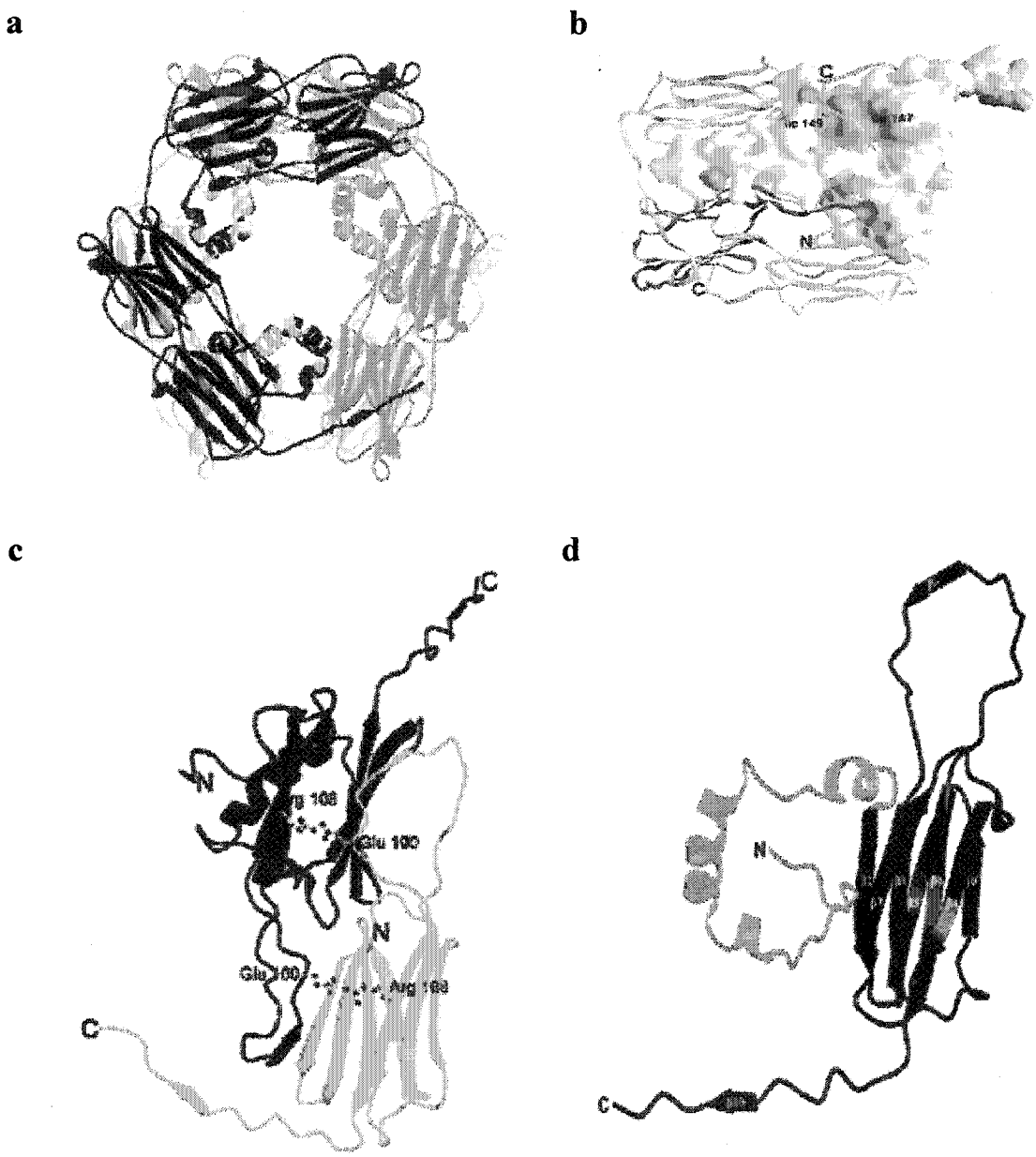

Figure 4

binding motif (I/VXI/V) conserved among sHSPs and covering a putative substrate binding site in the α-crystallin domain of the monomer in the adjacent dimer (Fig. 4b) (van Montfort *et al.*, 2001b).

1.2.2 sHSP Function

sHSPs suppress aggregation of nonnative proteins thereby conferring stress resistance to cells and their functional relevance is widespread. Active α-crystallin, wherein αA-crystallin and αB-crystallin exist in a molar ratio of approximately 3:1, is essential for refracting light and maintaining lens transparency (Bera *et al.*, 2002). In vertebrates, sHSPs interact directly with actin and intermediate filaments, potentially altering the filament assembly/disassembly equilibrium of cytoskeletal components (Perng *et al.*, 1999). αB-crystallin negatively regulates TNF-α, DNA damage and differentiation-induced apoptosis, and protects cells against genomic instability (Kamradt *et al.*, 2001; Kamradt *et al.*, 2002; Bai *et al.*, 2003). Overexpression of Hsp22 in the mitochondria of *D. melanogaster* motor neurons extends life span and increases resistance to oxidative injuries (Morrow *et al.*, 2004). Several proteins are associated *in vivo* with Hsp16.6 from the photosynthetic cyanobacterium *Synechocystis* during heat treatment, revealing the potential for sHSPs to protect cellular functions as diverse as transcription, translation, cell signaling, and secondary metabolism (Basha *et al.*, 2004). In bovine lens, helices in α-crystallin selectively recognize single-stranded and double-stranded DNA (Singh *et al.*, 1998; Bloemendal *et al.*, 1999), indicating potential relationships between sHSPs and nucleic acids *in vivo*. sHSPs may also be involved in the transient storage and protection of mRNA during stress-induced translation arrest (Scharf *et al.*, 1998; Kedersha *et al.*, 1999). Whether sHSPs bind RNA directly or indirectly via other proteins as intermediates

is uncertain. Studies on lens plasma membrane suggest that a subfraction of α-crystallin becomes buried in the membrane bilayer (Cobb and Petrash, 2000a), and the majority of heat-induced *Synechocystis* Hsp16.6 is associated with thylakoid membranes (Horúath *et al.*, 1998; Lee *et al.*, 2000), suggesting the involvement of these sHSPs in membrane fluidity regulation. It is thus reasonable to propose that upon stress, the cellular pool of sHSPs, at least in some organisms, is divided into two or more subfractions, including those responsible for protein chaperoning and those for membrane stability (Narberhaus, 2002b).

1.3 Mutational analysis of sHSPs

Mutations to sHSPs may affect structural stability and compromise chaperone function, and this is the subject of intensive study. For example, internal deletion mutations of human αA- and αB-crystallin lacking residues SRLFDQFFG at positions 20-28 and 21-29 respectively, yield oligomers of significantly reduced size and decreased stability to urea-induced denaturation, indicating the motif is an important determinant of quaternary structure (Pasta *et al.*, 2003). Removal of the N-terminus from *Mt* Hsp16.3 dissociates the nonameric oligomer into trimers, the building block of this sHSP (Koteiche and McHaourab, 2003). Deletion of the N-terminus of yeast Hsp26 reduces the twenty-four subunit complex to dimers and abolishes chaperone activity, indicating the structural and functional importance of the region (Stromer *et al.*, 2004). The N-terminal region may be buried within sHSP oligomers, involved in monomer-monomer interactions, and of critical importance for the association of sHSPs with nonnative proteins and the formation of large oligomeric complexes (Kim *et al.*, 1998; Stromer *et al.*, 2004; Usui *et al.*, 2004). For *Mj* Hsp16.5, however, an N-terminal-deleted mutant behaves similarly to

its wild type counterpart, suggesting this part of the protein does not have a critical structural role, but is important in organizing monomers before final oligomer assembly (Kim *et al.*, 2003b).

The α-crytallin domain mediates subunit interactions and is responsible for the formation of sHSP dimers and trimers (Feil *et al.*, 2001; Pasta *et al.*, 2004). Mutations in this domain may have dramatic consequences. For instance, variations at F94 in the core α-crytallin domain of HspH from the bacterium *Bradyrhizobium japonicum* disrupt function and dimerization, leading to monomer formation, whereas modification of G114, a conserved residue among sHSPs, impairs chaperone function without affecting oligomerization (Lentze *et al.*, 2003). Mutant R120G of αB-crystallin exhibits decreased β-sheet secondary structure, irregular tertiary and quaternary structure, the absence of a clear central cavity and a two-fold increase in oligomeric mass (Bova *et al.*, 1999b). R120G loses the ability to inhibit proteolytic activation of caspase-3 which affects apoptosis regulation (Kamradt *et al.*, 2002). Furthermore, R120G fails to stabilize the intermediate filament desmin and co-aggregates with this protein, leading to desmin-related myopathy (DRM) with symptoms similar to those caused by desmin mutations (Vicart *et al.*, 1998; Goldfarb *et al.*, 2004). The misfolding of R120G contributes to inclusion body formation, although their occurrence may be delayed or prevented by expression of wild type αB-crystallin or other chaperones (Chavez-Zobel *et al.*, 2003). Similarly, a mutation at the equivalent position in human αA-crystallin, R116C, results in impaired chaperone activity, increased oligomeric polydispersity and enhanced membrane association (Cobb and Petrash, 2000b), all potential influences in the pathogenesis of autosomal dominant congenital cataract (ADCC). R116C αA-crystallin

has a diminished protective ability against UVA radiation-induced lens epithelial cell apoptosis (Andley *et al.*, 2002). Missense mutations of K141 to either E or N in human HspB8 (Hsp22), a residue corresponding to R120 in αB-crystallin or R116 in αA-crystallin, lead to dysfunction of axonal transport and dysregulation of the cytoskeleton, causing motor neuron death in distal hereditary motor neuropathy (HMN) (Irobi *et al.*, 2004). Together, the results indicate a single arginine or lysine mutation in the core α-crystallin domain has dramatic effects on the structural integrity and chaperoning function of human sHSPs. Substantial changes caused by these mutations are likely due to the fact that the arginine and lysine residues are buried and potentially form salt bridges with residues of opposite charge. The disruption or absence of such salt bridges could lead to protein conformational changes and loss of function (Kumar *et al.*, 1999; Bera *et al.*, 2002).

Besides acting primarily as a solubilizing agent for sHSPs and sHSP-substrate complexes formed during stress, the C-terminal extension is characterized by structural flexibility and sequence diversity. Being generally polar and hydrophilic, this extension plays a vital role in chaperone activity by maintaining sHSP solubility and binding to oppositely charged residues of unfolding proteins which are then held by the hydrophobic N-terminal region of sHSPs (Derham and Harding, 1999). The C-terminal extension of sHSPs is susceptible to cleavage, and deletion of the region results in modified tertiary structure, compromised solubility and decreased chaperone function (Takemoto *et al.*, 1993; Andley *et al.*, 1996). For instance, mouse Hsp25 lacking the C-terminal extension fails to stabilize α-lactalbumin against precipitation following reduction by dithiothreitol, and is less stable at elevated temperatures than the wild type, suggesting that the C-

terminal extension is indispensable for full chaperone activity (Lindner *et al.*, 2000). Progressive deletion of the C-terminus from rat and human αA-crystallin leads to significant alteration of tertiary structure and dramatic decline in oligomer mass from approximately 550 kDa to 150 kDa (Thampi and Abraham, 2003), indicating a role in organization of higher order structures. Analysis of α-crystallin C-terminal truncations in hereditary cataractous rat lens demonstrated that a hydrophilic C-terminal extension is essential for chaperone activity, suggesting increased C-terminal truncation of α-crystallins in mutant lenses and reduction in chaperone function accelerates cataract formation (Takeuchi *et al.*, 2004). Single site mutations to the C-terminal extension also affect sHSPs. As an example, alternation of isoleucine residues in the conserved I/VXI/V motif, which has a propensity to participate in inter-subunit interactions, results in oligomeric dissociation and chaperone activity decline for bacterial and plant sHSPs (Studer *et al.*, 2002; Pasta *et al.*, 2004).

1.4 The brine shrimp, *Artemia franciscana*

The crustacean, *Artemia franciscana*, has a remarkable ability to tolerate environmental hardships. The organism inhabits aquatic environments of high salinity, subject to temperature extremes, desiccation, anoxia, and variable food reserves (Drinkwater and Clegg, 1991; Clegg *et al.*, 2000; MacRae, 2003). Two developmental pathways, namely ovoviviparous and oviparous, allow *Artemia* to survive these extremes (Fig. 5). Embryos developing via the ovoviviparous pathway are released from females as free-swimming nauplii or instar I larvae (MacRae, 2003). Alternatively, embryos undergoing oviparous development are arrested at the gastrula stage and then encyst. The cysts, composed of approximately 4000 cells enclosed in a shell permeable only to volatile molecules, enter a

Figure 5. Life history of *Artemia franciscana*

Fertilized *Artemia* oocytes may undergo ovoviviparous development where free-swimming nauplii are released (left). Alternatively, oviparous development occurs where development stops at late gastrulae and embryos encyst (top-left), enter diapause and are released from females (top-middle). Diapause continues until cysts are activated by environmental stimuli such as cold and desiccation (top-middle). Activated, post-diapause cysts develop into nauplii. However, if unfavorable conditions prevail, growth is arrested and cysts become quiescent until favorable conditions occur (Liang and MacRae, 1999).

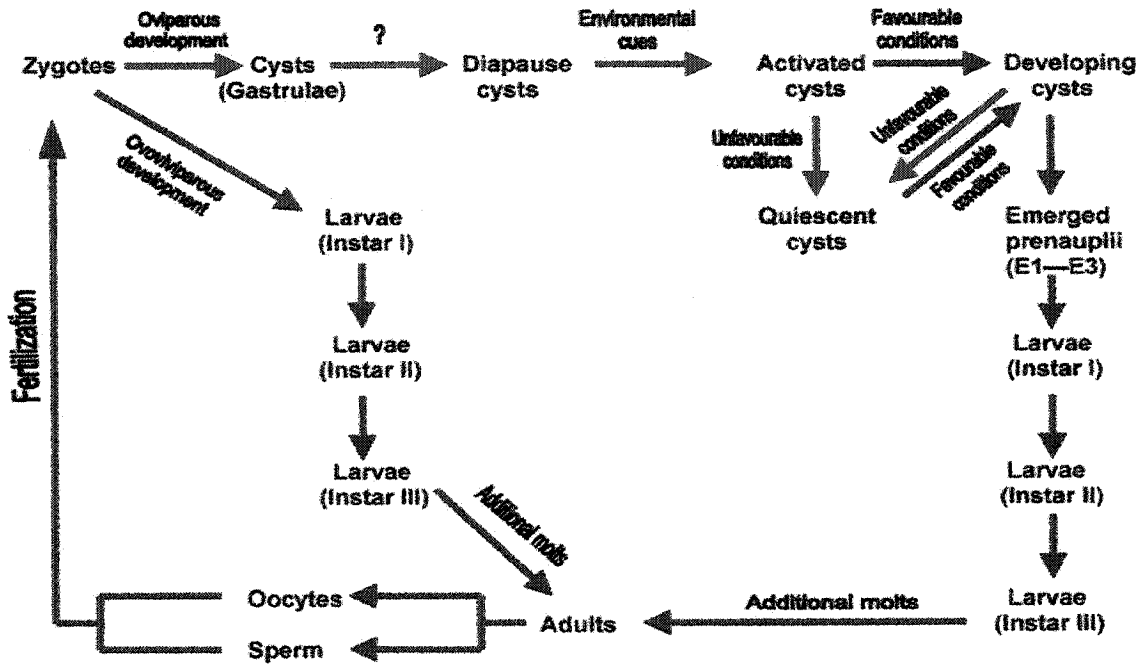
Oviparous development
Zygotes
Cysts (Gastrulae)
?
Diapause cysts
Environmental cues
Activated cysts
Favourable conditions
Developing cysts
Unfavourable conditions
Unfavourable conditions
Favourable conditions
Ovoviviparous development
Larvae (Instar I)
Quiescent cysts
Emerged prenaupli (E1—E3)
Larvae (Instar II)
Larvae (Instar I)
Larvae (Instar III)
Additional molts
Larvae (Instar II)
Fertilization
Oocytes
Sperm
Adults
Additional molts
Larvae (Instar III)

Figure 5

dormant state known as diapause, where the metabolic rate is too low to be detected experimentally (Jackson and Clegg, 1996; Clegg *et al.*, 2000; MacRae, 2003). Diapause continues, even under favorable conditions, until cysts are activated by the appropriate environmental stimulus, including desiccation and cold (Clegg *et al.*, 2000; MacRae, 2003). Upon activation, cysts resume development, provided that appropriate temperature, water content and oxygen are available (Drinkwater and Clegg, 1991; Clegg *et al.*, 1999). However, cysts remain quiescent if unfavorable conditions prevail.

Among organisms which experience diapause, encysted *Artemia* embryos possess an outstanding capability to tolerate environmental insults (Viner and Clegg, 2001). For example, post-diapause cysts will survive fully hydrated at physiological temperature in the absence of oxygen for four years, and the anoxic cysts maintain integrity even in the apparent absence of nuclear transcription, protein synthesis and ongoing energy metabolism (Hand, 1998; Clegg *et al.*, 1999; Liang and MacRae, 1999; van Breukelen *et al.*, 2000; Warner and Clegg, 2001). Interestingly, this appears contrary to the biological axiom that, upon normal hydration and temperature, cell maintenance requires a constant and substantial free energy flow (Warner and Clegg, 2001). Cysts have developed a mechanism to survive by which intracellular macromolecules and organelles are protected against irreversible denaturation due to water removal, heat, anoxia and reduced metabolism. The sHSPs, which function as molecular chaperones and may be developmentally regulated, are ideal candidates for this purpose.

1.5 p26, a small heat shock protein from *Artemia franciscana*

Diapause-destined embryos synthesize large amounts of a novel sHSP, namely p26, which is thought to act as a molecular chaperone during diapause, anoxia and other

stresses (MacRae, 2003). Composed of 20.8 kDa subunits, p26 forms oligomers as large as 34 subunits with a molecular mass of approximately 700 kDa (Liang *et al.*, 1997b; MacRae, 2003). This protein makes up approximately 10-15% of total non-yolk embryonic protein and is most abundant in the encysted embryo stage of the life cycle (Clegg *et al.*, 1994; Clegg *et al.*, 1995). Produced mainly in oviparously developing *Artemia,* p26 peaks in encysted embryos and remains constant during post-gastrula development until just before the emergence of nauplii from cysts (Liang and MacRae, 1999; MacRae, 2003). p26 is almost entirely missing from second instar larvae, and is neither detectable nor inducible in subsequent life stages (Clegg *et al.*, 1999; Liang and MacRae, 1999). Instead of being heat-inducible, p26 is developmentally regulated, as occurs for Hsp12.6 from *Caenorhabditis elegans*, Hsp17.6 from sunflower and multiple sHSPs from *D. melanogaster* (Morrow *et al.*, 2000; MacRae, 2003). During diapause, p26 exists in nuclei and cytoplasm (Jackson and Clegg, 1996; Clegg *et al.*, 2000). Upon diapause termination, most p26 resides in the cytoplasm, although about half re-enters nuclei if activated embryos experience anoxia or thermal stress (Clegg *et al.*, 1994; Clegg *et al.*, 1999). Cytoplasm-to-nuclei translocation of p26 also occurs *in vitro* when the pH of homogenates is reduced, and this is reversed by alkaline pH (Clegg *et al.*, 1995; Clegg *et al.*, 1999). The observation of p26 in discrete intranuclear compartments of *Artemia* cysts implies roles for the protein in specific processes (MacRae, 2003), perhaps including the inhibition of DNA replication which characterizes cyst development.

p26 exhibits molecular chaperone activity *in vitro*, protecting citrate synthase against heat induced inactivation and chaperoning *Artemia* tubulin which exposes hydrophobic amino acid residues as it ages (Liang *et al.*, 1997b; Viner and Clegg, 2001; Day *et al.*,

2003). Additionally, p26 is thought to protect intracellular proteins of encysted *Artemia* from stress-induced denaturation (Liang and MacRae, 1999; MacRae, 2003). p26 also confers thermotolerance on transformed bacteria and enhances stress resistance in transgenic *D. melanogaster* (Crack *et al.*, 2002; Malaviarachchi, 2002), further indicating that p26 functions as a molecular chaperone *in vivo*.

As a member of the sHSP family, p26 possesses a conserved α-crystallin domain, with secondary structure predicted to consist predominantly of β-pleated sheets (Liang *et al.*, 1997a), although how these sheets are organized was not investigated. Previous data showed that the C-terminus of p26 is more important than the N-terminus for conferring thermotolerance on *Escherichia coli* and formation of large oligomers is not a prerequisite for the chaperoning function of p26 (Crack *et al.*, 2002). When compared with other sHSPs, p26 has an N-terminus distinctly enriched in both glycine and arginine (MacRae, 2003), and a serine/threonine-enriched patch in the unusually long, polar and hydrophilic C-terminus. Such specific variances between p26 and other sHSPs suggest these regions are structurally and functionally important. In addition to these unique characteristics, p26 possesses highly conserved sites within the core α-crystallin domain. The purpose of the work described in this thesis was to analyze p26 structure and function. The results enhance our appreciation of *Artemia* development and have important implications for understanding the functional mechanisms of p26, while providing a model for the study of other sHSPs, many of which are involved in human diseases.

II. Materials and Methods

2.1 Site-directed mutagenesis of p26

Truncations, single amino acid substitutions and internal deletions of p26 cDNAs were generated by site-directed mutagenesis with the QuikChange™ Site-directed Mutagenesis kit (Stratagene, La Jolla, CA), using pRSET.C-p26-3-6-3 as template (Liang *et al.*, 1997a), and designated primers (Tables 1 & 2). Fifty µl PCR reaction mixtures included 5 µl of 10 × reaction buffer, 1 µl (50 ng) of DNA extracted with the *Wizard Plus* SV Miniprep DNA purification kit (Promega, Madison, WI) following the manufacturer's instructions, 1 µl (125 ng) of sense primer, 1 µl (125 ng) of anti-sense primer, 1 µl of dNTP mix and 41 µl of ddH_2O. One µl of *PfuTurbo* DNA polymerase (2.5 U/µl) was added and sample reactions were overlayed with 30 µl of mineral oil. Mixtures were incubated for 30 sec at 95 °C prior to multiple cycles of 30 sec at 95 °C, 1 min at 55 °C, 8 min at 68 °C. To produce truncated or internally deleted p26 cDNAs, 18 cycles were employed, for single amino acid substitutions 12 cycles sufficed. A PTC-100 programmable thermal controller (MJ Research, Inc, Watertown, MA) was employed. After cycling, the reactions were placed on ice for 2 min, then 1 µl of the restriction enzyme *Dpn* I (10 U/µl) was added to each amplification reaction prior to incubation at 37 °C for 1 h. For transformation, 50 µl of gently thawed *E. coli* XL1-blue supercompetent cells were placed in prechilled Falcon 2059 polypropylene tubes, 1 µl of the *Dpn* I-treated DNAs was added, and the mixtures were incubated on ice for 30 min. The transformation mixtures were heated for 45 sec at 42 °C, placed on ice for 2 min, and 0.5 ml of NZY^+ broth preheated to 42 °C was added. The transformation mixtures were

Table 1. Truncations of p26 cDNA

p26 variants	Amino acid residues deleted	Primer sequences
p26-NΔ36	1-36	5'-CTCGTGCCGATCAAAATGCCCTTCCGGAGAAG-3'
		5'-CTTCTCCGGAAGGGCATTTTGATCGGCACGAG-3'
p26-NΔ60	1-60	5'-CTCGTGCCGATCAAAATGTCCTTGAGGGACACAGC-3'
		5'-GCTGTGTCCCTCAAGGACATTTTGATCGGCACGAG-3'
p26-CΔ40	153-192	5'-GCTCACCAACAGAACGTTAATCTGCATTC-3'
		5'-GAATGCAGATTAACGTTCTGTTGGTGAGC-3'
p26-CΔ10	183-192	5'-GCTAGTTCAACTCCATAATCTGCATTC-3'
		5'-GAATGCAGATTATGGAGTTGAACTAGC-3'
p26-alpha	1-60	5'-CTCGTGCCGATCAAAATGTCCTTGAGGGACACAGC-3'
		5'-GCTGTGTCCCTCAAGGACATTTTGATCGGCACGAG-3'
	153-192	5'-GCTCACCAACAGAACGTTAATCTGCATTC-3'
		5'-GAATGCAGATTAACGTTCTGTTGGTGAGC-3'

Truncations of p26 cDNA were generated by site-directed mutagenesis using primers listed above in the right column. The name of each p26 variant, either cDNA or protein, is indicated in the left column and the positions of deleted amino acids are in the middle column.

Table 2. Single amino acid substitutions and internal deletions of p26 cDNA

Regions of p26	Mutations	Primer sequences
N-terminal region	W17R	5'-GGTATGACTGACCCAAGGTCTGATCCATTTGG-3'
		5'-CCAAATGGATCAGACCTTGGGTCAGTCATACC-3'
	D19A	5'-GACCCATGGTCTGCTCCATTTGGATTTGG-3'
		5'-CCAAATCCAAATGGAGCAGACCATGGGTC-3'
	P20A	5'-CCCATGGTCTGATGCATTTGGATTTGGTGGC-3'
		5'-GCCACCAAATCCAAATGCATCAGACCATGGG-3'
	F21R	5'-CCCATGGTCTGATCCACGTGGATTTGGTGGC-3'
		5'-GCCACCAAATCCACGTGGATCAGACCATGGG-3'
	G22A	5'-GGTCTGATCCATTTGCATTTGGTGGC-3'
		5'-GCCACCAAATGCAAATGGATCAGACC-3'
	"G" deletion (8-29:22)	5'-GGCACTTAACCCATGGTACATGGACCTTGATATTGAC-3'
		5'-GTCAATATCAAGGTCCATGTACCATGGGTTAAGTGCC-3'
	"R" deletion (36-45:10)	5'-GGACCTTGATATTGACGGTCCAGATACC-3'
		5'-GGTATCTGGACCGTCAATATCAAGGTCC-3'
α-crystallin domain	D67A	5'-GAGGGACACAGCTGCTGAATTTCAAGTTCAG-3'
		5'-CTGAACTTGAAATTCAGCAGCTGTGTCCCTC-3'
	F69R	5'-GGGACACAGCTGATGAACGTCAAGTTCAGC-3'
		5'-GCTGAACTTGACGTTCATCAGCTGTGTCCC-3'
	R110G	5'-GGACACGTACAAGGAGAATTTCGACGACG-3'
		5'-CGTCGTCGAAATTCTCCTTGTACGTGTCC-3'
	F112R	5'-CACGTACAAAGAGAACGTCGACGACG-3'
		5'-CGTCGTCGACGTTCTCTTTGTACGTG-3'
	R114A	5'-GAGAATTTCGAGCACGATACAGACTCCC-3'
		5'-GGGAGTCTGTATCGTGCTCGAAATTCTC-3'
	Y116D	5'-CGACGACGAGACAGACTCCCAGAACATGTC-3'
		5'-GACATGTTCTGGGAGTCTGTCTCGTCGTCG-3'
	G135A	5'-GTCATCAGATGCTGTCTTAACTATCC-3'
		5'-GGATAGTTAAGACAGCATCTGATGAC-3'
	L137R	5'-CAGATGGTGTCCGAACTATCCATGC-3'
		5'-GCATGGATAGTTCGGACACCATCTG-3'
	T138A	5'-GGTGTCTTAGCTATCCATGCTCCG-3'
		5'-CGGAGCATGGATAGCTAAGACACC-3'
C-terminal extension	"TS" deletion (169-186: 18)	5'-GGATTGAAGGGGGAAGATCAGGAGGTGC-3'
		5'-GCACCTCCTGATCTTCCCCCTTCAATCC-3'
	"GGAA" deletion	5'-CTCCAGCAAGAACAACAAGATCATAATCTGCATTC-3'
		5'-GAATGCAGATTATGATCTTGTTGTTCTTGCTGGAG-3'
	"AA" deletion	5'-CAAGATCAGGAGGTTAATCTGCATTC-3'
		5'-GAATGCAGATTAACCTCCTGATCTTG-3'

Single amino acid substitutions and internal deletions of p26 cDNA were generated by site-directed mutagenesis using the listed primers. The p26 regions which encompass mutations are indicated in the left column. Single amino acid substitutions are named

starting with the mutated amino acid, followed by its position, and then the replacing amino acid. "G" is the abbreviation for the modification where amino acid residues G8 to G29 are deleted; "R" is the internal deletion where residues R36 to R45 are lost; "TS" represents the internal deletion where residues T169 to T186 are missing; "GGAA" is the deletion where the last four C-terminal residues of p26 are removed; "AA" refers to the deletion which lacks the last two residues of p26. In later work, only four single amino acid substitutions generated in the α-crystallin domain including R110G, F112R, R114A, Y116D, and three internal deletions "G", "R", "TS" of p26 were selected for further studies.

incubated at 37 °C for 1 h with shaking at 225-250 rpm, after which 250 µl of each transformation mixture was spread on agar plates containing 50 µg/ml ampicillin (Sigma, St. Louis, MO) and incubated at 37 °C. Bacterial clones were selected randomly and propagated for DNA mini-preparation, with the identity of each mutant verified by DNA sequencing (DNA Sequencing Facility, Center for Applied Genomics, Hospital for Sick Children, Toronto, ON).

2.2 Cloning of p26 cDNAs in eukaryotic and prokaryotic expression vectors

For cloning in eukaryotic and prokaryotic expression vectors, p26 cDNA-containing pRSET.C plasmids were digested with *Bam* HI and *Xho* I, and electrophoresed in agarose gels from which inserts were recovered with the GFX™ PCR DNA and Gel Band purification kit (Amersham Biosciences, Piscataway, NJ). p26 cDNA, either full length or containing single amino acid substitutions and internal deletions was inserted into pcDNA4/TO/myc-His.A (Invitrogen, San Diego, CA), a eukaryotic expression vector which was pre-linearized with the same restriction enzymes, with T4 DNA ligase (MBI Fermentas, Hanover, MD) and constructs were transformed into *E. coli* strain DH5α (Invitrogen, Carlsbad, CA). These p26 cDNAs were also subcloned into pPROTet.E233 (Clontech Laboratories, Inc, Palo Alto, CA), a His-tag containing prokaryotic expression vector, between the *Bam* HI and *Xba* I sites. Full length and truncated forms of p26 cDNAs were cloned in pRSET.C and recovered by digestion with *Bam* HI and *Xho* I, before subsequently cloned into pSecCMV (Invitrogen, San Diego, CA) for expression in mammalian cells. p26-full which contained the full length p26 polypeptide, p26-NΔ60 where residues 1-60 were removed, and p26-alpha which comprised only the α-crystallin domain of p26 were also excised with *Bam* HI and *Xba* I and cloned into the eukaryotic

vector pcDNA4/His.A (Invitrogen, San Diego, CA) for expression as His-tagged fusion proteins. The vectors used in these experiments are listed in Table 3. After cloning, all inserts were sized by restriction digestion followed by electrophoresis in 1% agarose gels, and PCR fidelity was verified by DNA sequencing.

2.3 p26 cDNA expression in transiently transfected COS-1 cells

COS-1 cells were maintained at 37 °C under 5% CO_2 in Dulbecco's Modified Eagles Medium (DMEM) (Gibco, Burlington, ON) containing 10% fetal bovine serum (FBS, Gibco) and 2% penicillin/streptomycin (Gibco). For small scale transfections, 60 µl of DMEM lacking serum and antibiotics, 1 µg of purified plasmid DNA and 3 µl of SuperFect™ (Qiagen, Mississauga, ON) were mixed in 5 ml polypropylene tubes. The transfection mixtures were incubated at room temperature for 15 min, placed in individual wells of 6-well plates (Becton Dickinson Labware, Franklin Lakes, NJ) containing COS-1 cells grown to 60% confluency and incubated overnight at 37 °C. For large scale transfection, T75 culture flasks (Becton Dickinson Labware) were employed, with the amount of each transfection reagent 6 times that used for 6-well plates. Cells were trypsinized with trypsin-EDTA (Gibco) 24 h after transfection, centrifuged at 1,500 x *g* for 5 min and washed with 1 ml of phosphate buffered saline (PBS) (140 mM NaCl, 2.7 mM KCl, 8.0 mM Na_2HPO_4, 1.5 mM KH_2PO_4, pH 7.4). Cells were collected by centrifugation at 1,500 x *g* for 5 min, resuspended in 50 µl of lysis buffer consisting of 50 mM Tris-HCl, pH 7.8, 150 mM NaCl, 0.5% Nonidet P-40, 1 mM phenylmethylsulfonyl fluoride (PMSF) (Sigma), 1 µg/ml pepstatin A (Sigma) and 1 µg/ml leupeptin (Sigma) and incubated on ice for 20 min. Cell lysates were centrifuged at

Table 3. Vectors used for cloning and expression of p26 cDNA

Types of p26 cDNA mutations	Prokaryotic expression vectors and restriction sites (His-tagged)	Eukaryotic expression vectors and restriction sites
Truncations	pRSET.C *Bam* HI and *Xho* I	pSecCMV *Bam* HI and *Xba* I pcDNA4/His.A (His-tagged) *Bam* HI and *Xba* I
Single amino acid substitutions	pPROTet.E233 *Bam* HI and *Xba* I	pcDNA4/TO/myc-His.A *Bam* HI and *Xho* I
Internal deletions	pPROTet.E233 *Bam* HI and *Xba* I	pcDNA4/TO/myc-His.A *Bam* HI and *Xho* I

The vectors used for cloning and expression of p26 cDNAs in prokaryotic and eukaryotic cells are listed. The types of p26 cDNA variants are indicated in the left column. Vector names and restriction sites used in cloning are indicated in the remaining columns. "His-tagged" means the vector contains either a 6×His or a 6×HN tag.

10,000 × *g* for 10 min, supernatants were transferred to fresh tubes and protein concentrations determined by the Bradford assay (Bio-Rad, Hercules, CA).

2.4 SDS-polyacrylamide gel electrophoresis (SDS-PAGE), Western blotting and immunodetection of proteins

Equal amounts of cell-free extracts from COS-1 cells expressing p26 variants were electrophoresed in 12.5% SDS-polyacrylamide gels which were either stained with Coomassie Brilliant Blue R-250 (Sigma) or the proteins were transferred to nitrocellulose membranes (Bio-Rad, Hercules, CA). The membranes were rinsed briefly with TBS, and then stained with 2% Ponceau-S (Sigma) in 3% trichloroacetic acid (TCA) to check transfer efficiency. The membranes were incubated in 5% low fat Carnation milk powder in TBS-Tween for 45 min, followed by incubation for 30 min at room temperature with either anti-p26 antibody (Liang *et al.*, 1997a) diluted 1:10000 in HST (10 mM Tris, pH 7.4, 1 M NaCl, 0.5% (v/v) Tween 20) or Omni-probe (Santa Cruz Biotechnology, Inc., Santa Cruz, CA), an antibody recognizing the $(His)_6$/Xpress epitope region encoded by pRSET.C and diluted 1:2000 in HST buffer. The blots were washed twice for 3 min in TBS-Tween (10 mM Tris, pH 7.4, 0.14 M NaCl, 0.1% (v/v) Tween 20), twice for 3 min in HST, and once for 3 min in TBS-Tween, before incubation for 30 min with horseradish peroxidase (HRP)-conjugated goat anti-rabbit IgG antibody diluted 1:10000 in HST or HRP-conjugated goat anti-mouse IgG antibody (Jackson ImmunoResearch) diluted 1:5000 in HST. The immunoconjugates were detected with the Western Lightning Enhanced Chemiluminescence (ECL) Reagent Plus (PerkinElmer Life Sciences, Boston, MA) using Fuji medical X-ray film (Fuji Photo Film Co., Ltd, Tokyo).

2.5 Immunolocalization of p26 in transfected COS-1 cells

Twenty-four h after transfection, cells cultured on cover-slips were fixed for 20 min at room temperature in 4% paraformaldehyde, rinsed twice with PBS and permeabilized for 5 min in PBS containing 0.2% (v/v) Triton X-100 (PBS-Triton). Each cover-slip received 35 µl of anti-p26 antibody diluted 1:500 in PBS-Triton and was incubated for 30 min. The cells were washed three times with PBS-Triton, then incubated for 20 min at room temperature with 35 µl of fluorescein isothiocyanate (FITC)-conjugated goat anti-rabbit IgG antibody (Jackson ImmunoResearch) diluted 1:500 in PBS-Triton. The cells were washed three times with PBS-Triton, incubated with RNaseA (Amersham Biosciences, Baie d'Urfe, Quebec) at 5 mg/ml for 10 min and stained with propidium iodide (Sigma) at 0.4 mg/ml for 2 min. Cover-slips were rinsed with PBS-Triton, PBS, and distilled water before being placed on slides with Vectashield™ mounting medium (Vector Laboratories, Burlingame, CA). Cells expressing His-tagged p26 fusion proteins were stained with Omni-probe diluted in PBS-Triton, followed by FITC-conjugated goat anti-mouse IgG antibody (Jackson ImmunoResearch). Immunofluorescently stained cells were examined with a Wild Leitz Aristoplan microscope (Wild Leitz Ltd, Heerbrugg, Switzerland) and a Zeiss 410 inverted confocal laser scanning microscope (Carl Zeiss, Thornwood, NY).

2.6 p26 oligomer formation in COS-1 cells

Transfected COS-1 cells grown to confluency in T75 culture flasks and collected as described above were incubated on ice for 20 min in lysis buffer (50 mM Tris-HCl, pH 7.8, 150 mM NaCl, 1% (v/v) Nonidet P-40,) containing 1 mM PMSF (Sigma), 1 µg/ml pepstatin A (Sigma) and 1 µg/ml leupeptin (Sigma), before centrifugation at 10,000 × *g*

for 10 min. Sucrose gradients of 10-50% were prepared by layering 5 ml of 10% (w/v) sucrose on 5 ml of 50% (w/v) sucrose in 0.1 M Tris/glycine buffer, pH 7.4, in 12 ml tubes and centrifuging at 200,000 × *g* for 3 h at 15 °C. Equal amounts of protein extract from transfected COS-1 cells were applied to individual gradients and centrifuged at 200,000 × *g* for 21 h at 4 °C followed by collection of 0.8 ml fractions. Fifteen µl from each fraction was electrophoresed in 12.5% SDS polyacrylamide gels, blotted to nitrocellulose, and probed with either anti-p26 antibody or Omni-probe as described previously. Molecular mass standards, namely alpha-lactalbumin (14.2 kDa), carbonic anhydrase (29 kDa), bovine serum albumin (66 kDa), alcohol dehydrogenase (150 kDa), apoferritin (443 kDa), and thyroglobulin (669 kDa) (Sigma) were centrifuged separately and their locations determined by measuring the A_{280} of gradient fractions.

2.7 Expression of p26 cDNA in *E. coli*

pRSET.C vectors containing full length and truncated p26 cDNAs were transferred into *E. coli* BL21(DE3)pLysS (Novagen, Madison, WI). For expression of p26, 2 ml of LB medium containing 50 µg/ml ampicillin was inoculated with a single *E. coli* colony and incubated overnight with shaking at 37 °C. The cultures were added to 50 ml of LB medium containing 50 µg/ml ampicillin in 125 ml Erlenmeyer flasks and incubated with shaking at 37°C until the A_{600} of cultures reached 0.5-0.7. Isopropyl-1-thio-β-D-galactopyranoside (IPTG) (Sigma) was then added to a final concentration of 1 mM and incubation continued for 6 h. The cultures were cooled on ice for 5 min, and centrifuged at 5,000 × *g* for 5 min at 4 °C. The cell pellets were washed once with 1 × Extraction/Wash buffer (50 mM Na_3PO_4, 300 mM NaCl, pH 7.5) and resuspended in 4 ml of the same buffer, prior to addition of 100 µg/ml lysozyme (Sigma), 1 mM PMSF

(Sigma), 1 μg/ml pepstatin A (Sigma) and 1 μg/ml leupeptin (Sigma). After multiple freeze-thaw cycles, the mixtures were incubated at 30 °C for 15 min, cooled on ice and sonicated three times for 10 sec using a Branson Sonifier™ 150 (Branson Ultrasonics, Danbury, CT) at medium setting with intermittent cooling on ice for 30 sec. The sonicated cells were centrifuged at 12,000 × *g* for 20 min at 4 °C, the supernatants recovered and protein concentrations ascertained with the Bradford assay kit (Bio-Rad, Hercules, CA).

For the expression of p26 cDNA containing single amino acid substitutions and internal deletions, recombinant vectors constructed with pPROTet.E233 were transformed into *E. coli* BL21PRO (Clontech Laboratories, Inc., Mississauga, ON). Single colonies were picked from LB plates containing 50 μg/ml spectinomycin (Sigma) and 34 μg/ml chloramphenicol (Sigma), inoculated in 2 ml of LB medium and incubated overnight at 37 °C. Fifty ml of LB medium containing spectinomycin/chloramphenicol were inoculated with each overnight culture, and incubated with shaking at 37 °C until the A_{600} reached 0.5-0.7. Anhydrotetracycline (aTc) (Clontech Laboratories) was added to a final concentration of 100 ng/ml, and the incubation continued for 6 h. Cell-free extracts were prepared as just described.

2.8 Purification of p26

Five ml aliquots of thoroughly resuspended BD TALON resin (BD Biosciences Clontech, Mississauga, ON) were transferred to sterile 50 ml tubes, centrifuged at 700 × *g* for 2 min, and the pellets were resuspended in 10 bed volumes of 1 × Extraction/Wash buffer (50 mM Na_3PO_4, 300 mM NaCl, 10 mM Imidazole, pH 7.5) prior to brief agitation. After re-centrifugation at 700 × *g* for 2 min, the resin was pelleted, and the

wash was repeated. Bacterial cell-free extracts were added to the resin, and the mixtures were agitated gently at room temperature for 20 min on a platform shaker, before centrifugation at 700 × g for 5 min. The supernatants were removed carefully, the resin was washed with gentle agitation in 10 bed volumes of 1 × Extraction/Wash buffer for 10 min and centrifuged at 700 × g for 5 min, after which the wash was repeated. One bed volume of the 1 × Extraction/Wash buffer was added, the resuspended resin was transferred to 2 ml BD TALON™ affinity gravity-flow columns (BD Biosciences Clontech) and allowed to settle out of suspension. The buffer was drained and columns were washed once with 5 bed volumes of 1 × Extraction/Wash buffer. The polyhistidine-tagged proteins were eluted by adding 5 bed volumes of 1 × Elution buffer (50 mM Na_3PO_4, 300 mM NaCl, 150 mM Imidazole, pH 7.5) to columns, 500-µl fractions were collected and the A_{280} of each fraction measured. The purified samples were dialyzed for 4 h at room temperature with one change of buffer, then overnight at 4 °C against 10 mM NaH_2PO_4, pH 7.1. Dialyzed samples were concentrated in CentriprepYM-10 centrifugal filter devices (Amicon Bioseparations, Billerica, MA) following manufacturer's instructions.

2.9 Oligomerization of p26

Half-ml samples of p26-containing cell-free extracts from either transfected COS-1 cells or transformed bacteria, and purified samples of p26, were applied to continuous 10-50% (w/v) sucrose gradients, which were prepared with 5 ml of 10% (w/v) sucrose and 5 ml of 50% (w/v) sucrose in 0.1 M Tris/Glycine buffer, pH 7.4, using a gradient maker (MRA, Boston, MA). The gradients were centrifuged at 200,000 × *g* for 12 h at 4 °C in an SW41-TI Beckman rotor. Tube bottoms were punctured with a 21-gauge needle after

centrifugation, 0.8 ml fractions were collected and 15 µl from each fraction was electrophoresed in 12.5% SDS-polyacrylamide gels before blotting to nitrocellulose for immunodetection. For purified truncated versions of p26, the A_{280} of each gradient fraction was measured with a SPECTRAmax *PLUS* microplate spectrophotometer (Molecular Devices, Sunnyvale, CA). The number of p26 monomers per oligomer was calculated using a p26 molecular mass of 20.8 kDa as determined by GENERUNNER (version 3.05, Hastings Software, Inc.) with corrections for protein modifications as necessary. Alpha-lactalbumin (14.2 kDa), carbonic anhydrase (29 kDa), bovine serum albumin (66 kDa), alcohol dehydrogenase (150 kDa), apoferritin (443 kDa), and thyroglobulin (669 kDa) (Sigma) were centrifuged separately and their locations determined in sucrose gradients by measuring the A_{280} of each gradient fraction.

2.10 p26-induced thermotolerance in *E. coli*

To examine thermotolerance induction in *E. coli* expressing p26, 2 ml of LB medium containing either ampicillin/IPTG or spectinomycin/chloramphenicol/anhydrotetracycline was inoculated with single bacterial colonies and incubated overnight at 37 °C with shaking. Upon 1:10 dilution in Falcon 2059 polypropylene tubes (Becton Dickinson Labware, Franklin Lakes, NJ), cultures were transferred to a 54 °C water bath and 100 µl samples were removed at 0, 15, 30, 45 and 60 min. Samples were diluted in cold LB medium and kept on ice before plated on LB agar and incubated at 37 °C overnight. All colony-forming units were counted, and data from three separate heat shock experiments were pooled in order to assess survival. Between data groups, two-sample t-tests were performed at a confidence level of 95.0% with a statistical software MINITAB 14.12.0 (Minitab Inc., State College, PA) to evaluate the significance of difference which was

accepted at the $P < 0.05$ level. To ensure that bacteria contained p26, small amounts of cells were collected before heating, homogenized, and electrophoresed in 12.5% SDS-polyacrylamide gels, followed by transfer to nitrocellulose membranes and immunodetection of p26.

2.11 *In vitro* chaperone activity of p26

2.11.1 Citrate synthase aggregation

A 0.178 mM stock solution of dimeric citrate synthase (Sigma) was diluted with 40 mM HEPES/KOH buffer, pH 7.5 to a final concentration of 150 nM in 1.0 ml cuvettes and heated at 43 °C with 37.5 nM, 75 nM, 150 nM, 300 nM, 600 nM, 1.2 μM and 2.4 μM of purified, bacterially-produced p26. p26 molarity in reaction mixtures was based on monomeric molecular masses of p26 variants. Heat induced aggregation of citrate synthase was monitored by measuring solution turbidity at 360 nm with a SPECTRAmax *PLUS* spectrophotometer (Molecular Devices) every 2 min for 1 h. Bovine serum albumin (BSA) (Sigma) and immunoglobulin G (IgG) (Sigma) were used at final concentrations of 600 nM or 1.2 μM to evaluate non-specific protection for citrate synthase.

2.11.2 Citrate synthase inactivation

Citrate synthase was incubated in the presence and absence of p26 at 43 °C, small aliquots of the enzyme were withdrawn at various time points during heat denaturation and enzyme activity was measured. Reaction mixtures contained 940 μl of TE (50 mM Tris-HCl, pH 7.5, 2 mM EDTA), 10 μl of 10 mM oxaloacetic acid (OAA) (Sigma), 10 μl of 10 mM 5,5'-Dithiobis (2-nitrobenzoic acid) (DTNB) (Sigma) and 30 μl of 5 mM acetyl-CoA (Sigma). The reaction, initiated by adding 10 μl of 150 nM citrate synthase,

was monitored at 25 °C as an increase in absorption at 412 nm which was determined with a SPECTRAmax *PLUS* spectrophotometer (Molecular Devices).

2.11.3 Insulin aggregation

In 300 µl reaction systems (10 mM phosphate buffer, 100 mM NaCl, pH 7.4) prepared in a 96-well plate, insulin (Sigma) was dissolved to a final concentration of 0.023 mg/ml (4.0 µM), while p26 was added to final concentrations of 0.05 µM, 0.1 µM, 0.2 µM, 0.4 µM, 0.8 µM, 1.6 µM and 3.2 µM. Dithiothreitol (DTT) (Sigma) was added to a final concentration of 20 mM in each well and the aggregation extent was measured at 25 °C by monitoring light scattering at 400 nm in a SPECTRAmax *PLUS* spectrophotometer (Molecular Devices) for 30 min at 2 min intervals.

2.12 Far-UV circular dichroism measurements

Far-UV circular dichroism (CD) spectra were recorded over 180-260 nm in a JASCO J-810/A001960750 spectropolarimeter (Japan Spectroscopic, Tokyo, Japan). At 25 °C, a 0.1 cm path length quartz cuvette containing purified p26 at 0.2 mg/ml in 10 mM NaH_2PO_4, pH 7.1, was employed, and an average of 3 scans was taken for each spectrum with a bandwidth of 2 nm, with all scans corrected for buffer and smoothed to eliminate background noise. Secondary structure parameters were calculated with the CDNN v2.1 deconvolution program (Martin-Luther-Universität Halle-Wittenberg, Germany).

2.13 Intrinsic tryptophan fluorescence and ANS-binding measurements

Purified p26 was diluted in 10 mM NaH_2PO_4, pH 7.1 to a final concentration of 0.06 mg/ml and fluorescence spectra were measured at 25 °C in 96-well plates with a SPECTRAmax GEMINIXS fluorescence spectrophotometer (Molecular Devices). The emission wavelength was set at 340 nm with a 2 nm band pass, and fluorescence

excitation was detected over a range of 250-310 nm to determine the maximal absorbance wavelength. Then, the excitation wavelength was set to 280 nm with a 2 nm band pass, and fluorescence emission was detected over a range of 310-400 nm. Each spectrum was recorded in duplicate using two independent sample preparations.

Two µl of 8.0 mM ANS (Molecular Probes, Eugene, OR) stock prepared in 10 mM NaH_2PO_4, pH 7.1 were added to 198 µl of each protein sample, and the mixtures were incubated for 5 min at either 25 °C or 43 °C. The excitation wavelength was set to 388 nm with a band pass of 8 nm, and the emission wavelength was set to 473 nm with a band pass of 8 nm. Measurements were taken with an AMINCO Bowman series z luminescence spectrometer (AMINCO, Rochester, NY) equipped with a thermostated circular water-bath, and with all conditions chosen to minimize inner filter effects. A standard curve was constructed with a series of ANS concentrations from 0.025 to 1.0 µM for future reference.

2.14 p26 purification from *Artemia* cysts

2.14.1 Preparation of Artemia cell-free extracts

Encysted *Artemia* embryos (cysts) (INVE Aquaculture, Inc., Ogden, UT) were hydrated in distilled water at 4 °C for 3 h, collected on a Buchner funnel, washed with cold distilled water and homogenized with a Retsch motorized mortar and pestle (Brinkman Instruments Canada, Rexdale, ON) in PIPES buffer (100 mM Pipes, 1 mM EGTA, 1 mM $MgCl_2$, pH 6.5). The homogenates were centrifuged at 16,000 × *g* for 10 min at 4 °C and the supernatants were passed through two layers of Miracloth (Calbiochem, La Jolla, CA) before centrifugation at 40,000 × *g* for 30 min at 4 °C. The upper two thirds of each

supernatant was transferred to a fresh tube and re-centrifuged for 20 min. The resulting supernatants were used immediately or frozen at –80 °C.

2.14.2 Purification of IgG from rabbit serum and p26 from Artemia cell-free extracts

Preparation of IgG from anti-p26 serum, coupling of purified IgG to protein A Sepharose™ CL-4B (Amersham Biosciences, Baie d'Urfe, Quebec), and purification of p26 were performed as described previously (Liang *et al.*, 1997b).

2.15 Effect of pH on p26 oligomers

Cell-free extracts of encysted *Artemia* embryos were prepared as just described, except that the PIPES buffer for homogenization was at either pH 6.5 or 7.0. Either immediately after preparation, or following incubation at room temperature for 30 min, supernatants were centrifuged at 200,000 × *g* for 12 h at 4 °C in 10-50% continuous sucrose gradients at the pH used for homogenization. The gradients were fractionated and 10 µl of each sample was electrophoresed in SDS-polyacrylamide gels, blotted to nitrocellulose and probed with anti-p26 antibody as described above.

2.16 Effect of heat shock on p26 oligomers

Ten g of *Artemia* cysts in 500 ml of distilled H_2O were brought to 22 °C, then heated to 50 °C over 1 h with vigorous aeration in a Programmable/Digital Immersion Circulator (VWR, Mississauga, ON). Heat shocked and control cysts, the latter incubated on ice for 30 min, were homogenized separately by hand for 2 min in a chilled mortar and pestle in 35 ml of cold HPC (1 mM $CaCl_2$, 0.05 mM PIPES, 6.4% Hexylene glycol, pH 7.0) (Liang *et al.*, 1997a), followed by one passage in a Dounce homogenizer, filtration through Miracloth, and centrifugation at 2,000 × *g* for 10 min at 4 °C to pellet nuclei. Supernatants were centrifuged at 40,000 × *g* for 30 min at 4 °C, and the upper two thirds

was placed in a fresh tube and re-centrifuged for 20 min. Supernatants were centrifuged in 10-50% continuous sucrose gradients, fractionated and analyzed on western blots with anti-p26 antibody after SDS-PAGE.

The nuclei-containing pellets from above were rinsed twice with 40 ml of HPC, resuspended in 17.5 ml of the same buffer, applied to 25 ml cushions of 75% (v/v) Percoll (Sigma) in 150 mM NaCl, 14 mM $MgCl_2$, 16 mM Tris, pH 7.0, and centrifuged at 16,000 × *g* for 30 min at 4 °C in a Beckman JS-13.1 swinging bucket rotor. Cloudy layers were transferred to fresh tubes, brought to 15 ml with HPC, placed on a 25 ml Percoll cushion and centrifuged as above. Nuclei were recovered, mixed with an equal volume of HPC, centrifuged at 16,000 x *g* for 30 min at 4 °C, and the pellets were suspended in 1.0 ml of HPC. Samples were stained with 0.4% DAPI (Molecular Probes, Eugene, OR) and examined microscopically. Nuclei from control and heat shocked embryos were lysed in treatment buffer, electrophoresed in 12.5% SDS polyacrylamide gels, blotted to nitrocellulose and probed with anti-p26 antibody. For sucrose density gradient centrifugation, extracts were prepared by suspending purified nuclei in 1.0 ml of ice cold extraction buffer (20 mM HEPES/KOH, 2.5 mM $MgCl_2$, 0.42 M NaCl, 25% (v/v) glycerol, 0.2 mM EDTA, 0.5 mM DTT, pH 7.9) containing 1 mM PMSF, 1 μg/ml pepstatin A and 1 μg/ml leupeptin, and sonicating three times for 10 sec using a Branson Sonifier™ 150 at medium setting with intermittent cooling on ice for 30 sec. The sonicated samples were incubated on ice for 30 min, and then centrifuged at 25,000 × *g* for 30 min at 4 °C with supernatants collected. Nuclear extracts were centrifuged in 10-50% continuous sucrose gradients at 200,000 × *g* for 12 h at 4 °C. The gradients were

fractionated and samples were electrophoresed in SDS polyacrylamide gels, blotted to nitrocellulose and probed with antibody to localize p26.

2.17 Modeling of p26 structure

To model the three-dimensional structure of p26, the Swiss-Model Protein Modeling Server (version 36.0003, Biozentrum University Basel, Basel and Swiss institute of Bioinformatics, Geneva, Switzerland and GlaxoSmithKline R&D S.A., Raleigh, NC, US) (Guex and Peitsch, 1997; Guex *et al.*, 1999; Schwede *et al.*, 2003) was applied. Wheat *Ta* Hsp16.9 (ExPDB entry code: 1GME) was used as a template for sequence alignment when the "alignment interface" function of Swiss-Model was employed, with the resulting alignment as a guide for modeling. The structure of p26 was modeled encompassing A2~P158 corresponding to S2~G151 of *Ta* Hsp16.9, and was shown in a monomer, with partial sequence of p26 C-terminal (A159~A192) deleted for alignment optimization. The returned three-dimensional model was improved with the "improve fit" function of Swiss-PdbViewer (version 3.7, GlaxoSmithKline R&D, Geneva, Switzerland) and sent for a second round modeling.

III. Results

3.1 p26 truncations

3.1.1 Generation and cloning of p26 cDNAs

Five truncated p26 cDNAs were generated by site-directed mutagenesis, with pRSET.C-p26-3-6-3 (Liang *et al.*, 1997), a prokaryotic expression vector containing full length p26 cDNA as template. Six different cDNAs were obtained, including p26-full-His, encoding the full length p26 polypeptide; p26-NΔ36-His, residues 1-36 deleted; p26-NΔ60-His, residues 1-60 removed; p26-CΔ40-His, final forty residues eliminated; p26-CΔ10-His, lacking the last ten residues; p26-alpha-His, missing residues 1-60 and 153-192, thereby consisting only of the α-crystallin domain (Fig. 6). All p26 cDNAs generated by site-directed mutagenesis contained, in addition to the p26 coding sequence, an amino-terminal peptide of 13 residues encoded by p26-3-6-3, the His-tag and the Xpress epitope region. The presence of the His-tag is indicated by "–His" in the name of the p26 cDNA or protein. To examine the size of each cloned cDNA, minipreped pRSET.C plasmids as p26 constructs were double digested with *Bam* HI and *Xho* I, and the digestion products were electrophoresed in 1% agarose gels, revealing bands of insert DNAs at the expected positions (not shown). p26 constructs derived from pRSET.C-p26-3-6-3 were used for expression in prokaryotic systems. The p26 cDNAs recovered from previously used storage vector pCRII (Crack *et al.*, 2002) were subcloned into pSecCMV for expression in COS-1 cells. p26-full, p26-NΔ60 and p26-alpha were also subcloned into pcDNA4/His.A for expression as His-tagged fusion proteins. All cloned p26 cDNA fragments were sized by electrophoresis in 1% agarose gels after restriction digestion of recombinant plasmids, with PCR fidelity confirmed by DNA sequencing (not shown).

Figure 6. Schematic representation and sequence of p26 cDNAs

a, truncations of p26 cDNAs generated by site-directed mutagenesis were cloned in the prokaryotic expression vector pRSET.C and the eukaryotic expression vectors pSecCMV and pcDNA4/His.A. The primers used for site-directed mutagenesis are listed in Table 1. The box labeled 6xHis is a His-tag-encoding sequence present in the vectors pRSET.C and pcDNA4/His.A; b, amino acid sequence of p26 (NCBI accession number AAB87967). The amino acid residues removed to generate p26-NΔ60 and p26-CΔ40 are shaded and those for p26-NΔ36 and p26-CΔ10 are shaded and bold.

a

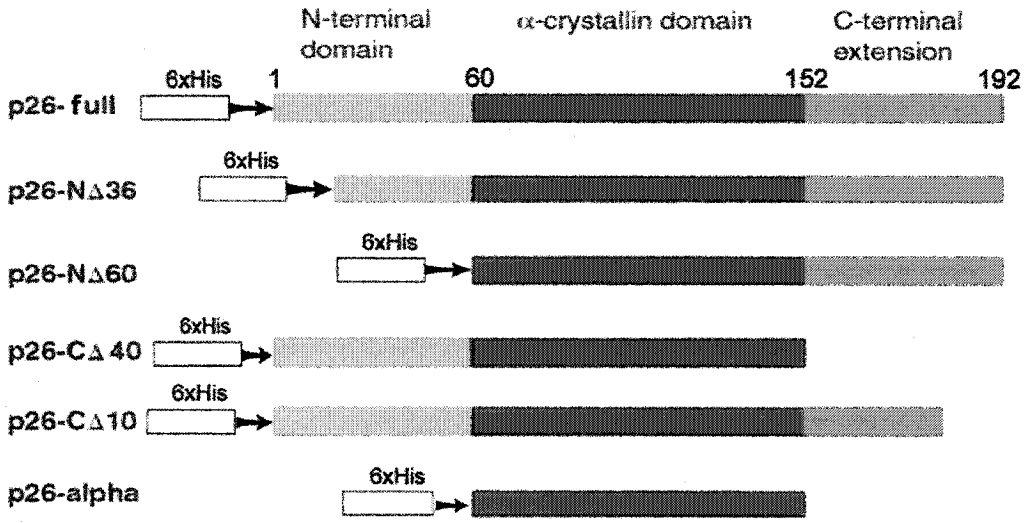

b

MALNPWYGGFGGMTDPWSDPFGFGGFGGGMDLDIDRPFRRRMMRRGPDTSRALKELATPG

SLRDTADEFQVQLDVGHFLPNEITVKTTDDDILVHGKHDERSDEYGHVQREFRRRYRLPEHVKPE

SVSSTLSSDGVLTIHAPKTALSSPTERIVPITPAPAVGRIEGGTTGTTTGSTASSTPARTTRSGGAA

Figure 6

3.1.2 p26 expression in bacteria

IPTG induction of transformed *E. coli* BL21(DE3)pLysS yielded polypeptides on western blots of the appropriate sizes that reacted with Omni-probe, although bands corresponding to p26 were not readily visible in Coomassie blue stained gels (Figs. 7a, b). With the exception of p26-NΔ60-His and p26-alpha-His, all of the polypeptides were recognized by anti-p26 antibody (not shown). Subsequent to purification on TALON™ affinity columns, single bands of the expected size appeared on Coomassie blue stained gels (Fig. 7c). These polypeptides reacted strongly with Omni-probe (Fig. 7d) indicating they were His-tagged p26, although purified p26-NΔ60-His and p26-alpha-His again failed to react with anti-p26 antibody. Protein bands were not detected on blots containing extract from *E. coli* transformed with vector lacking p26 cDNA (Figs. 7a, b, lane 7).

3.1.3 p26 oligomer formation

The molecular mass of oligomers assembled from purified p26-full-His synthesized in *E. coli* BL21(DE3)pLysS ranged from 25.8 kDa to 600 kDa, with the peak at about 150 kDa, or 6 monomers per oligomer (Fig. 8, Table 4). The oligomers assembled with full length p26 were larger than those obtained with truncated proteins, although oligomers of p26-CΔ10-His were similar in mass. At the other extreme, p26-NΔ60-His and p26-alpha-His migrated predominately as monomers and dimers, although larger complexes occurred. Oligomers assembled from other p26 variants were intermediate in mass to those just described.

Figure 7. Purification of p26 synthesized in *E. coli*

Cell free extracts from transformed *E. coli* induced with IPTG were electrophoresed in SDS polyacrylamide gels and either stained with Coomassie blue (a) or blotted to nitrocellulose and reacted with Omni-probe (b). Proteins purified by affinity chromatography were electrophoresed in SDS polyacrylamide gels and either stained with Coomassie blue (c), or blotted to nitrocellulose and reacted with Omni-probe (d). The lanes contained: 1, p26-NΔ36-His; 2, p26-NΔ60-His; 3, p26-alpha-His; 4, p26-CΔ40-His; 5, p26-CΔ10-His; 6, p26-full-His; 7, vector lacking p26 cDNA. All lanes received 10 μl of sample. M, molecular mass markers of 97, 66, 45, 31, 21 and 14 kDa.

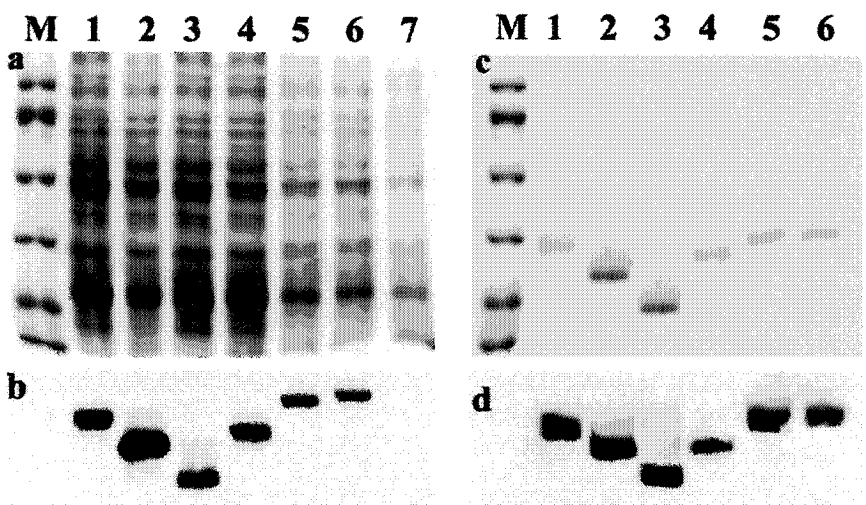

Figure 7

Figure 8. Oligomer formation by purified p26

Bacterially produced p26 purified to apparent homogeneity by affinity chromatography was centrifuged at 200,000 x *g* for 12 h at 4 °C on 10-50% sucrose gradients. The gradients were fractionated and the A_{280} of each fraction was plotted against fraction number. The top of each gradient is to the right and fractions are numbered across the bottom. The molecular mass markers, alpha-lactalbumin, 14.2 kDa; carbonic anhydrase, 29 kDa; bovine serum albumin, 66 kDa; alcohol dehydrogenase, 150 kDa; apoferritin, 443 kDa; and thyroglobulin, 669 kDa are indicated by numbered arrows.

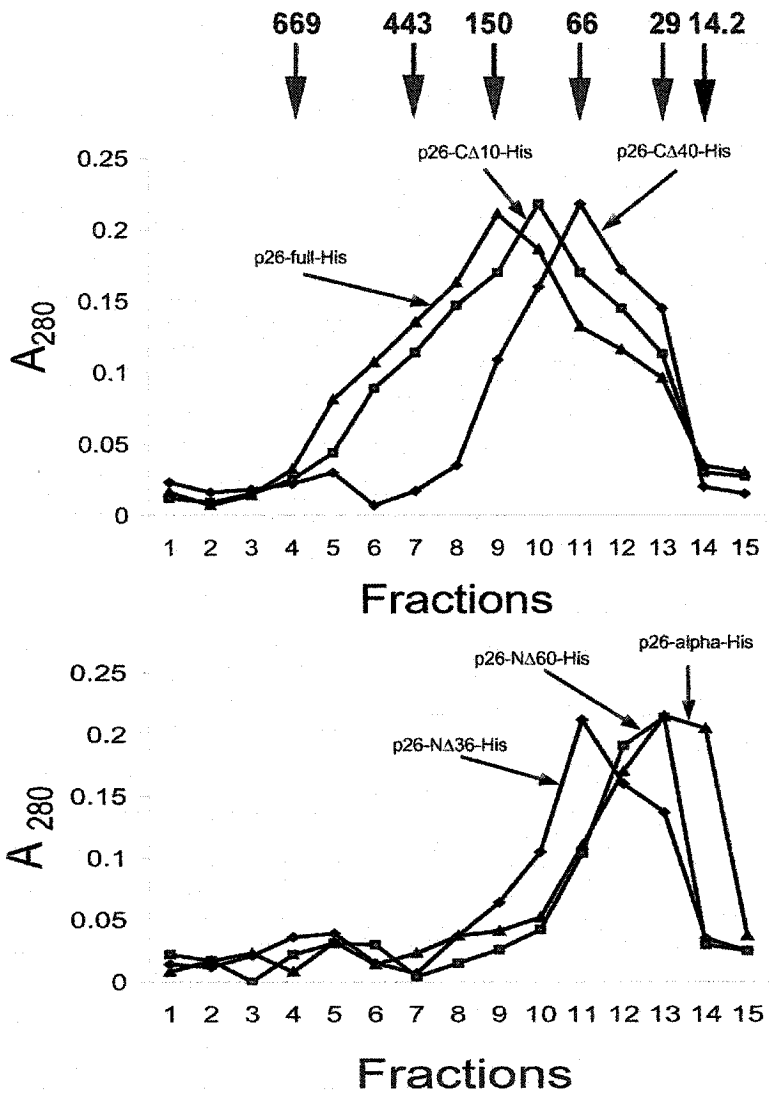
669
443
150
66
29
14.2
p26-CΔ10-His
p26-CΔ40-His
p26-full-His
A280
0.25
0.2
0.15
0.1
0.05
0
1 2 3 4 5 6 7 8 9 10 11 12 13 14 15
Fractions
p26-NΔ60-His
p26-alpha-His
p26-NΔ36-His
A 280
0.25
0.2
0.15
0.1
0.05
0
1 2 3 4 5 6 7 8 9 10 11 12 13 14 15
Fractions

Figure 8

Table 4. Oligomerization of p26 purified from *E. coli* BL21(DE3)pLysS

p26 variant	Monomer mass (kDa)	Oligomer Mass		Monomer number (peak)
		range (kDa)	peak (kDa)	
p26-full-His	25.8	26-600	150	6
p26-NΔ36-His	22.0	22-110	66	3
p26-NΔ60-His	19.2	19-58	19-38	1-2
p26-alpha-His	15.5	16-62	16-32	1-2
p26-CΔ40-His	22.1	22-220	66	3
p26-CΔ10-His	24.9	25-500	125	5

The molecular mass of oligomers produced by p26 purified from transformed *E. coli* BL21(DE3)pLysS was determined by reading the A_{280} of samples obtained by fractionation of sucrose density gradients. Monomer mass refers to the molecular mass of p26 polypeptides. Oligomer mass range represents the smallest to largest oligomers observed while oligomer mass peak refers to the mass of the most prevalent oligomer. Monomer number peak refers to the number of subunits in the most prevalent oligomer.

3.1.4 Chaperone activity

Purified p26-full-His possessed the greatest chaperone activity and p26-alpha-His the least, as determined by heat-induced denaturation of citrate synthase, although all variants provided some protection (Fig. 9). At a chaperone to target molar ratio of 4:1 (p26 monomer to citrate synthase dimer), or 1:1.5 if the peak oligomer size of p26-full-His is used for comparison, citrate synthase denaturation was inhibited almost completely after 1 h at 43 °C (Fig. 9a). At a 1:4 molar ratio of p26-full-His to citrate synthase, or 1:24 (oligomer to dimer), purified p26 reduced the heat-induced turbidity increase by approximately 25% (Fig. 9e). In contrast, p26-alpha-His almost completely lost chaperone activity even at molar ratios of 4:1 (Fig. 9). p26-NΔ60-His was marginally better than p26-alpha-His as a chaperone, followed by p26-NΔ36-His and p26-CΔ40-His which were similar to one another. p26-CΔ10-His approached p26-full-His in chaperone potency especially at high concentrations. In contrast, BSA and IgG at 600 nM provided almost no protection at all upon heating of citrate synthase (Fig. 9f).

3.1.5 Synthesis and oligomerization of p26 in transfected mammalian cells

Except for p26-NΔ60 and p26-alpha, which reacted exclusively with Omni-probe, protein extracts from COS-1 cells transfected with p26 cDNA-containing expression vectors yielded polypeptides of the expected size on western blots when probed with anti-p26 antibody (Fig. 10). Neither primary antibody gave protein bands on blots with extracts from COS-1 cells transfected with vectors lacking p26 cDNA (not shown). Full length p26 synthesized in COS-1 cells produced oligomers as large as 512 kDa and composed of up to 21 monomers, with monomer number essentially the same in the presence and absence of His-tag (Figs. 11a, b). Oligomers assembled with p26-CΔ10

Figure 9. p26 chaperone activity

Bacterially produced p26 purified to apparent homogeneity was heated at 43 °C for 1 h with 150 nm citrate synthase and solution turbidity was measured at A_{360}. p26 was at final concentrations of: a, 600 nM; b, 300 nM; c, 150 nM; d, 75 nM; e, 37.5 nM. The curves are: 1, No p26; 2, p26-alpha-His; 3, p26-NΔ60-His; 4, p26-NΔ36-His; 5, p26-CΔ40-His; 6, p26-CΔ10-His; 7, p26-full-His and they occupy the same relative positions in panels a-e. Panel f contains 150 nM citrate synthase incubated in the absence of other proteins (1) but with either 600 nM BSA (2) or 600 nM IgG (3).

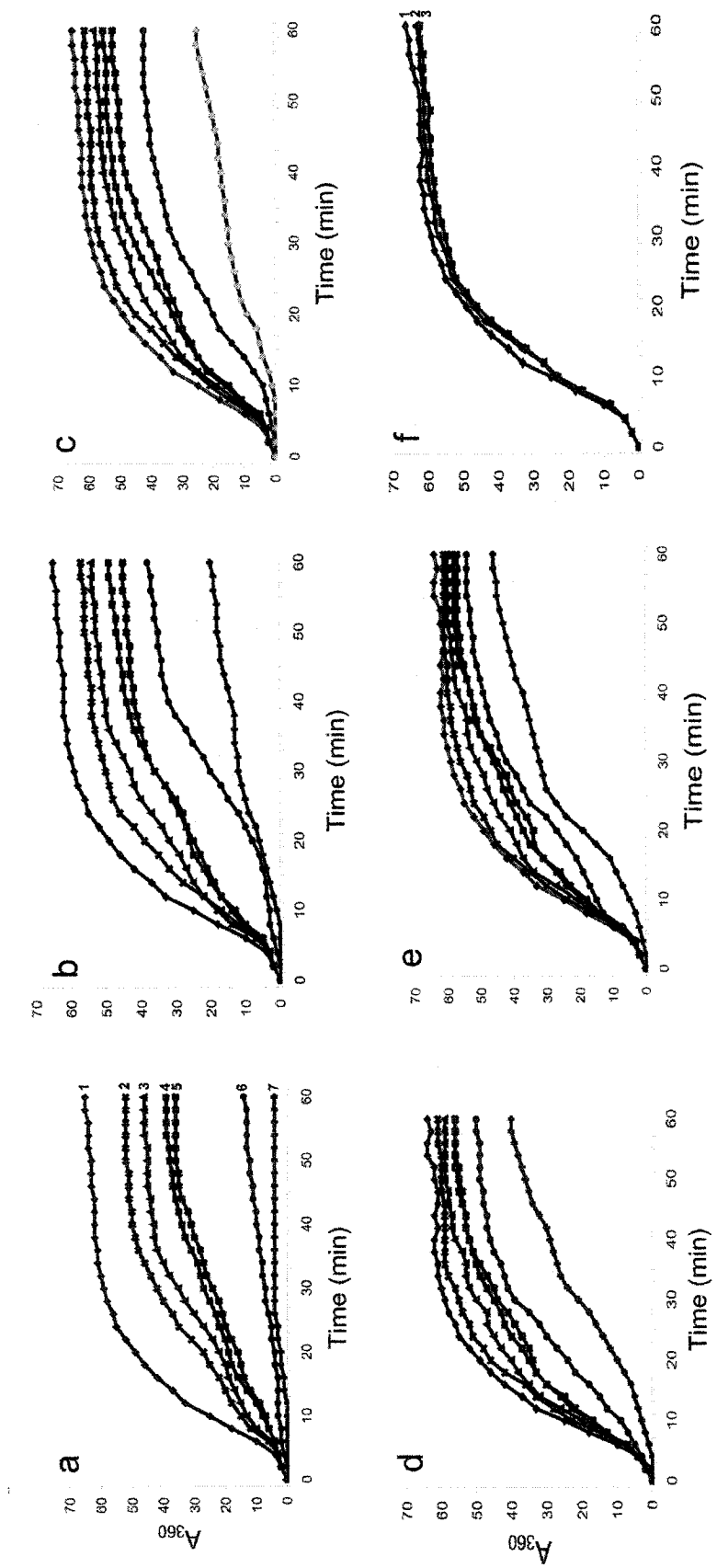

Figure 9

Figure 10. p26 synthesis in transfected COS-1 cells

Extracts prepared from COS-1 cells transfected with the pSecCMV eukaryotic expression vector containing p26 cDNAs were electrophoresed in SDS polyacrylamide gels and either stained with Coomassie blue (a) or transferred to nitrocellulose and stained with anti-p26 antibody followed by HRP-conjugated goat anti-rabbit IgG antibody (b). Each lane received 10 μl of extract from cells transfected with 1, p26-NΔ36; 2, p26-NΔ60; 3, p26-alpha; 4, p26-CΔ40; 5, p26-CΔ10; 6, p26-full. M, molecular mass markers of 97, 66, 45, 31, 21 and 14 kDa. Western blots containing extracts from COS-1 cells transfected with the pcDNA4/His.A expression vector containing p26 cDNAs and prepared as just described were stained with either anti-p26 antibody followed by HRP-conjugated goat anti-rabbit IgG antibody (c) or Omni-probe followed by HRP-conjugated goat anti-mouse IgG (d). Each lane in c and d received 10 μl of extract from cells transfected with 1, p26-full-His; 2, p26-NΔ60-His; p26-alpha-His.

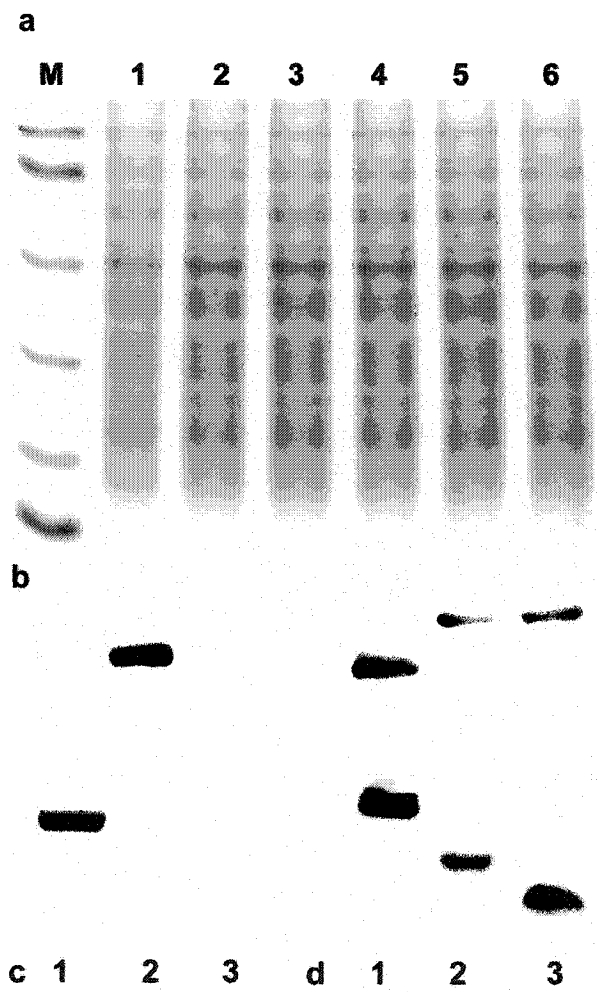

Figure 10

Figure 11. p26 oligomer formation in transfected COS-1 cells

Extracts prepared from COS-1 cells transiently transfected with p26-containing vectors were centrifuged in 10-50% sucrose gradients and 15 µl samples from each fraction were electrophoresed in SDS polyacrylamide gels, transferred to nitrocellulose, and probed with either anti-p26 antibody followed by HRP-conjugated goat anti-rabbit IgG (a, c, d, e) or Omni-probe followed by HRP-conjugated goat anti-mouse IgG (b, f, g).The gradients contained, a, p26-full; b, p26-full-His; c, p26-CΔ10; d, p26-CΔ40; e, p26-NΔ36; f, p26-NΔ60-His; g, p26-alpha-His. The top of each gradient is to the right and fractions are numbered across the top. The positions of molecular mass markers, alpha-lactalbumin, 14.2 kDa; carbonic anhydrase, 29 kDa; bovine serum albumin, 66 kDa; alcohol dehydrogenase, 150 kDa; apoferritin, 443 kDa; and thyroglobulin, 669 kDa are indicated by numbered arrows.

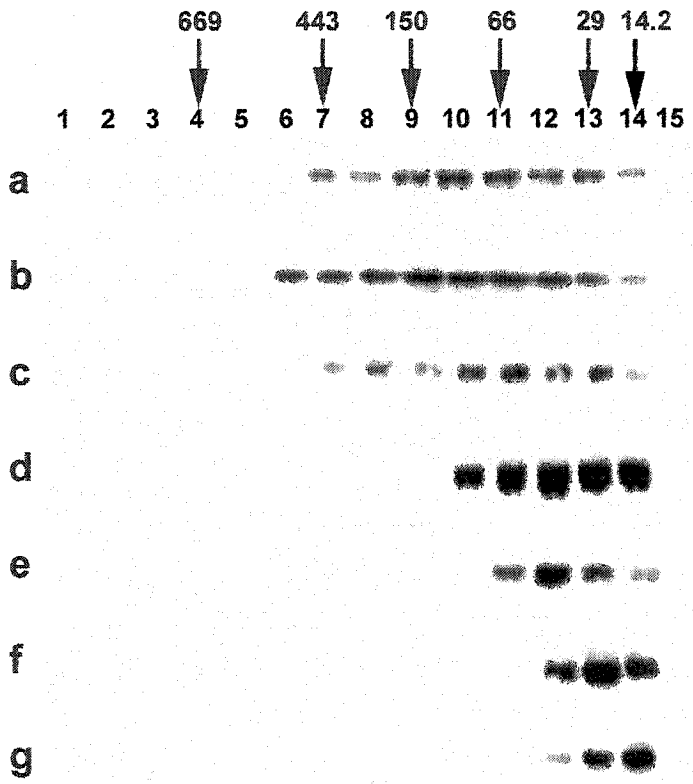

Figure 11

were close in size to those produced from full length p26 (Fig. 11c), but removal of the complete C-terminal extension gave oligomers of a narrower size range and smaller mass (Fig. 11d). Oligomer mass became progressively smaller upon sequential removal of the N-terminus (Figs. 11e, f) with polypeptides encoded by p26-NΔ60-His present as monomers and dimers, as was true for p26-alpha-His (Fig. 11g), although the latter was more enriched in monomers. The properties of p26 oligomers produced in COS-1 cells are summarized in Table 5.

3.1.6 Intracellular localization of truncated p26 in COS-1 cells

In order to monitor p26 synthesis, transiently transfected COS-1 cells were stained with anti-p26 antibody or Omni-probe and propidium iodide, revealing that polypeptides encoded by p26-full and p26-full-His (Figs. 12a, b) and the C-terminal truncations, p26-CΔ40 (Fig. 12c) and p26-CΔ10 (Fig. 12d), localized predominantly to the cytoplasm. In contrast, upon N-terminal truncation p26 occurred in cytoplasm and nuclei, the latter shown by yellow staining (overlapping of red and green). p26-NΔ36 encoded polypeptides entered the nuclei of only some transfected cells (Figs. 12e, f), but polypeptides p26-NΔ60/p26-NΔ60-His lacking the N-terminus (Figs. 12g, h), or p26-alpha/p26-alpha-His composed of the α-crystallin domain (Figs. 12i, j), resided in the nuclei of all transfected cells, indicating that the His-tag had no effect on p26 localization. The results, in concert with analysis of oligomer formation, suggested that oligomer disassembly is responsible for p26 movement into nuclei of COS-1 cells, and by extrapolation, the nuclei of encysted *Artemia* embryos.

Table 5. Oligomerization of p26 synthesized in transfected COS-1 cells

p26 variant	Monomer mass (kDa)	Oligomer Mass		Monomer number peak
		range (kDa)	peak (kDa)	
p26-full	20.8	21-437	104	5
p26-full-His	24.4	24-512	146	6
p26-CΔ10	19.9	20-438	100	5
p26-CΔ40	17.1	17-103	51	3
p26-NΔ36	17.0	17-68	51	3
p26-NΔ60-His	17.7	18-53	18-35	1-2
p26-alpha-His	14.0	14-56	14-28	1-2

The molecular mass of p26 oligomers was determined by immunoprobing of samples electrophoresed in SDS polyacrylamide gels and transferred to western blots after sucrose gradient centrifugation. Monomer mass refers to the molecular mass of p26 polypeptides. Oligomer mass range represents the smallest to largest oligomers observed while oligomer mass peak refers to the mass of the most prevalent oligomer. Monomer number peak refers to the number of subunits in the most prevalent oligomer.

Figure 12. p26 intracellular localization in transfected COS-1 cells

COS-1 cells transfected with the p26 cDNA-containing vector pSecCMV were incubated with antibody to p26 followed by FITC-conjugated goat anti-rabbit IgG antibody (green) (a, c, d, e, f). Cells transfected with the p26 cDNA-containing vector pcDNA4/His.A were exposed to anti-p26 antibody followed by FITC-conjugated goat anti-rabbit IgG (green) (g,i) or to Omni-probe followed by FITC-conjugated goat anti-mouse IgG (green) (b, h, j). Nuclei were stained with propidium iodide (red) and samples were examined by confocal microscopy. a, p26-full; b, p26-full-His; c, p26-CΔ40; d, p26-CΔ10; e and f, p26-NΔ36; g, p26-NΔ60; h, p26-NΔ60-His; i, p26-alpha; j, p26-alpha-His. The scale bar represents 50 μm and all figures are the same magnification.

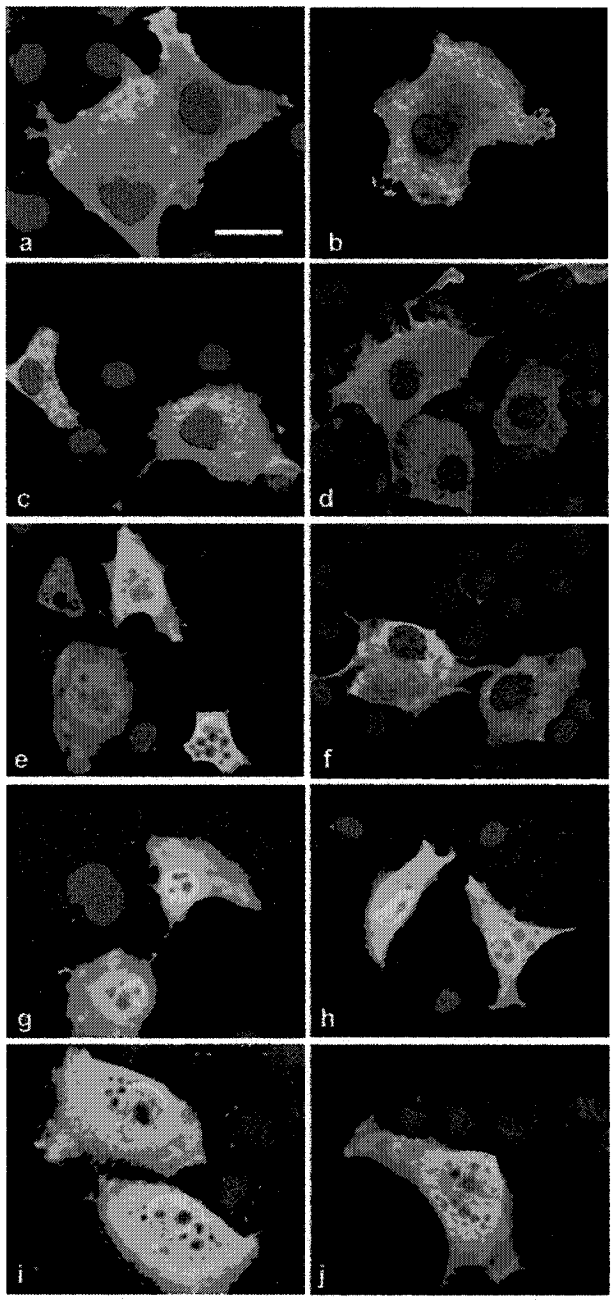

Figure 12

3.1.7 Effects of pH and heat shock on oligomer size of p26 from *Artemia* embryos

p26 moves into the nuclei of *Artemia* embryos upon exposure to reduced pH *in vitro* and upon heat shock *in vivo* by an unknown mechanism that, as suggested by the previous results, entails oligomer mass reduction. However, the p26 oligomers obtained from *Artemia* cysts homogenized at either pH 6.5 or 7.0 were identical in mass, whether or not they were incubated for 30 min at RT before gradient centrifugation (Fig. 13a-d). p26 migrated into the nuclei of heat shocked *Artemia* embryos under the conditions used in this work (Figs. 14a, b), but the size of p26 oligomers in extracts from cysts (Figs. 14c, d) and nuclei (Figs. 14e, f) remained constantly similar. The p26 in nuclear extracts tended to smear upon electrophoresis and blotting, probably due to the presence of DNA.

3.2 Single amino acid substitutions of the p26 α-crystallin domain

3.2.1 Mutation and cloning of p26 cDNAs

Four single amino acid substitutions in the α-crystallin domain of p26, namely R110G, F112R, R114A and Y116D, were generated by site-directed mutagenesis using the template pRSET.C-p26-3-6-3 (Liang *et al.*, 1997). The mutated cDNAs, along with wild type (WT) cDNA were then cloned into the eukaryotic expression vector pcDNA4/TO/myc-His.A (in this thesis, WT is equivalent to full length). The p26 cDNA-containing pcDNA4/TO/myc-His.A plasmids were digested with *Bam* HI and *Xba* I, with the inserts ligated into the His-tag containing prokaryotic expression vector pPROTet.E233. The sizes of insert cDNAs in eukaryotic and prokaryotic expression constructs were examined by restriction digestion, and the identity of each cDNA was confirmed by automated DNA sequencing (not shown).

Figure 13. p26 oligomer size is unaffected by pH

Protein extracts obtained from *Artemia* cysts prepared at either pH 7.0 (a, c) or pH 6.5 (b, d), were centrifuged in 10-50% continuous sucrose gradients either immediately after preparation (a, b), or following incubation at room temperature for 30 min (c, d). Fifteen μl fractions from each gradient were electrophoresed in 12.5% SDS polyacrylamide gels, transferred to nitrocellulose, and probed with anti-p26 antibody followed by HRP-conjugated goat anti-rabbit IgG. The top of each gradient is to the right and fractions are numbered across the top. The positions of molecular mass markers, alpha-lactalbumin, 14.2 kDa; carbonic anhydrase, 29 kDa; bovine serum albumin, 66 kDa; alcohol dehydrogenase, 150 kDa; apoferritin, 443 kDa; and thyroglobulin, 669 kDa are indicated by numbered arrows.

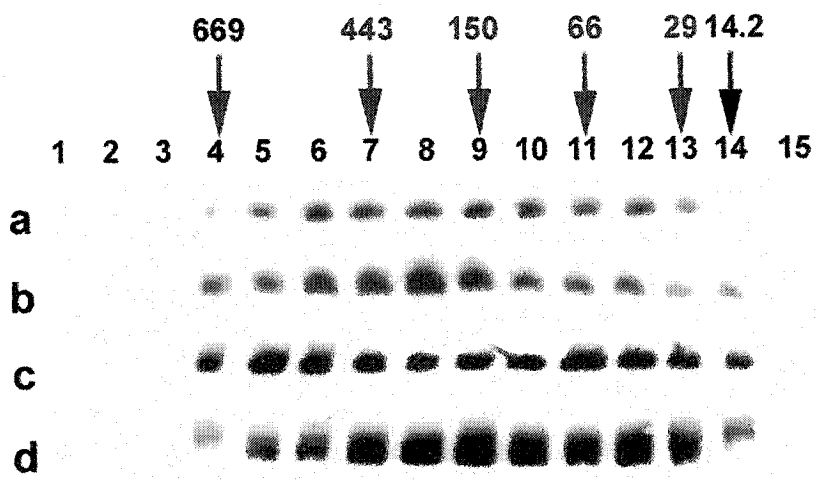

Figure 13

Figure 14. p26 oligomer size is unaffected by heat shock

Extracts prepared from heat shocked *Artemia* cysts and their nuclei were electrophoresed in SDS polyacrylamide gels and either stained with Coomassie blue (a) or blotted to nitrocellulose and stained with anti-p26 antibody (b). The lanes contained: 1, total cyst extract, heat shocked; 2, total cyst extract, control; 3, nuclear extract, heat shocked; 4, nuclear extract, control. Total extract from heated (c) and control (d) cysts and nuclear extracts from heated (e) and control (f) cysts were centrifuged in continuous 10-50% sucrose gradients and 15 µl fractions from each gradient were electrophoresed in SDS polyacrylamide gels, transferred to nitrocellulose, and probed with anti-p26 antibody followed by HRP-conjugated goat anti-rabbit IgG. The top of each gradient is to the right and fractions are numbered across the top. The positions of molecular mass markers, alpha-lactalbumin, 14.2 kDa; carbonic anhydrase, 29 kDa; bovine serum albumin, 66 kDa; alcohol dehydrogenase, 150 kDa; apoferritin, 443 kDa; and thyroglobulin, 669 kDa are indicated by numbered arrows.

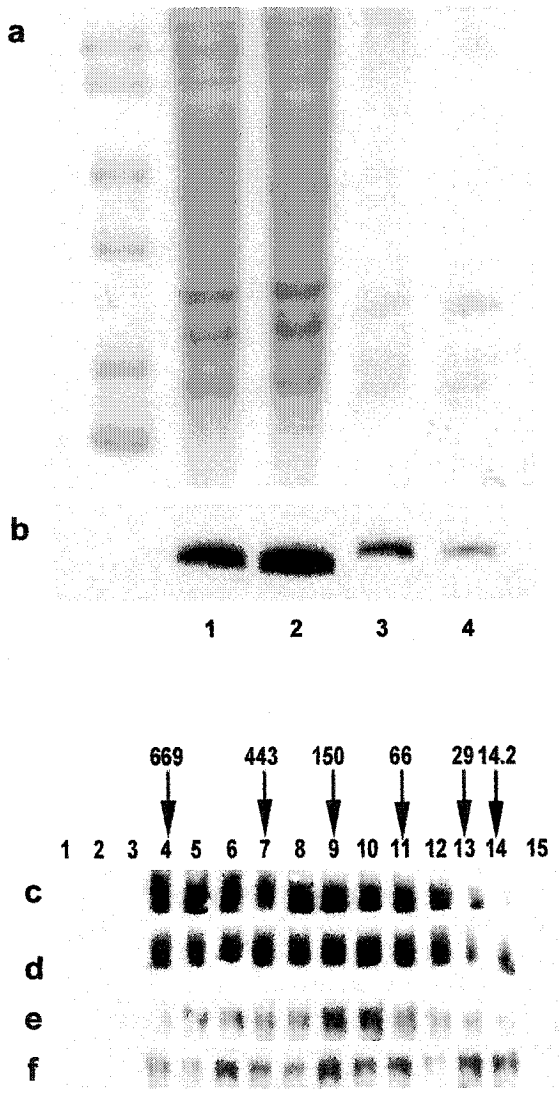

Figure 14

3.2.2 Purification of p26 produced in bacteria

The pPROTet.E233 constructs were transformed into *E. coli* strain BL21PRO, and p26 expression was induced with anhydrotetracycline (aTc). After electrophoresis, light bands corresponding in expected size to p26 variants were visible in Coomassie blue stained SDS polyacrylamide gels, and these polypeptides reacted with antibody to p26 (Figs. 15a, b). Extract from *E. coli* transformed with vector without p26 cDNA lacked anti-p26 antibody reactive polypeptides (Figs. 15a, b, lane 6). After purification on TALON™ affinity columns, single bands of the expected size were seen on Coomassie blue stained gels (Fig. 15c) and these polypeptides reacted strongly with antibody to p26 (Fig. 15d). Each fusion protein of recombinant p26 expressed in *E. coli* BL21PRO contained, in addition to the p26 sequence (20.8 kDa), a 6×HN-tag followed by 14 amino acids prior to the multiple cloning site (3.2 kDa) and an amino-terminal peptide of 13 residues encoded by p26-3-6-3 but not part of the p26 sequence (1.5 kDa).

3.2.3 Oligomer formation by bacterially produced p26

Oligomers formed by each p26 mutant were similar in mass before and after purification from bacterial extracts (Figs. 16a, b). The molecular mass of oligomers assembled from WT p26 ranged from approximately 29 kDa to 669 kDa and this range was greater than for any p26 containing single amino acid substitutions. Among the four mutants, the range in oligomer mass was greatest for R114A, narrowest for F112R, and intermediate for R110G and Y116D. WT p26 exhibited the largest oligomers at 669 kDa, whereas for the modified p26 variants, R114A had the largest oligomers, although they were still smaller than for WT, and the maximum oligomer mass was smallest for F112R. These results are summarized in Table 6, with the median oligomer mass and monomer

Figure 15. Purification of p26 synthesized in *E. coli* BL21PRO

Cell free extracts from transformed *E. coli* BL21PRO induced with aTc were electrophoresed in SDS polyacrylamide gels and either stained with Coomassie blue (a) or blotted to nitrocellulose and reacted with antibody to p26 (b). Proteins purified by affinity chromatography were electrophoresed in SDS polyacrylamide gels and either stained with Coomassie blue (c), or blotted to nitrocellulose and reacted with antibody to p26 (d). The lanes contained: 1, R110G; 2, F112R; 3, R114A; 4, Y116D; 5, WT; 6, vector lacking p26 cDNA. Arrow, p26. All lanes received 10 µl of sample. M, molecular mass markers of 97, 66, 45, 31, 21 and 14 kDa.

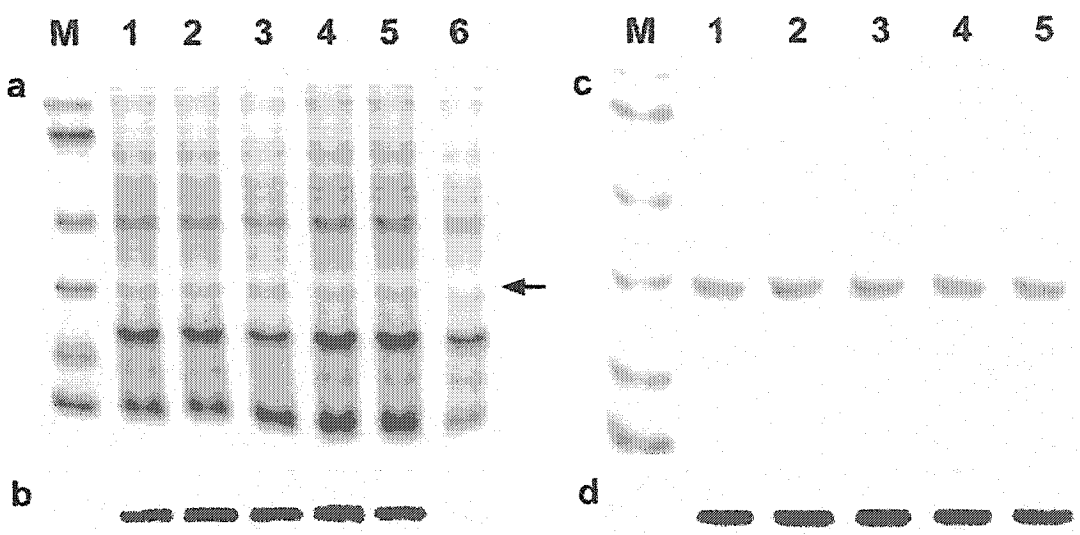

Figure 15

Figure 16. Oligomer formation by p26 synthesized in *E. coli* BL21PRO

Bacterially produced p26 either before (a) or after purification to apparent homogeneity by affinity chromatography (b) was centrifuged at 200,000 x *g* for 12 h at 4 °C on 10-50% continuous sucrose gradients. The gradients were fractionated and 15-µl samples from each fraction were electrophoresed in SDS polyacrylamide gels, blotted to nitrocellulose and reacted with antibody to p26 followed by HRP-conjugated goat anti-rabbit IgG. The top of each gradient is to the right and fractions are numbered across the top. The molecular mass markers, alpha-lactalbumin, 14.2 kDa; carbonic anhydrase, 29 kDa; bovine serum albumin, 66 kDa; alcohol dehydrogenase, 150 kDa; apoferritin, 443 kDa; and thyroglobulin, 669 kDa are indicated by numbered arrows.

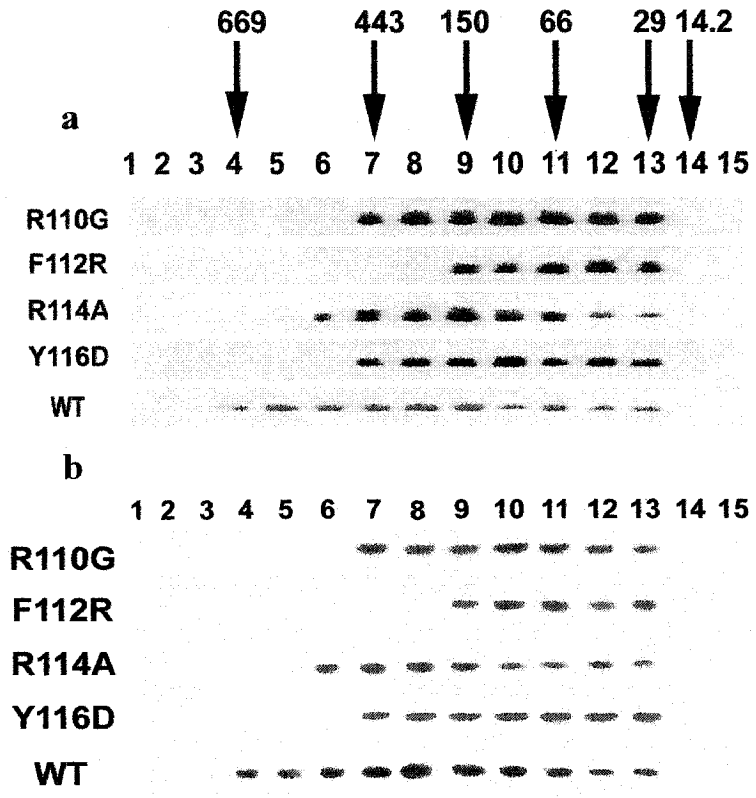
669
443
150
66
29
14.2
a
1 2 3 4 5 6 7 8 9 10 11 12 13 14 15
R110G
F112R
R114A
Y116D
WT
b
1 2 3 4 5 6 7 8 9 10 11 12 13 14 15
R110G
F112R
R114A
Y116D
WT

Figure 16

Table 6. Oligomerization of p26 produced in *E. coli* BL21PRO

p26 variant	Monomer mass (kDa)	Oligomer Mass		Median monomer number
		Range (kDa)	Median (kDa)	
R110G	25.4	29-443	100	4
F112R	25.5	29-150	75	3
R114A	25.4	29-500	125	5
Y116D	25.5	29-443	100	4
WT	25.5	29-669	200	8

The molecular mass of p26 oligomers produced by transformed *E. coli* BL21PRO was determined by sucrose density gradient centrifugation. Monomer mass refers to the molecular mass of p26 polypeptides. Oligomer mass range represents the smallest to largest oligomers observed while median oligomer mass refers to the mass of the median size oligomer. Median monomer number refers to the number of subunits in the median size oligomer.

number given for each p26 variant. R114A is unusual within the latter comparison in that there was a greater number of oligomers above the median position than below, thus the median values may represent underestimations.

3.2.4 p26 induced bacterial thermotolerance

E. coli BL21PRO expressing all variants of recombinant p26 examined in this study were significantly more thermotolerant than bacteria containing only the pPROTet.E233 vector which did not survive heat shock, and of these, bacteria producing WT p26 were the most resistant to heat stress (Fig. 17). The levels of thermotolerance induced by expression of R110G, F112R and Y116D were similar to each other ($P > 0.05$) and significantly higher than the thermotolerance conferred by R114A ($P < 0.05$).

3.2.5 Chaperone activity of WT and modified p26

3.2.5.1 p26 protects citrate synthase against heat-induced aggregation

Purified WT p26 possessed the greatest chaperone activity and R114A the least, as determined by heat-induced aggregation of citrate synthase, although all variants provided protection (Fig. 18). At final p26 concentrations of 1200 nM and 600 nM when chaperone to target molar ratio is 8:1 and 4:1 respectively (p26 monomer to citrate synthase dimer), or 1:1 and 0.5:1 respectively if the median oligomer size of WT p26 is used for comparison, citrate synthase aggregation was inhibited almost completely for 1 h at 43 °C (Figs. 18a, b). At a final p26 concentration of 37.5 nM, wherein the molar ratio of WT p26 to citrate synthase is 1:4, or 1:32 if the median oligomer size of p26 is used for comparison, purified WT p26 reduced heat-induced turbidity by 46% (Fig. 18f). At each concentration from 37.5 nM to 1200 nM, mutants R110G, F112R and Y116D possessed similar levels of chaperone activity, significantly better than R114A, but less

Figure 17. Thermotolerance of transformed bacteria

Transformed *E. coli* BL21PRO were incubated at 54 °C for periods up to 1 h, diluted and plated in duplicate on LB agar followed by incubation at 37 °C for 16 h. Colonies were counted and the Log_{10} values of colony forming units (CFU) per ml were plotted against the length of heat shock in min. Bacteria containing the pPROTet.E233 vector lacking a p26 cDNA insert did not survive the 60 min heat shock. Results are averaged from three independent experiments.

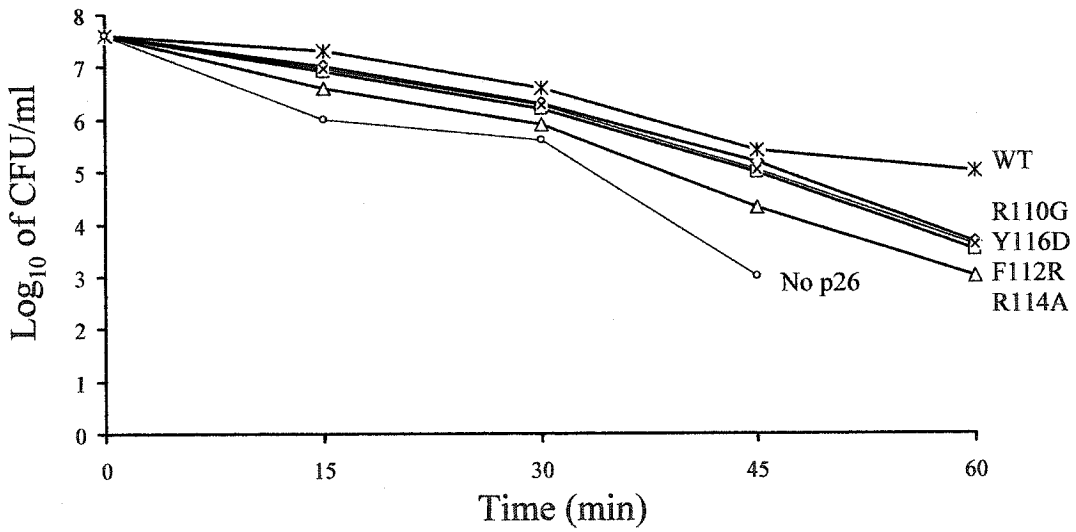
8
7
6
5
4
3
2
1
0
Log10 of CFU/ml
0
15
30
45
60
Time (min)
WT
R110G
Y116D
F112R
R114A
No p26

Figure 17

Figure 18. p26 chaperone activity on citrate synthase

Bacterially produced p26 purified to apparent homogeneity was heated at 43 °C for 1 h with 150 nM citrate synthase, and solution turbidity was measured at 360 nm. The final concentrations of p26 based on monomer molecular mass were: a, 1200 nM; b, 600 nM; c, 300 nM; d, 150 nM; e, 75 nM; f, 37.5 nM. The curves are: 1, No p26; 2, R114A; 3, F112R; 4, Y116D; 5, R110G; 6, WT, and they occupy the same relative positions in a-f.

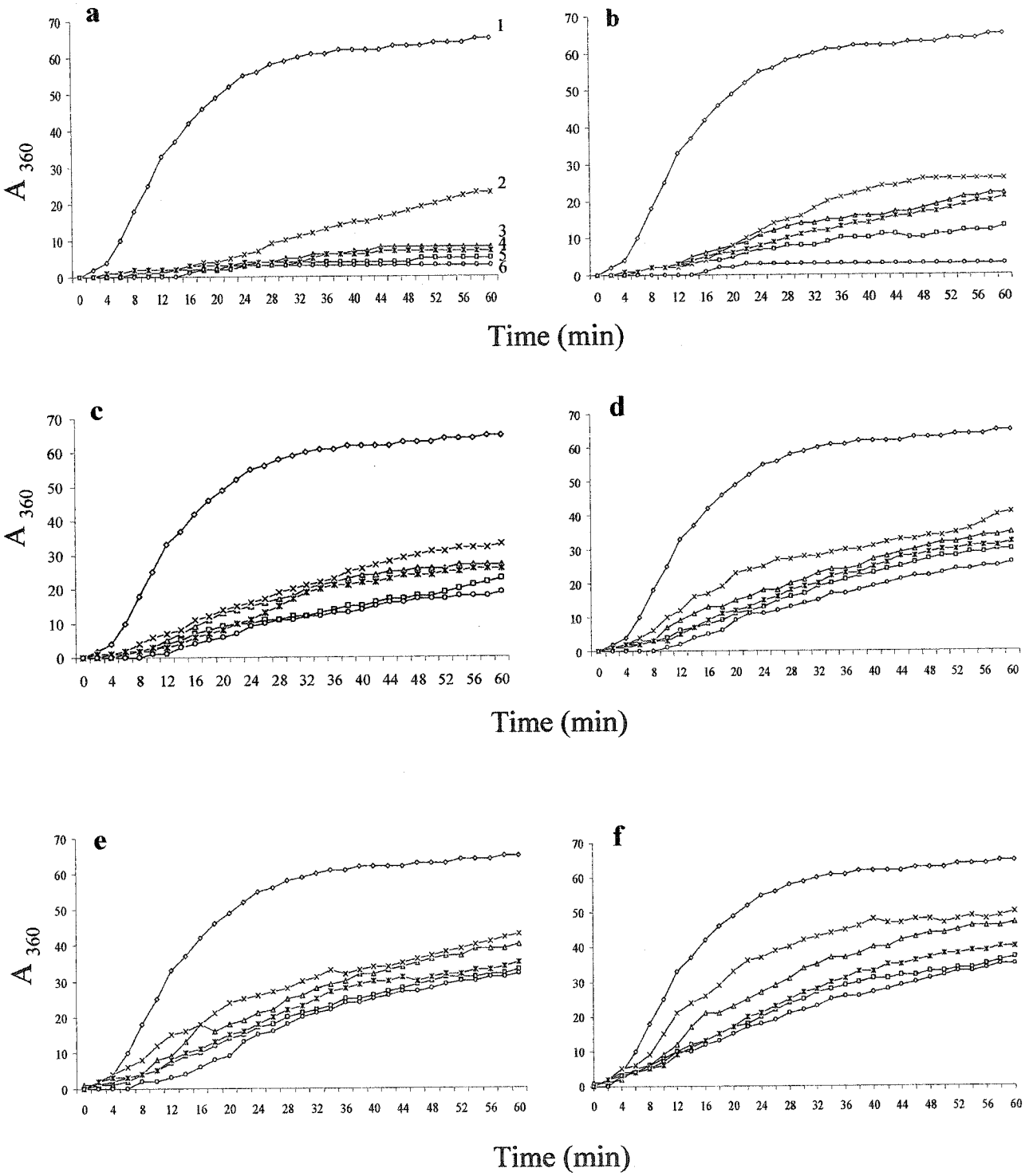

Figure 18

than WT (Fig. 18a-f). R110G, F112R and Y116D almost completely inhibited citrate synthase aggregation at 1200 nM (Fig. 18a), while R114A only reached this chaperone level at 2400 nM (not shown), twice the concentration required for other p26 variants. However, R114A still offered a significant amount of protection to citrate synthase even at lower ratios to substrate. BSA and IgG at 1200 nM provided almost no protection upon heating of citrate synthase when compared to the solution containing only enzyme (not shown).

3.2.5.2 p26 prevents citrate synthase from heat-induced inactivation

WT p26 protected citrate synthase against heat induced inactivation more effectively than any of the modified variants (Fig. 19). Of the tested samples, R114A exhibited the least protection at each chaperone concentration, this in contrast to R110G, F112R and Y116D which were more effective although not as good as WT. When the concentration of WT p26 reached 1200 nM, only limited enzyme inactivation occurred, with the detected enzyme activity almost the same as those determined for samples containing citrate synthase before heat shock (not shown).

3.2.5.3 p26 protects insulin against DTT-induced aggregation

WT p26 was the most effective in preventing DTT-induced insulin aggregation (Fig. 20), with R114A the least effective, and R110G, F112R and Y116D moderately better than R114A. At 0.1 μM, WT p26 inhibited insulin aggregation by 39% after 30 min, and the aggregation was almost completely suppressed at 1.6 μM. At this concentration, the molar ratio of chaperone to target is 0.4:1 (monomer to monomer), or 0.05:1 if the median oligomer size of WT p26 is used for comparison. BSA and IgG at 1.6 μM did not inhibit insulin aggregation (not shown).

Figure 19. Citrate synthase inactivation

Citrate synthase at 150 nM was heated at 43 °C for 1 h in either the absence or the presence of p26 and the enzyme activity remaining was determined. p26 concentrations were at 1200 nM, 600 nM, 300 nM, 150 nM, 75 nM, 37.5 nM. The p26 variants tested were: 1, R110G; 2, F112R; 3, R114A; 4, Y116D; 5, WT; 6, No p26, and they are in the same order at each concentration tested.

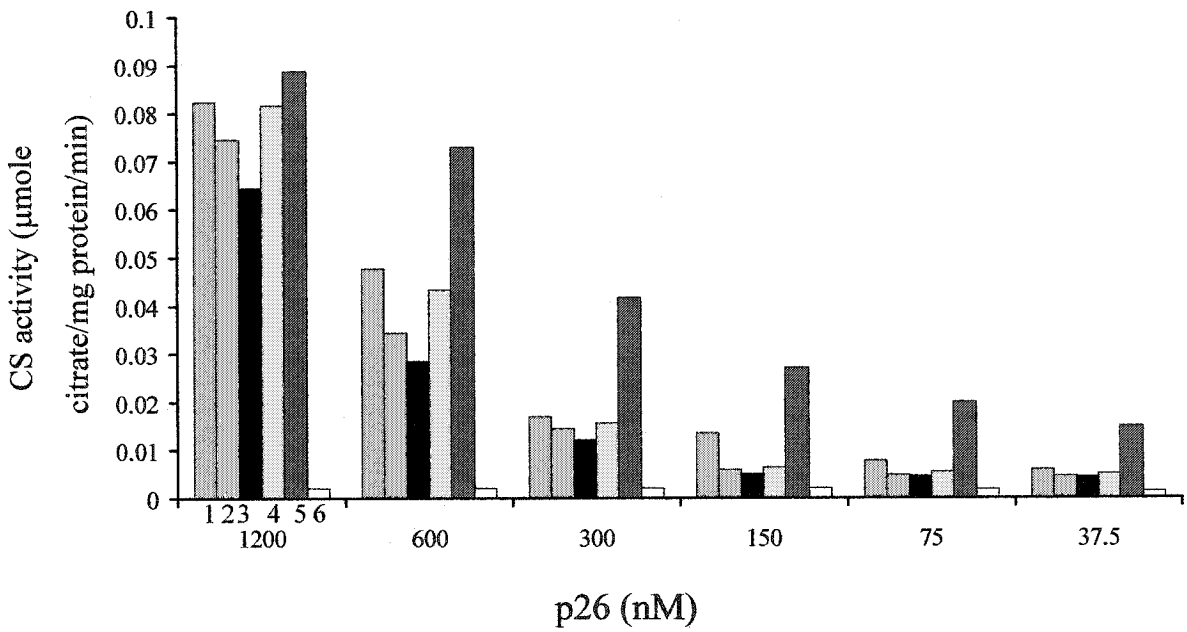
CS activity (µmole citrate/mg protein/min)
0.1
0.09
0.08
0.07
0.06
0.05
0.04
0.03
0.02
0.01
0
1 2 3 4 5 6
1200
600
300
150
75
37.5
p26 (nM)

Figure 19

Figure 20. Insulin aggregation

Bacterially produced p26 purified to apparent homogeneity was incubated with insulin for 30 min in the presence of DTT and solution turbidity was measured at 400 nm. The p26 variants tested were: 1, R110G; 2, F112R; 3, R114A; 4, Y116D; 5, WT; 6, No p26, and they are in the same order in each histogram group.

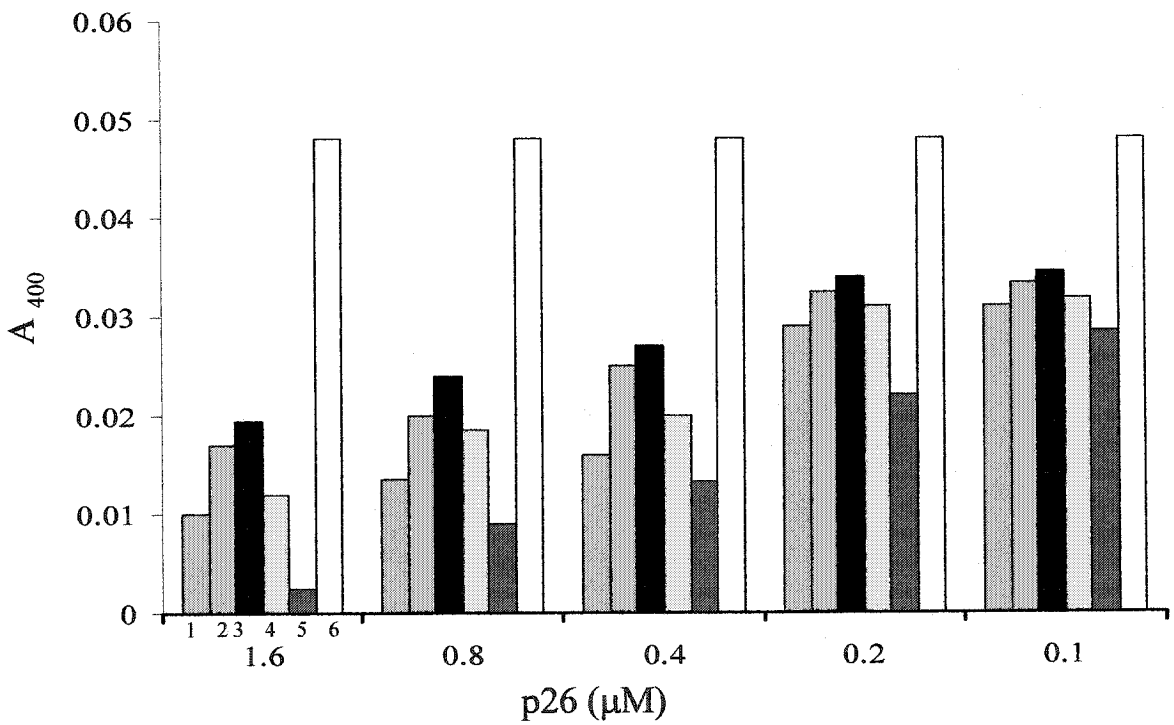

Figure 20

3.2.6 p26 localization in transfected COS-1 cells

Transiently transfected COS-1 cells were immunofluorescently stained and examined by confocal laser scanning microscopy. WT p26 was localized predominantly in the cytoplasm of transfected cells (Fig. 21a). Mutants R110G, F112R and Y116D occurred in the cytoplasm but not in all nuclei of transfected cells (Figs. 21b, c, d). R114A was found in the cytoplasm and nuclei of all transfected COS-1 cells (Fig. 21e).

3.2.7 Oligomerization of p26 in COS-1 cells

The molecular mass of WT p26 oligomers assembled in COS-1 cells ranged from approximately 14.2 kDa to 500 kDa which was similar to that of R114A (Fig. 22). Among the four mutants, F112R exhibited the narrowest range in oligomer size, while R110G and Y116D were intermediate. The oligomeric pattern of each sample from COS-1 was generally similar to that from *E. coli* (Fig. 16), except that maximal oligomer mass for WT p26 was reduced. The results are summarized in Table 7.

3.2.8 The secondary structure of p26 was modified upon mutation

Far-UV CD spectra of WT p26 purified from transformed bacteria had a negative shoulder near 214 nm and a positive shoulder near 194 nm (Fig. 23-1), these characteristic of β-sheets. p26 from *Artemia* had similar negative and positive peaks (Fig. 23-2). Most of the α-crystallin domain mutants possessed a wider negative shoulder encompassing approximately 220 nm to 208 nm, with each mutant showing a positive shoulder near 194 nm (Figs. 23-3-6). Among them, R114A gave the greatest peaks for both the negative and positive shoulders, with higher intensities than other mutants and WT (Fig. 23-5). The calculated secondary structure elements of each sample are listed in Table 8, indicating decreased β-structure and increased α-helical constituents for the

Figure 21. p26 localization in transfected COS-1 cells

COS-1 cells transiently transfected with the p26 cDNA-containing vector pcDNA/4/TO/myc-His.A were incubated with antibody to p26 followed by FITC-conjugated goat anti-rabbit IgG antibody (green). Nuclei were stained with propidium iodide (red). a, WT; b, R110G; c, F112R; d, Y116D; e, R114A. The scale bar represents 100 μm and all figures are the same magnification.

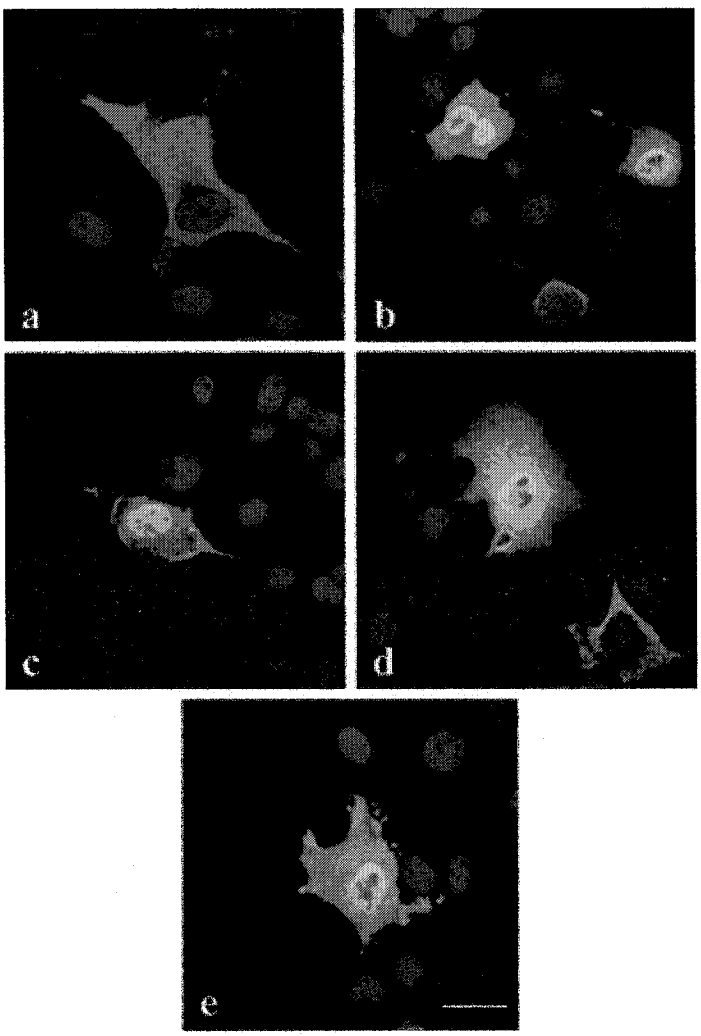

Figure 21

Figure 22. Oligomer formation of p26 in transfected COS-1 cells

Extracts prepared from COS-1 cells transiently transfected with p26-containing vectors were centrifuged in 10-50% continuous sucrose gradients. The gradients were fractionated and 15-µl samples from each fraction were electrophoresed in SDS polyacrylamide gels, blotted to nitrocellulose and probed with antibody to p26 followed by HRP-conjugated goat anti-rabbit IgG antibody. The top of each gradient is to the right and fractions are numbered across the top. The molecular mass markers, alpha-lactalbumin, 14.2 kDa; carbonic anhydrase, 29 kDa; bovine serum albumin, 66 kDa; alcohol dehydrogenase, 150 kDa; apoferritin, 443 kDa; and thyroglobulin, 669 kDa are indicated by numbered arrows.

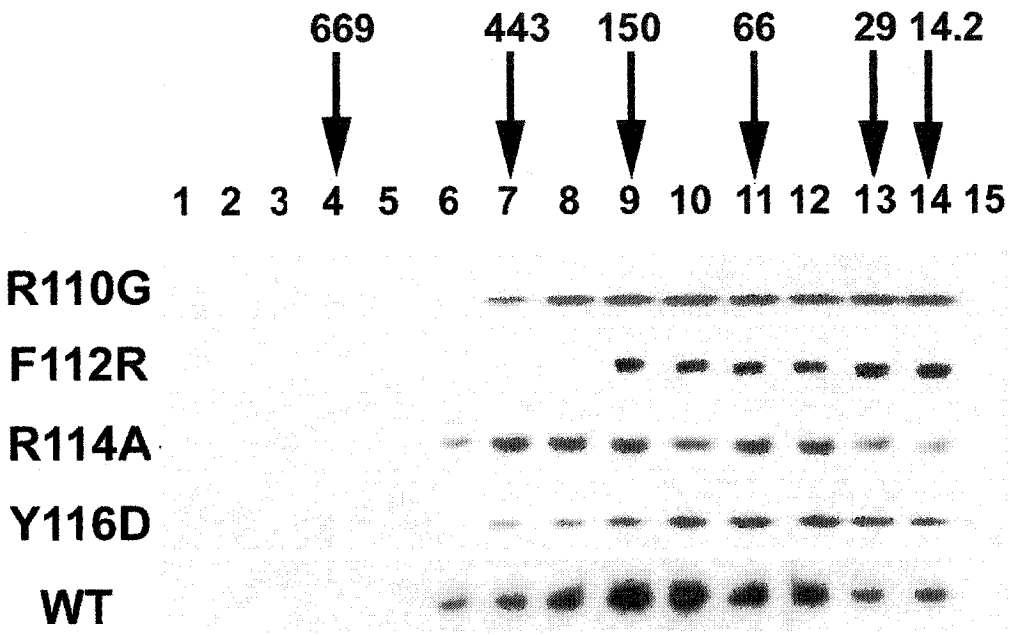
669
443
150
66
29
14.2
1 2 3 4 5 6 7 8 9 10 11 12 13 14 15
R110G
F112R
R114A
Y116D
WT

Figure 22

Table 7. Oligomerization of p26 synthesized in transfected COS-1 cells

p26 variant	Monomer mass (kDa)	Oligomer Mass		Median monomer number
		Range (kDa)	Median (kDa)	
R110G	20.7	14.2-443	80	4
F112R	20.8	14.2-150	60	3
R114A	20.7	14.2-500	100	5
Y116D	20.8	14.2-443	80	4
WT	20.8	14.2-500	100	5

The molecular mass of p26 oligomers produced by COS-1 cells was determined by immunoprobing samples electrophoresed in SDS-polyacrylamide gels and transferred to western blots after sucrose gradient centrifugation. Monomer mass refers to the molecular mass of p26 polypeptides. Oligomer mass range represents the smallest to largest oligomers observed while median oligomer mass refers to the mass of the median size oligomer. Median monomer number refers to the number of subunits in the median size oligomer.

Figure 23. Far-UV circular dichroism spectra of p26

Each spectrum represents the average of 3 scans of purified p26 dissolved in 10 mM NaH_2PO_4, pH 7.1, at a final concentration of 0.2 mg/ml. The absorption data were expressed as molar ellipticity in degrees cm^2/dmol (m deg). 1, WT from bacteria; 2, WT from *Artemia*; 3, R110G; 4, F112R; 5, R114A; 6, Y116D.

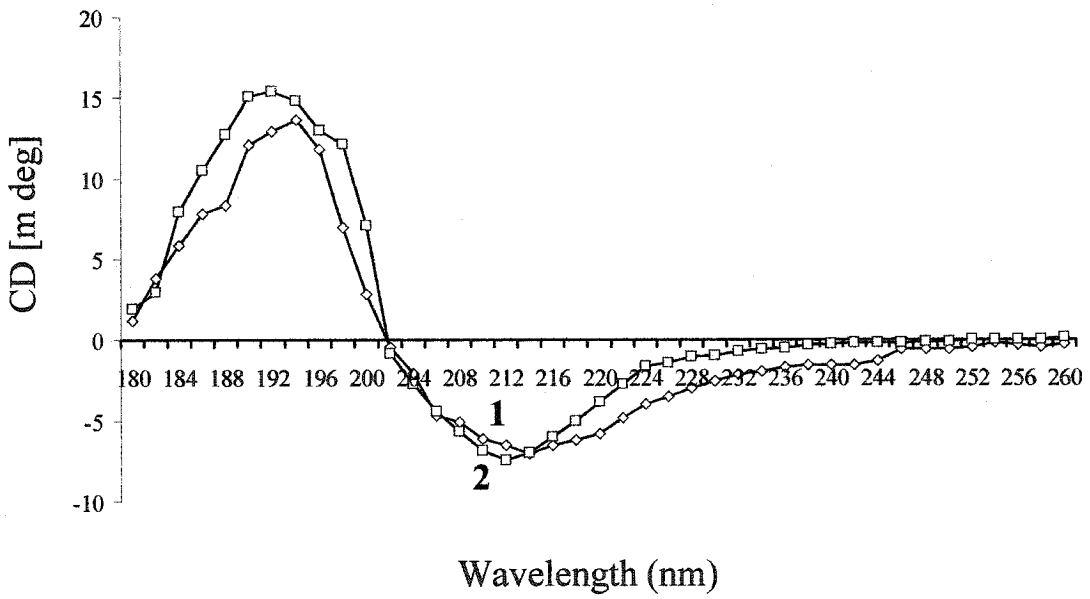
CD [m deg]
20
15
10
5
0
-5
-10
180 184 188 192 196 200 204 208 212 216 220 224 228 232 236 240 244 248 252 256 260
1
2
Wavelength (nm)

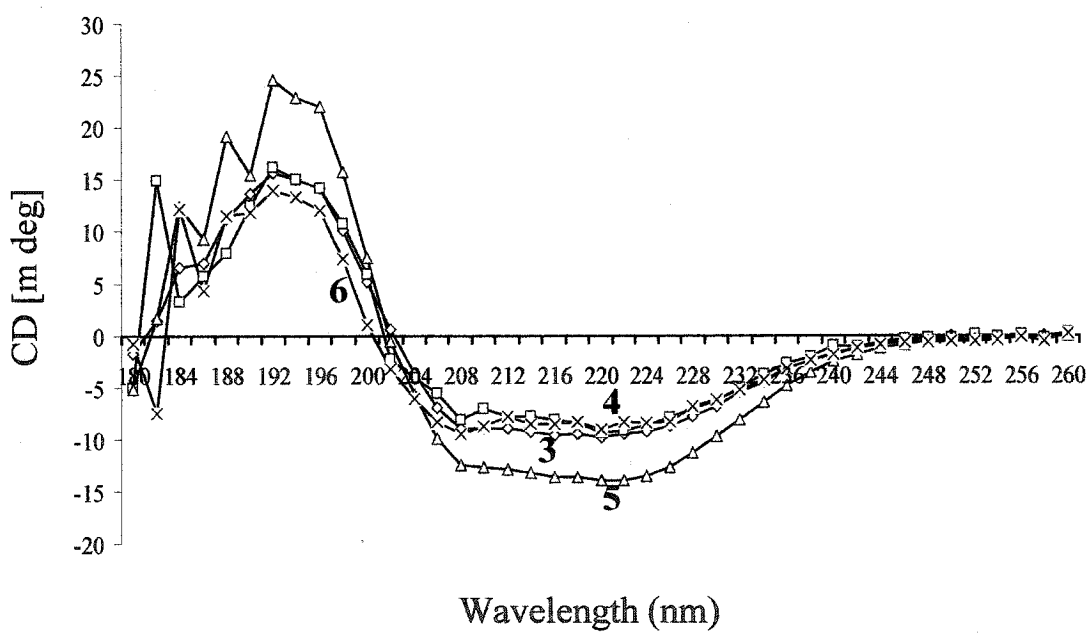
CD [m deg]
30
25
20
15
10
5
0
-5
-10
-15
-20
180 184 188 192 196 200 204 208 212 216 220 224 228 232 236 240 244 248 252 256 260
6
4
3
5
Wavelength (nm)

Figure 23

Table 8. Secondary structure elements of p26 calculated from CD spectra

Elements	R110G (%)	F112R (%)	R114A (%)	Y116D (%)	WT (*E. coli*) (%)	WT (*Artemia*) (%)
α-helix	20.3	20.2	25.7	19.3	17.7	17.7
β-antiparallel	18.0	18.2	12.9	20.5	21.6	23.0
β-parallel	10.2	10.2	9.7	10.1	10.3	10.0
β-turn	16.7	16.6	16.9	16.9	16.5	16.8
Random coil	34.8	34.8	34.9	33.3	34.0	32.5

Secondary structure elements of p26 were calculated with the CDNN v2.1 deconvolution program, with the percentage of α-helix, β-antiparallel, β-parallel, β-turn and random coil indicated for each sample.

variants, with these observations most pronounced for R114A.

3.2.9 Fluorescence studies of p26 revealed altered tertiary structure and reduced surface hydrophobicity

Fluorescence emission of each sample was detected over a range of 310-400 nm with an excitation wavelength at 280 nm. WT p26 from bacteria gave a maximal emission peak at 344 nm, while WT from *Artemia* was at 352 nm, with the former thus blue-shifted over the latter, although their emission intensities were similar (Fig. 24-1, 2). In comparison, all mutants exhibited reduced emission intensities, with the peaks of R110G, F112R, Y116D at 344 nm and the peak of R114A at 358 nm (Fig. 24-3-6). The intensity of R114A was the lowest with a red-shift in comparison with other samples (Fig. 24-5), indicating altered microenvironments and mobilities for aromatic amino acid residues.

ANS-binding experiments were carried out at an excitation wavelength of 388 nm with an emission wavelength at 473 nm. WT p26 from bacteria and *Artemia* gave similar fluorescence intensities (Fig. 25), but all four mutants exhibited decreased ANS-binding capacity when compared with WT at either 25 °C or 43 °C. Among them R114A possessed the lowest ability to bind ANS. When tested at 25 °C, the fluorescence intensity of R114A was 45.5% that of WT from bacteria, and at 43 °C, it was 40.1%. With elevated temperature, the fluorescence intensity of each sample increased. For instance, the emission of p26 from *Artemia* at 43 °C was 73.9% higher than at 25 °C. However, the relative increases in fluorescence intensity of mutants when temperature changed from 25 °C to 43 °C were less remarkable than that of WT. As an example, the increase of R110G was 19.4%, in contrast to that of WT from *E. coli* as 72.4%.

Figure 24. Intrinsic fluorescence of p26

Purified p26 was diluted in 10 mM NaH_2PO_4, pH 7.1 to a final concentration of 0.06 mg/ml. The excitation wavelength was set to 280 nm with a 2 nm band pass and fluorescence emission was detected over a range of 310-400 nm. Each spectra was recorded in duplicate using two independent sample preparations. 1, WT from bacteria; 2, WT from *Artemia*; 3, R110G; 4, F112R; 5, R114A; 6, Y116D.

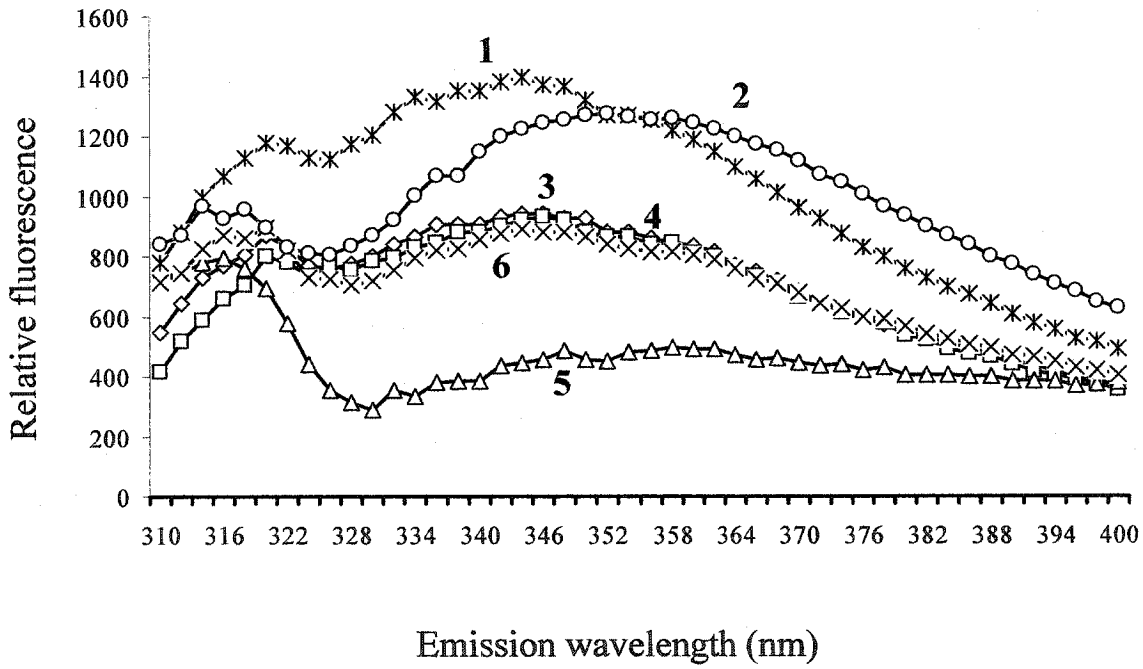
1600
1400
1200
1000
800
600
400
200
0
Relative fluorescence
1
2
3
4
5
6
310 316 322 328 334 340 346 352 358 364 370 376 382 388 394 400
Emission wavelength (nm)

Figure 24

Figure 25. Surface hydrophobicity of p26

Purified p26 solutions at 0.06 mg/ml in 10 mM NaH_2PO_4, pH 7.1 were oversaturated with ANS and the fluorescence was measured with an excitation wavelength at 388 nm, a band pass of 8 nm, and an emission wavelength set to 473 nm with a band pass of 8 nm. Measurements were carried out at either 25 °C (shaded columns) or 43 °C (filled columns). The fluorescence generated by buffer containing ANS but no p26 was subtracted from the readings for each sample.

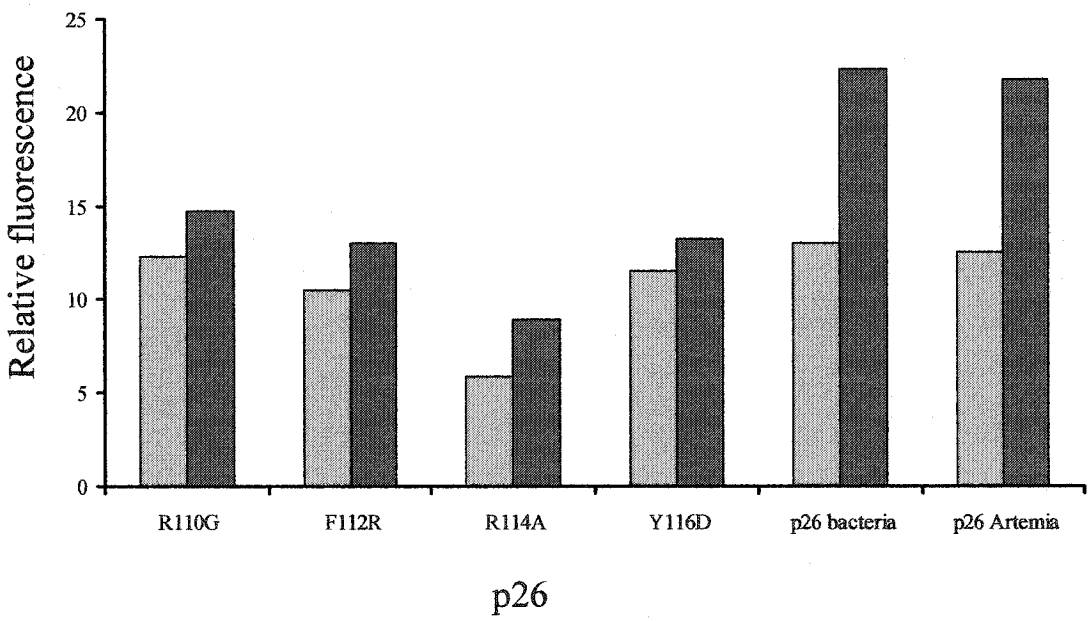
Relative fluorescence
25
20
15
10
5
0
R110G
F112R
R114A
Y116D
p26 bacteria
p26 Artemia
p26

Figure 25

3.3 Internal deletions of p26

3.3.1 Mutation and cloning of p26 cDNAs

Three internal deletions of p26, namely "G" (multiple glycine deletion), "R" (multiple arginine deletion), and "TS" (multiple serine/threonine deletion) were generated by site-directed mutagenesis using pRSET.C-p26-3-6-3 as template. Extracted plasmids for the mutants were digested with *Bam* HI and *Xho* I and the products were electrophoresed in 1% agarose gels, revealing DNA inserts at the expected positions. The identity of each insert cDNA was confirmed by DNA sequencing (not shown). The modified and WT cDNAs were then subcloned between the *Bam* HI and *Xho* I restriction sites of the eukaryotic expression vector pcDNA4/TO/myc-His.A. These p26 cDNA containing constructs were digested with *Bam* HI and *Xba* I and the resulting DNA fragments were ligated into the prokaryotic expression vector pPROTet.E233. The sizes of cDNAs inserted into eukaryotic and prokaryotic expression vectors were examined by restriction digestion, and their identities confirmed by automated DNA sequencing (not shown).

3.3.2 Purification of p26 synthesized in bacteria

The pPROTet.E233 constructs were transformed into *E. coli* strain BL21PRO, and expression was induced with anhydrotetracycline. Cell-free extracts containing expressed polypeptides were electrophoresed in SDS polyacrylamide gels, blotted to nitrocellulose and reacted with antibody to p26. Bands corresponding in size to p26 variants were visible in Coomassie blue stained gels and these polypeptides reacted with antibody to p26 (Figs. 26a, b). The "TS" construct gave the lowest yield and protein bands were not detected on blots containing extract from *E. coli* transformed with vector only. Upon purification with BD TALON™ IMAC system, single bands of the expected size

Figure 26. Purification of p26 synthesized in *E. coli* BL21PRO

Cell free extracts from transformed *E. coli* BL21PRO induced with aTc were electrophoresed in SDS polyacrylamide gels and either stained with Coomassie blue (a) or blotted to nitrocellulose and reacted with antibody to p26 (b). Proteins purified by affinity chromatography were electrophoresed in SDS polyacrylamide gels and either stained with Coomassie blue (c), or blotted to nitrocellulose and reacted with antibody to p26 (d). The lanes contained: 1, "G"; 2, "R"; 3, "TS"; 4, WT; 5, vector lacking p26 cDNA. Arrow, p26. All lanes received 10 µl of sample. M, molecular mass markers of 97, 66, 45, 31, 21 and 14 kDa.

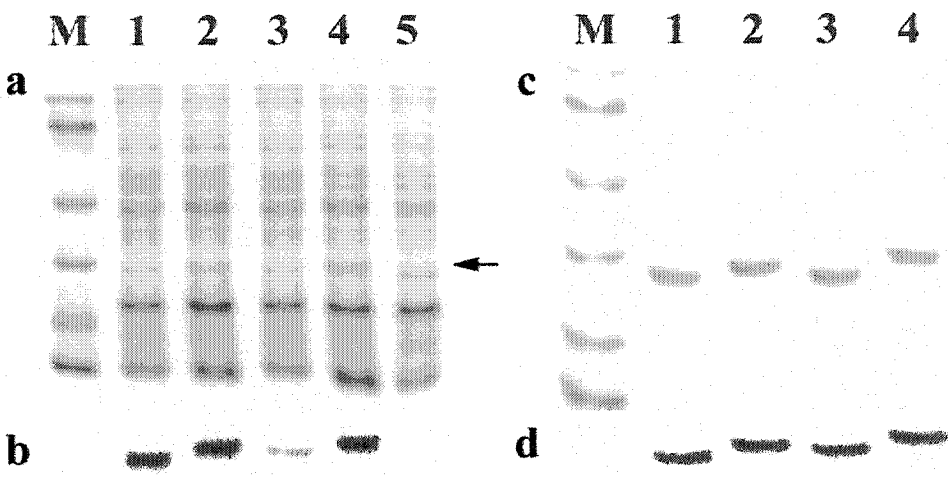

Figure 26

appeared on Coomassie blue stained gels and these polypeptides reacted with antibody to p26 on western blots (Figs. 26c, d).

3.3.3 p26 oligomer formation

The oligomer size of each bacterially expressed p26 variant was similar before and after purification (Figs. 27a, b). The molecular mass of oligomers assembled from purified WT p26 synthesized in *E. coli* ranged from 29 kDa to 669 kDa, whereas the range was 14 kDa to 443 kDa for "G" and 14 kDa to 300 kDa for "R" and "TS". The median mass of WT oligomers was greater than for any of the mutants. The results are summarized in Table 9.

3.3.4 Bacterial thermotolerance

E. coli BL21PRO expressing all variants of recombinant p26 examined in this study were significantly more thermotolerant than bacteria containing only the pPROTet.E233 vector which did not survive heat shock, and of these, bacteria producing WT p26 were the most resistant to heat stress (Fig. 28). The levels of thermotolerance induced by expression of "G" and "TS" were similar to each other ($P > 0.05$) and significantly higher than the thermotolerance conferred by variant "R" ($P < 0.05$).

3.3.5 Chaperone activity

3.3.5.1 p26 protects citrate synthase againt heat-induced aggregation

Purified WT p26 possessed the greatest chaperone activity, while mutant "R" exhibited the least, as determined by heat-induced aggregation of citrate synthase, although all mutants provided some protection (Fig. 29). At final WT p26 concentrations of 1200 nM and 600 nM when chaperone to target molar ratio is 8:1 and 4:1 respectively (p26 monomer to citrate synthase dimer), or 1:1 and 0.5:1 respectively if the median oligomer

Figure 27. Oligomer formation by p26 synthesized in *E. coli* BL21PRO

Bacterially produced p26 either before (a) or after purification to apparent homogeneity (b) was centrifuged at 200,000 x *g* for 12 h at 4 °C on 10-50% continuous sucrose gradients. The gradients were fractionated and 15-µl samples from each fraction were electrophoresed in SDS polyacrylamide gels, blotted to nitrocellulose and reacted with antibody to p26 followed by HRP-conjugated goat anti-rabbit IgG. The top of each gradient is to the right and fractions are numbered across the top. The molecular mass markers, alpha-lactalbumin, 14.2 kDa; carbonic anhydrase, 29 kDa; bovine serum albumin, 66 kDa; alcohol dehydrogenase, 150 kDa; apoferritin, 443 kDa; and thyroglobulin, 669 kDa are indicated by numbered arrows.

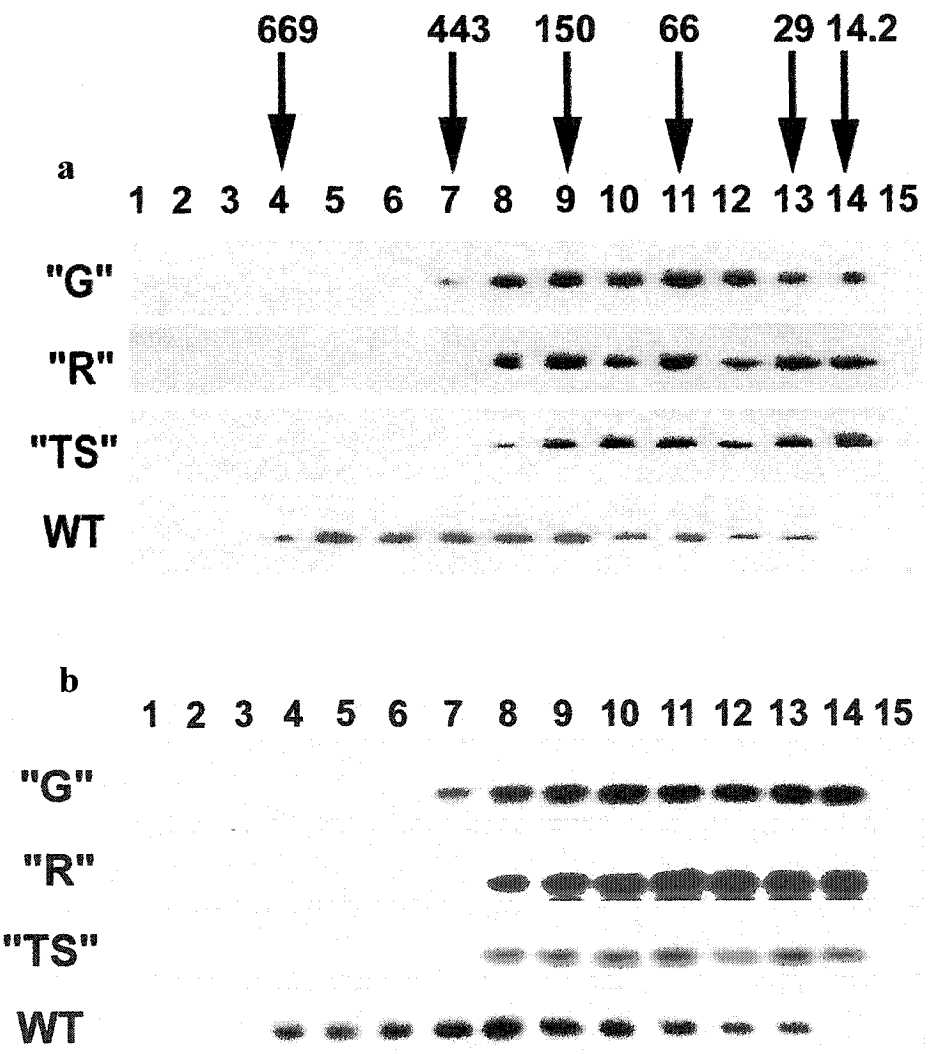
669
443
150
66
29
14.2
a
1 2 3 4 5 6 7 8 9 10 11 12 13 14 15
"G"
"R"
"TS"
WT
b
1 2 3 4 5 6 7 8 9 10 11 12 13 14 15
"G"
"R"
"TS"
WT

Figure 27

Table 9. Oligomerization of p26 produced in *E. coli* BL21PRO

p26 variant	Monomer mass (kDa)	Oligomer Mass		Median monomer number
		Range (kDa)	Median (kDa)	
"G"	23.7	14-443	95	4
"R"	24.1	14-300	66	3
"TS"	23.8	14-300	66	3
WT	25.5	29-669	200	8

The molecular mass of p26 oligomers produced by transformed *E. coli* BL21PRO was determined by sucrose density gradient centrifugation. Monomer mass refers to the molecular mass of p26 polypeptides. Oligomer mass range represents the smallest to largest oligomers observed while median oligomer mass refers to the mass of the median size oligomer. Median monomer number refers to the number of subunits in the median size oligomer.

Figure 28. Thermotolerance of transformed bacteria

Transformed *E. coli* BL21PRO were incubated at 54 °C for periods up to 1 h, diluted and plated in duplicate on LB agar followed by incubation at 37 °C for 16 h. Colonies were counted and the Log_{10} values of colony forming units (CFU) per ml were plotted against the length of heat shock in min. Bacteria containing the pPROTet.E233 vector lacking a p26 cDNA insert did not survive the 60 min heat shock. Results are averaged from three independent experiments.

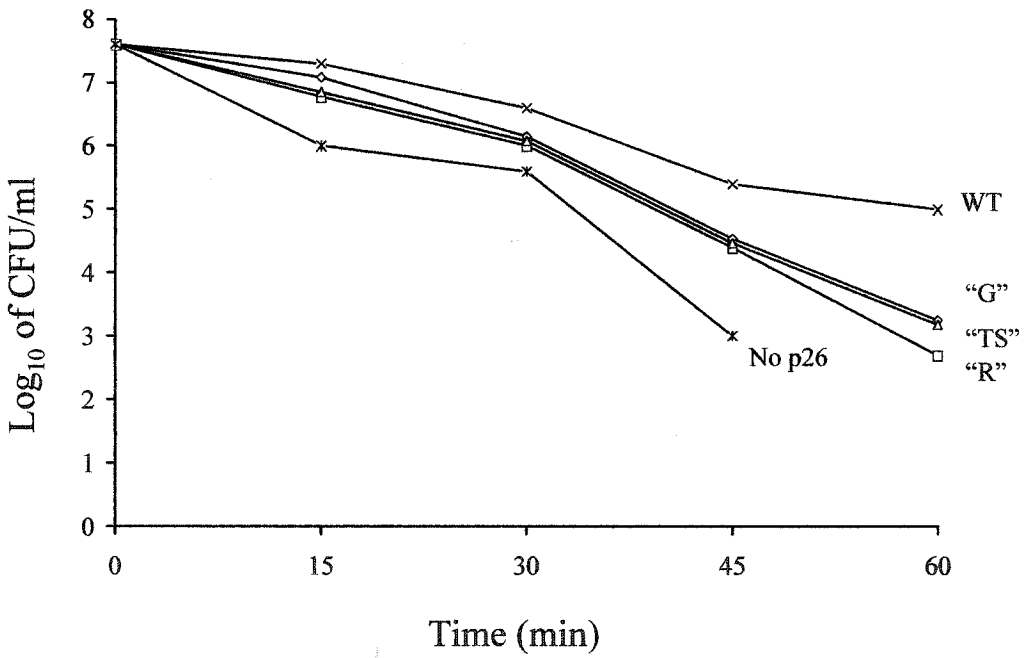

Figure 28

Figure 29. p26 chaperone activity on citrate synthase

Bacterially produced p26 purified to apparent homogeneity was heated at 43 °C for 1 h with 150 nM citrate synthase, and solution turbidity was measured at 360 nm. The final concentrations of p26 based on monomer molecular mass were: a, 1200 nM; b, 600 nM; c, 300 nM; d, 150 nM; e, 75 nM; f, 37.5 nM. The curves are: 1, No p26; 2, "R"; 3, "TS"; 4, "G"; 5, WT, and they occupy the same relative positions in a-f.

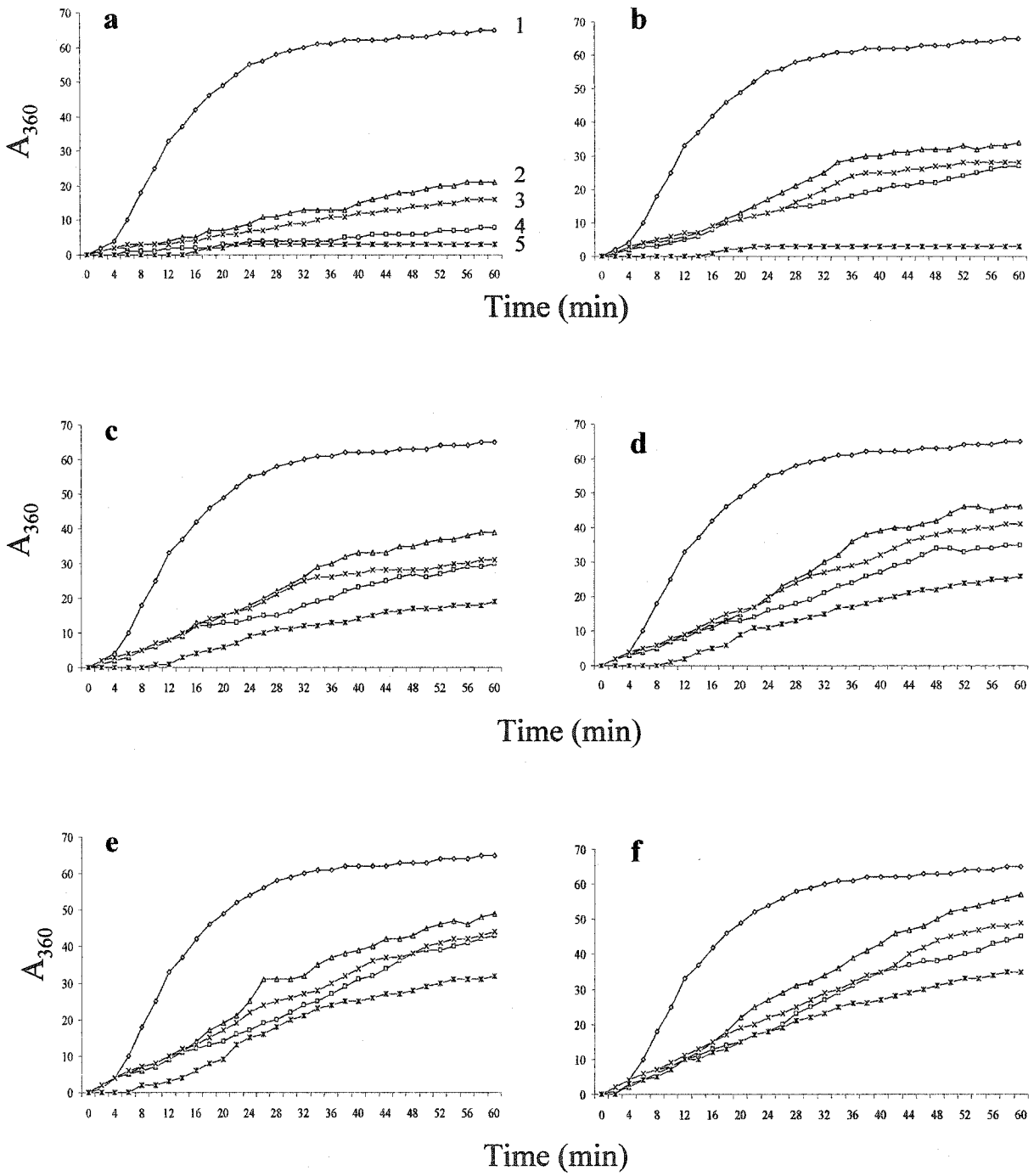

Figure 29

size of WT p26 is used for comparison, citrate synthase aggregation was inhibited almost completely for 1 h at 43 °C (Figs. 29a, b). At a final p26 concentration of 37.5 nM, where the molar ratio of WT p26 to citrate synthase is 1:4, or 1:32 if the median oligomer size of p26 is used for comparison, purified WT p26 reduced heat-induced turbidity by 46% after 1 h at 43 °C (Fig. 29f). WT p26 at each concentration from 37.5 nM to 1200 nM gave the best protection, mutants "G", "TS" and "R" followed in decreasing order of activity (Figs. 29a-f). None of the three mutants with internal deletions completely inhibited the aggregation of citrate synthase at 1200 nM (Fig. 29a), nor were higher concentrations more effective (not shown). However, "R", the least effective chaperone, still offered a significant amount of protection to citrate synthase even at the lowest ratio to substrate tested. BSA and IgG at 1200 nM provided almost no protection when heated with citrate synthase (not shown).

3.3.5.2 p26 prevents citrate synthase from heat-induced inactivation

WT p26 was the most effective in protecting citrate synthase against heat induced inactivation, followed by "G" and "TS" which were very similar and then "R" which exhibited the least protection at each chaperone concentration (Fig. 30). When the concentration of WT p26 was 1200 nM, the enzyme activity remaining after 1 h at 43 °C was almost the same as in samples containing citrate synthase before heat shock (not shown).

3.3.5.3 p26 protects insulin against DTT-induced aggregation

Purified WT p26 was the most effective in preventing DTT-induced denaturation of insulin at room temperature (Fig. 31), whereas mutant "R" had the least ability to protect insulin. Mutants "G" and "TS" provided an intermediate level of protection. At 0.1 μM,

Figure 30. Citrate synthase inactivation

Citrate synthase at 150 nM was heated at 43 °C for 1 h in either the absence or the presence of p26 and the enzyme activity remaining was determined. p26 concentrations were at 1200 nM, 600 nM, 300 nM, 150 nM, 75 nM, 37.5 nM. The p26 variants tested were: 1, "G"; 2, "R"; 3, "TS"; 4, WT; 5, No p26, and they are in the same order at each concentration tested.

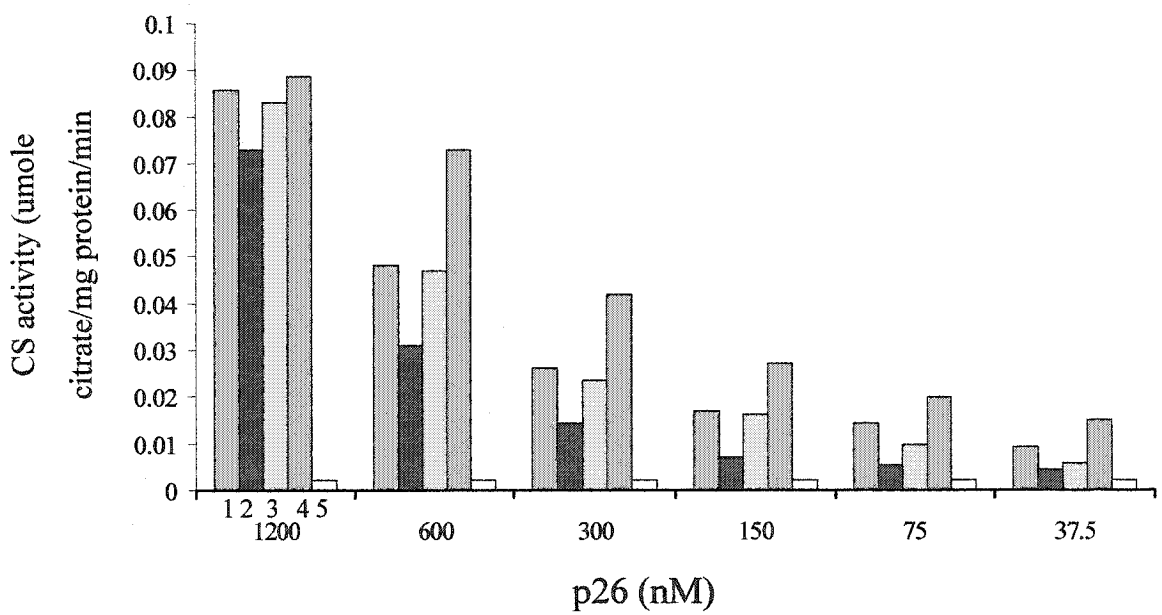
CS activity (umole citrate/mg protein/min
0.1
0.09
0.08
0.07
0.06
0.05
0.04
0.03
0.02
0.01
0
1 2 3 4 5
1200
600
300
150
75
37.5
p26 (nM)

Figure 30

Figure 31. Insulin aggregation

Bacterially produced p26 purified to apparent homogeneity was incubated with insulin for 30 min in the presence of DTT and solution turbidity was measured at 400 nm. The p26 variants tested were: 1, "G"; 2, "R"; 3, "TS"; 4, WT; 5, No p26, and they are in the same order in each histogram group.

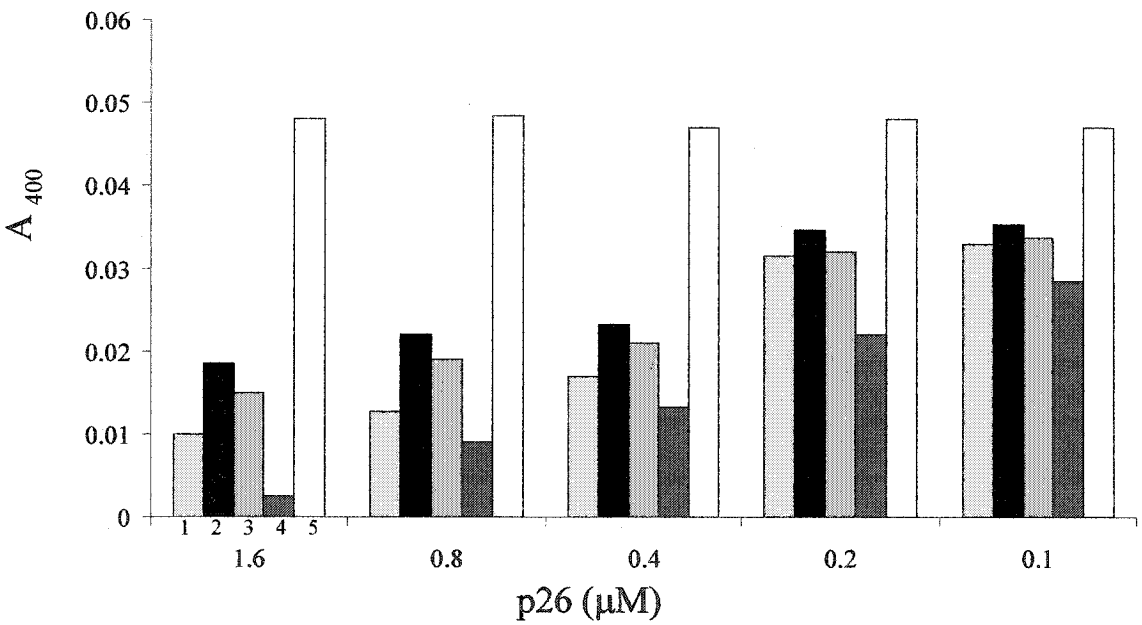

Figure 31

WT p26 inhibited insulin aggregation by 39% after 30 min, and the aggregation was almost completely suppressed at 1.6 μM. At this concentration, the molar ratio of chaperone to target is 0.4:1 (monomer to monomer), or 0.05:1 if the median oligomer size of WT p26 is used for comparison. BSA and IgG at 1.6 μM did not inhibit insulin aggregation (not shown).

3.3.6 Immunolocalization of p26 in COS-1 cells

Transiently transfected COS-1 cells were immunofluorescently stained and examined by confocal laser scanning microscopy. WT p26 was localized predominantly in the cytoplasm of transfected cells (Fig. 32a). Mutants "G" and "TS" occurred in the cytoplasm of all transfected cells and the nuclei of some (Figs. 32b, c), whereas "R" was found in the cytoplasm and nuclei of all transfected COS-1 cells (Fig. 32d).

3.3.7 Expression and oligomerization of p26 in COS-1 cells

The molecular mass of WT p26 oligomers assembled in COS-1 cells ranged from approximately 14 kDa to 500 kDa which was broader than for the mutants (Fig. 33). Among the four mutants, "G" exhibited slightly broader range in oligomer size than "R" and "TS". The oligomeric pattern of each sample from COS-1 was generally similar to that from *E. coli* (Fig. 27), except that maximal oligomer mass for WT p26 was reduced. The results are summarized in Table 10.

3.3.8 The seconday structure of p26 was altered by mutation

Far-UV CD spectra of WT p26 purified from either transformed bacteria or *Artemia* cysts had a negative shoulder near 214 nm and a positive shoulder near 194 nm, these characteristic of β-sheets (Fig. 34). The mutants with internal deletions possessed wider negative shoulders encompassing approximately 220 nm to 208 nm, with each mutant

Figure 32. p26 localization in transfected COS-1 cells

COS-1 cells transiently transfected with the p26 cDNA-containing vector pcDNA/4/TO/myc-His.A were incubated with antibody to p26 followed by FITC-conjugated goat anti-rabbit IgG antibody (green). Nuclei were stained with propidium iodide (red). a, WT; b, "G"; c, "TS"; d, "R". The scale bar represents 100 μm and all figures are the same magnification.

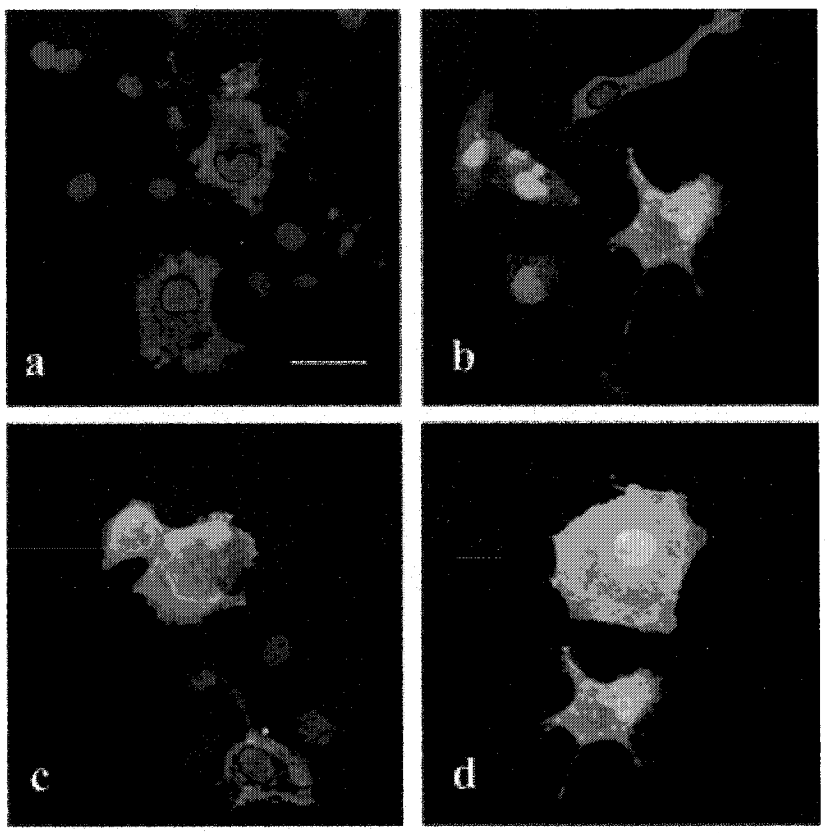

Figure 32

Figure 33. Oligomer formation of p26 in transiently transfected COS-1 cells

Extracts prepared from COS-1 cells transiently transfected with p26-containing vectors were centrifuged in 10-50% continuous sucrose gradients. The gradients were fractionated and 15-μl samples from each fraction were electrophoresed in SDS polyacrylamide gels, blotted to nitrocellulose and probed with antibody to p26 followed by HRP-conjugated goat anti-rabbit IgG antibody. The top of each gradient is to the right and fractions are numbered across the top. The molecular mass markers, alpha-lactalbumin, 14.2 kDa; carbonic anhydrase, 29 kDa; bovine serum albumin, 66 kDa; alcohol dehydrogenase, 150 kDa; apoferritin, 443 kDa; and thyroglobulin, 669 kDa are indicated by numbered arrows.

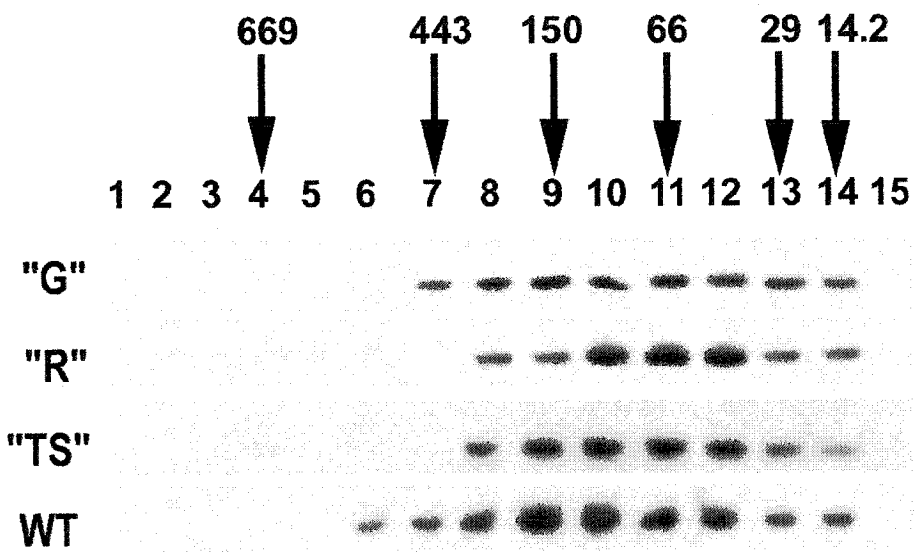

Figure 33

Table 10. Oligomerization of p26 synthesized in transfected COS-1 cells

p26 variant	Monomer mass (kDa)	Oligomer Mass		Median monomer number
		Range (kDa)	Median (kDa)	
"G"	18.7	14-443	80	4
"R"	19.4	14-300	66	3
"TS"	19.1	14-300	66	3
WT	20.8	14-500	100	5

The molecular mass of p26 oligomers produced by COS-1 cells was determined by immunoprobing samples electrophoresed in SDS-polyacrylamide gels and transferred to membranes for Western blots after sucrose gradient centrifugation. Monomer mass refers to the molecular mass of p26 polypeptides. Oligomer mass range represents the smallest to largest oligomers observed while median oligomer mass refers to the mass of the median size oligomer. Median monomer number refers to the number of subunits in the median size oligomer.

Figure 34. Far-UV circular dichroism spectra of p26

Each spectrum represents the average of 3 scans of purified p26 dissolved in 10 mM NaH_2PO_4, pH 7.1, at a final concentration of 0.2 mg/ml. The absorption data were expressed as molar ellipticity in degrees cm^2/dmol (m deg). Tested samples are: 1, WT from bacteria; 2, WT from *Artemia*; 3, "G"; 4, "R"; 5, "TS".

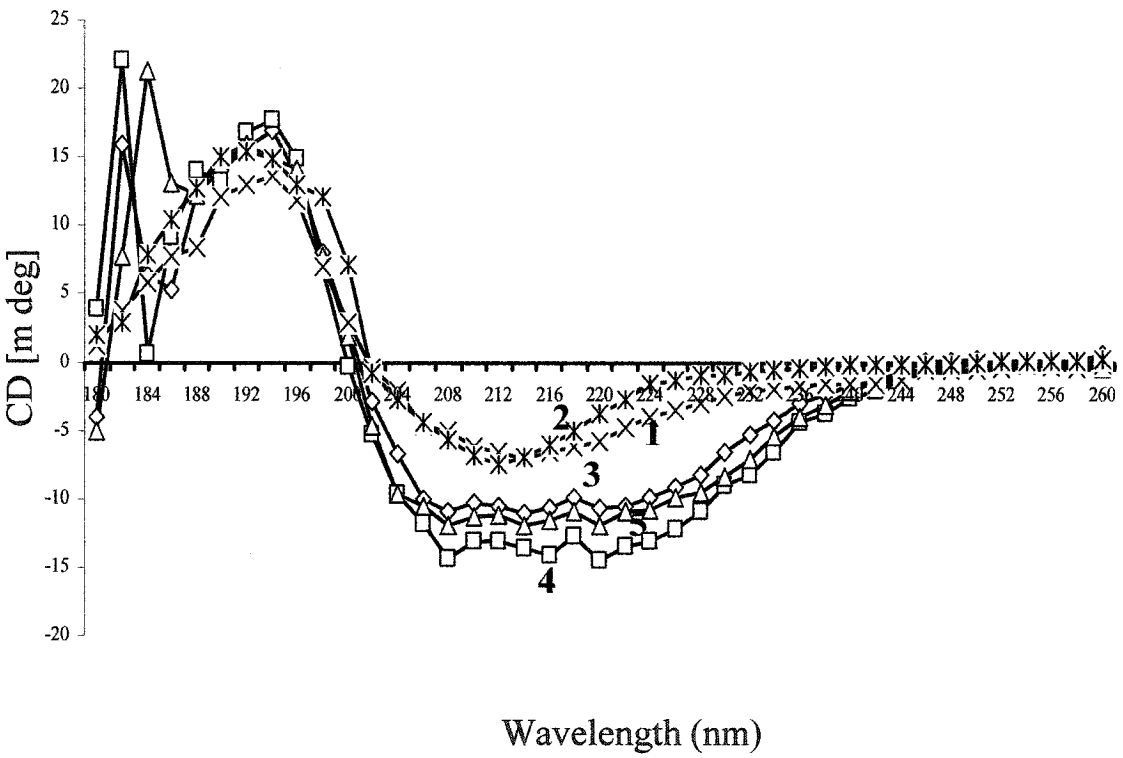
CD [m deg]
25
20
15
10
5
0
-5
-10
-15
-20
180
184
188
192
196
200
204
208
212
216
220
224
228
232
236
240
244
248
252
256
260
1
2
3
4
5
Wavelength (nm)

Figure 34

showing a positive shoulder near 194 nm. Among all p26 variants examined, "R" gave the greatest peak for both the negative and positive shoulders. The calculated secondary structure elements of each sample are listed in Table 11, indicating decreased β-structure and increased α-helical constituents for the variants, with these characteristics most pronounced for "R".

3.3.9 Tertiary structure and surface hydrophobicity were affected by mutation

Fluorescence emission of each sample was detected over a range of 310-400 nm with an excitation wavelength at 280 nm. WT p26 from bacteria gave a maximal emission peak at 344 nm, while WT from *Artemia* was at 352 nm, with the former thus blue-shifted over the latter, although their emission intensities were similar (Fig. 35). In comparison, all mutants exhibited reduced emission intensities, with the peak of "G" and "TS" at 348 nm and "R" at 360 nm. The fluorescence intensity of "R" was the lowest with a red-shift in comparison with other samples. The results indicate altered microenvironments and mobilities for aromatic residues.

ANS-binding experiments were carried out at an excitation wavelength of 388 nm with an emission wavelength at 473 nm. WT p26 from bacteria and *Artemia* gave similar fluorescence intensities (Fig. 36), but all three mutants exhibited decreased ANS-binding capacity when compared with WT at either 25 °C or 43 °C. Among them "R" possessed the lowest ability to bind ANS. When tested at 25 °C, the fluorescence intensity of "R" was 38.5% that of WT from bacteria, and at 43 °C, it was only 28.7%. With elevated temperature, the fluorescence of each sample increased. For instance, the emission of p26 from *Artemia* at 43 °C was 73.9% higher than at 25 °C. However, the relative increases in fluorescence intensity of mutants when temperature changed from 25 °C to 43 °C were

Table 11. Secondary structure elements of p26 calculated from CD spectra

Elements	"G" (%)	"R" (%)	"TS" (%)	WT (*E. coli*) (%)	WT (*Artemia*) (%)
α-helix	21.8	24.9	22.2	17.7	17.7
β-antiparallel	17.8	15.6	16.4	21.6	23.0
β-parallel	9.8	9.4	9.5	10.3	10.0
β-turn	17.1	17.4	17.5	16.5	16.8
Random coil	33.5	32.7	34.4	34.0	32.5

Secondary structure elements of p26 were calculated with the CDNN v2.1 deconvolution program, with the percentage of α-helix, β-antiparallel, β-parallel, β-turn and random coil indicated for each sample.

Figure 35. Intrinsic fluorescence of p26

Purified p26 was diluted in 10 mM NaH_2PO_4, pH 7.1 to a final concentration of 0.06 mg/ml. The excitation wavelength was set to 280 nm with a 2 nm band pass and fluorescence emission was detected over a range of 310-400 nm. Each spectrum was recorded in duplicate using two independent sample preparations. 1, WT from bacteria; 2, WT from *Artemia*; 3, "G"; 4, "R"; 5, "TS".

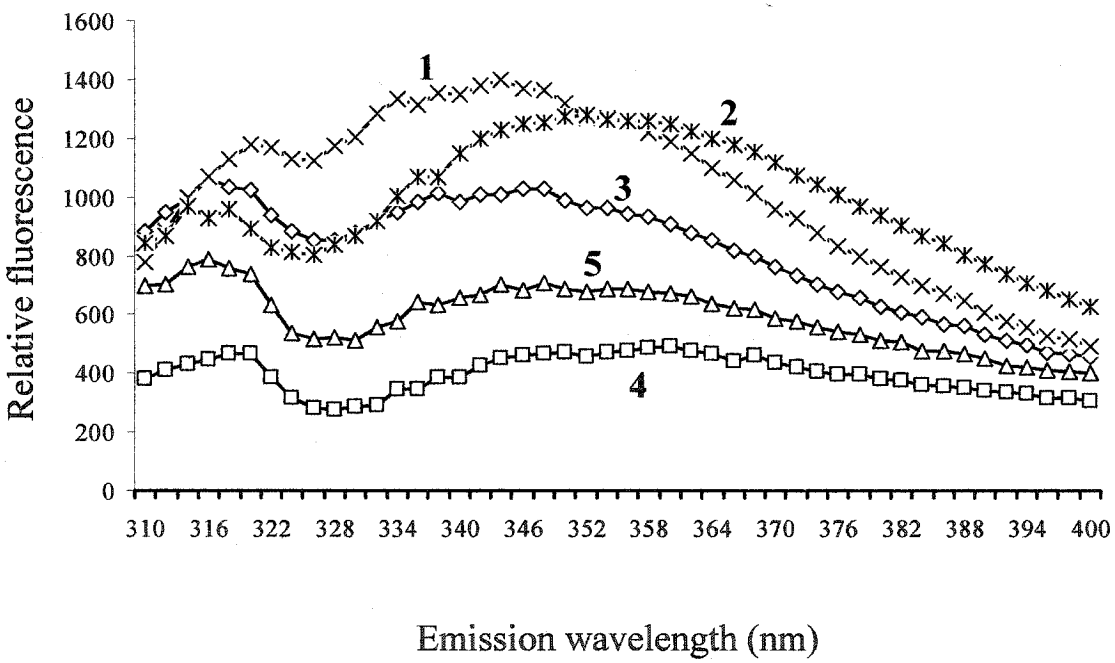
1600
1400
1200
1000
800
600
400
200
0
Relative fluorescence
1
2
3
4
5
310 316 322 328 334 340 346 352 358 364 370 376 382 388 394 400
Emission wavelength (nm)

Figure 35

Figure 36. Surface hydrophobicity of p26

Purified p26 at 0.06 mg/ml in 10 mM NaH_2PO_4, pH 7.1 was oversaturated with ANS and the fluorescence was measured with an excitation wavelength at 388 nm, a band pass of 8 nm, and an emission wavelength set to 473 nm with a band pass of 8 nm. Measurements were carried out at either 25 °C (shaded columns) or 43 °C (filled columns). Tested samples are: 1, "G"; 2, "R"; 3, "TS"; 4, WT from bacteria; 5, WT from *Artemia*. The fluorescence generated by buffer containing ANS but no p26 was subtracted from the readings for each sample.

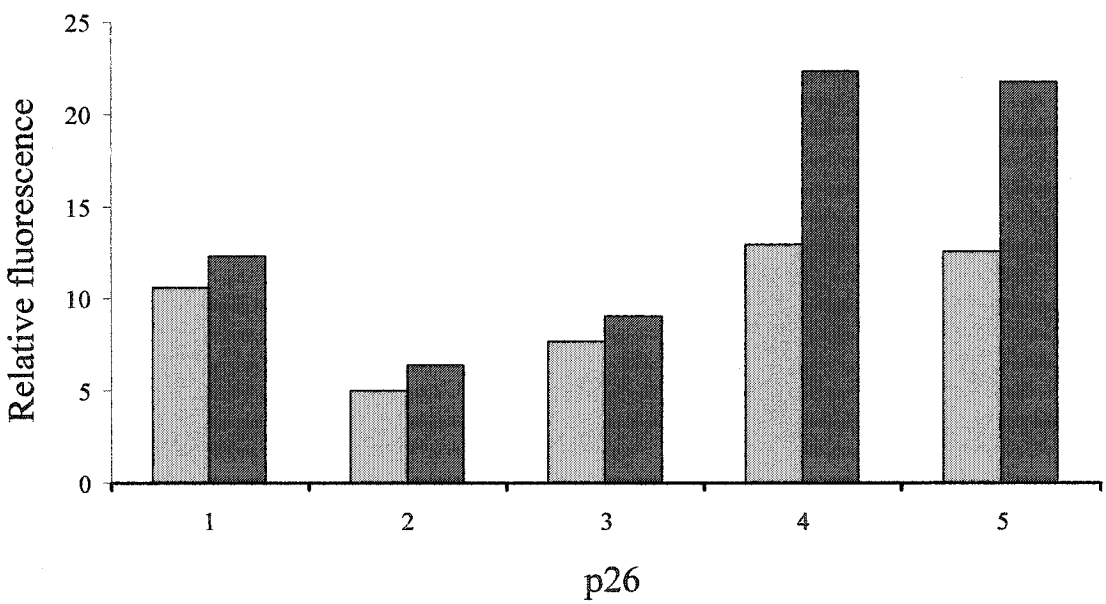

Figure 36

less remarkable than for WT. As an example, the increase for "R" was 27.9%, in contrast to WT from *E. coli* which was 72.4%.

3.4 Comparative modeling of p26 structure

The 29% sequence identity between α-crystallin domains of p26 and wheat *Ta* Hsp16.9 allowed generation of a p26 model based on the crystal structure of *Ta* Hsp16.9 (Fig. 37). The overall sequence identity between these two sHsps was 20%, and the lack of significant sequence identity between p26 and *Ta* Hsp16.9 C-terminal extensions precluded modeling this portion of p26. Thus, residues A159 to A192 were deleted from the p26 sequence for a better alignment interface. The similarity between the proteins indicates each p26 monomer contains a buried N-terminal region, a partially exposed α-crystallin domain and a solvent-accessible C-terminal extension, as initially shown for *Ta* Hsp16.9 (van Montfort *et al.*, 2001b). The α-crystallin domain of p26 forms an immunoglobulin-like fold composed of eight β-strands organized into two anti-parallel β-sheets. In the p26 model, loop 1 composed of residues 22GFGGFGGGMDL32 is located in the center of the N-terminal region, whereas loop 2 composed of residues 58TPGLSR63 is in the region connecting the N-terminal region and α-crystallin domain. Loop 3 (102SDEYGHVQRE111) protrudes from β-sheets of the α-crystallin domain and corresponds to the loop encompassing the β6 strand in *Ta* Hsp16.9. Loop 4 (132SSDGV136) equates to a sequence connecting β8 and β9 of *Ta* Hsp16.9. Residues 153IVPITP158 form the partial C-terminal extension of p26, and this sequence corresponds to a stretch close to the β10 strand in the C-terminal extension of *Ta* Hsp16.9. Hydrophobic residues I147 and I149 of *Ta* Hsp16.9 bind in a hydrophobic groove between strands β4 and β8 of a neighboring monomer in intact oligomers.

Figure 37. Comparative modeling of p26

Wheat *Ta* Hsp16.9 was used as a template for sequence alignment with the "alignment interface" program of Swiss-Model. The p26 residues A2-P158, corresponding to S2-G151 of *Ta* Hsp16.9 were used for modeling and the result is shown as a monomer, with C-terminal residues A159-A192 deleted for alignment optimization. The returned three-dimensional model was enhanced with the "improve fit" function of Swiss-PdbViewer and sent for second round modeling. Internal deletions "G" and "R" are indicated by labeled arrows; the location of the four α-crystallin domain single amino acid substitutions in strands β6-β7 (arrow labeled) are hidden from view by overlaying strands β2-β3 (arrow labeled) (a). The arrow-labeled A2 and P158 position the first and last amino acid residues, respectively, in the p26 model. The N-terminal region, α-crystallin domain and C-terminal extension are indicated by labeled arrows. Loops within the p26 monomer are indicated in b, and the large loop of the wheat *Ta* Hsp16.9 monomer corresponding to p26 loop 3 is indicated in c.

a

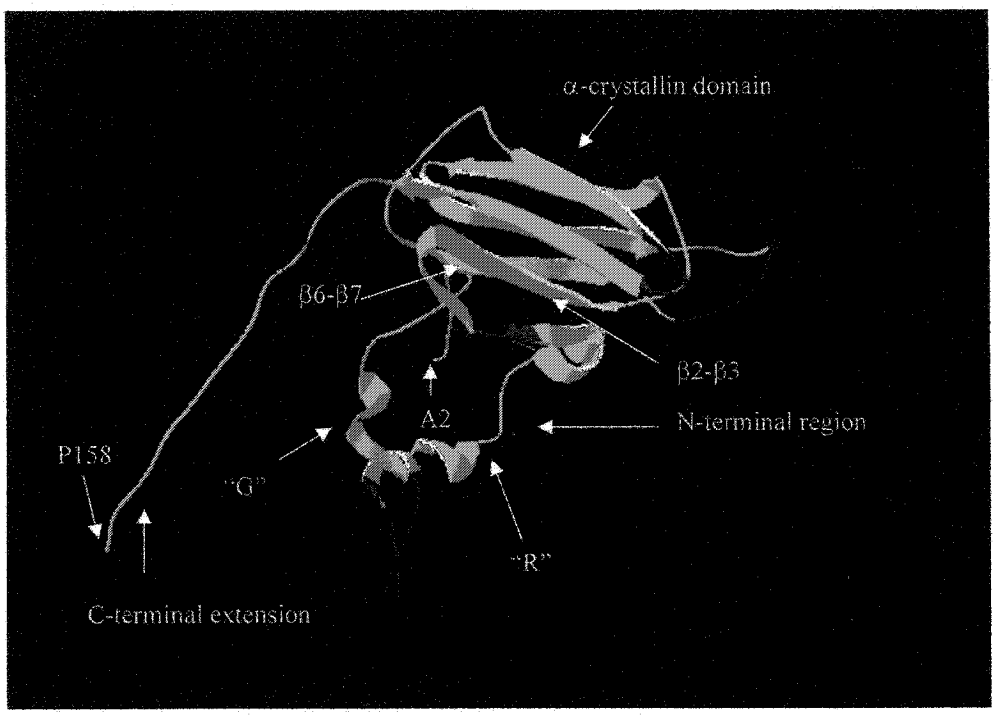

b

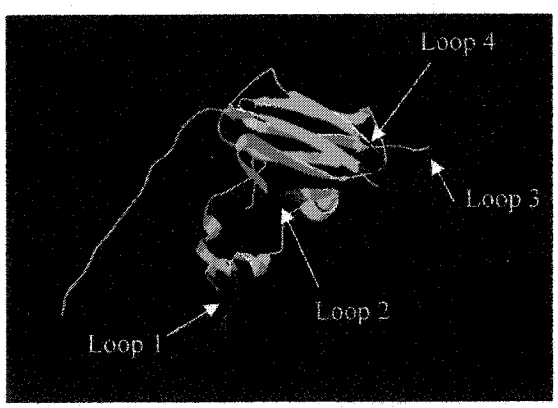

c

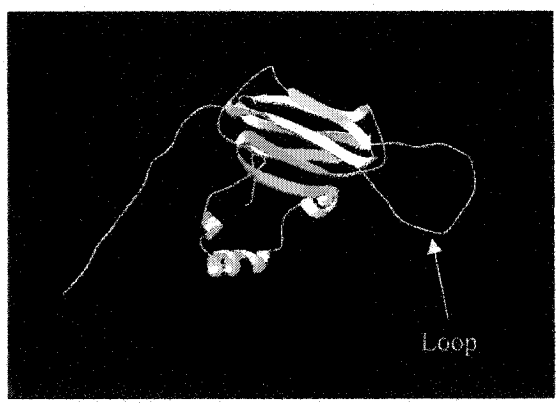

Figure 37

IV. Discussion

p26 exists in large amounts in encysted *Artemia* embryos, and is thought to play an important role in protecting embryos against environmental hardships. As the only crustacean sHSP described in detail so far, p26 has the ability to effectively prevent proteins from irreversible aggregation during *Artemia* development. p26 structure and function were characterized by site-directed mutagenesis in this work, which allows a further appreciation of p26 relevance during embryo diapause, desiccation and other stress, thereby also shedding light on the functional mechanisms of sHSPs in human diseases.

4.1 Sequence analysis of p26

Like most sHSPs, p26 is composed of three regions, with the conserved "α-crystallin domain" as the hallmark of this protein family. p26 was predicted to lack α-helical constituents in the α-crystallin domain, which consists predominantly of β-sheets (Liang *et al.*, 1997a). p26 forms oligomers and exhibits chaperone activity *in vivo* and *in vitro* (Liang *et al.*, 1997b; Crack *et al.*, 2002), characteristics potentially dominated by conserved sequences. The p26 α-crystallin domain is flanked by the 60-residue N-terminus and the 40-residue C-terminus, both of limited similarity to corresponding regions in other sHSPs. The nonconserved N-terminal region and C-terminal extension may determine the distinct properties of p26. As compared with other sHSPs, a unique characteristic of the p26 N-terminal region is the presence of 10 glycines in the first 29 amino acid residues, which are in a 22-residue peptide. Other sHSPs usually have only 3 or 4 glycines in the equivalent region. Seven arginines occur between residues 36-51 of p26, with 6 distributed in a 10-residue group. The first 60 residues of p26 share limited

sequence identity with other sHSPs, but exhibit a weak similarity in terms of the enrichment in glycine, arginine and phenylalanine. p26 shares many highly conserved residues with other sHSPs in the central α-crystallin domain, especially in the sequence 110REFRRRY116. Mutations to the arginine residues equivalent to R114 of p26 in αA- and αB-crystallin result in autosomal dominant congenital cataract and desmin-related myopathy, respectively (Litt *et al.*, 1998; Vicart *et al.*, 1998).

The sHSP C-terminal extension is variable in length and sequence from species to species, being absent from *C. elegans* Hsp12.6, while reaching 49 residues in *Drosophila* Hsp27 and 50 residues in *Artemia* p26 (Leroux *et al.*, 1997a; Liang *et al.*, 1997a; de Jong *et al.*, 1998b). Composed predominantly of polar and charged amino acid residues, the C-terminal extension solubilizes either sHSP oligomers or the complexes formed between sHSPs and substrates (Lindner *et al.*, 2000). Removal of this extension will likely decrease protein solubility and compromise chaperone function. The p26 C-terminal extension encompasses a serine/threonine-enriched stretch, wherein 13 serines or threonines exist within 24 residues. The structural and functional relevance of this motif was unexplored prior to this work.

4.2 Oligomerization of p26

Most sHSPs tend to assemble into large oligomeric complexes as a prerequisite for chaperone activity. Native p26 extracted from *Artemia* cysts forms polydisperse oligomers with a maximum mass of 669 kDa composed of up to 32 subunits, as is also true for recombinant p26 from bacteria although there are more smaller oligomers (Crack *et al.*, 2002). p26 oligomers in COS-1 cells are from 20.8 kDa to 500 kDa. p26 appears as particles about 15 nm in diameter as determined by electron microscopy, and they are

similar in size to human αB-crystallin and Hsp27, native bovine α-crystallin, and yeast Hsp26 (Clegg *et al.*, 1999; Haslbeck *et al.*, 1999; Haley *et al.*, 2000). The oligomeric polydispersity of p26 contrasts to *Mj* Hsp16.5 which consists of 24 monomers organized into a spherical complex, *Ta* Hsp16.9 existing as a dodecamer assembled into double disks and *Mt* Hsp16.3 which forms a triangular structure as a nonamer composed of three trimers (Kim *et al.*, 1998; van Montfort *et al.*, 2001b; Abulimiti *et al.*, 2003).

The 17WSDPF21 motif in p26 is conserved and corresponds to 15SWEPF19 in Chinese hamster Hsp27, a sequence important in oligomer formation and chaperone activity (Theriault *et al.*, 2004). This motif was missing in truncations p26-NΔ36 and p26-NΔ60, and the absence of higher order oligomers in both cases suggests the involvement of this sequence in oligomer assembly, a proposal currently under study. Mutated *Mj* Hsp16.5 lacking the first N-terminal 12 amino acid residues fails to assemble into spherical oligomers, indicating the region is required for oligomer organization (Kim *et al.*, 2003a). Other N-terminal hydrophobic elements may contribute to p26 structural organization, with the deleted residues 1-36 and 1-60 possessing 72.2% and 61.7% hydrophobicity, respectively, both higher than the 51% hydrophobicity of the p26 full-length sequence.

Truncated p26 consisting of only the α-crystallin domain existed predominantly as dimers and monomers. The α-crystallin domains of many sHSPs assemble into dimers rather than larger oligomers, while oligomer assembly and dynamics are controlled by the N-terminal region (Koteiche and McHaourab, 2002; Stromer *et al.*, 2004). For example, analysis of yeast Hsp26 revealed that the N-terminal region is critical for formation of Hsp26 large oligomers (Stromer *et al.*, 2004). This is consistent with data presented in

this thesis and corroborates the importance of the p26 N-terminal region in oligomer assembly. An interesting point is that sHSP oligomerization is insensitive to sequence extension at the N-terminus (Leroux *et al.*, 1997b; Muchowski *et al.*, 1997). For example, adding a tail of 4 kDa to the *C. elegans* Hsp16-2 N-terminal did not disturb oligomerization, and after fusion of the 42 kDa maltose-binding protein to the N-terminus of αB-crystallin, the recombinant protein remained as high molecular mass oligomers displaying full chaperone function (Leroux *et al.*, 1997b; Muchowski *et al.*, 1997). In this work, an elongation of approximately 5 kDa to the WT p26 N-terminus did not interfere with oligomer assembly dramatically.

Removal of 10 C-terminal residues had little effect on p26. However, deleting the entire C-terminal extension including the conserved I/V-X-I/V (as VPI for p26) reduced oligomerization more dramatically, and a similar case occurred for *B. japonicum* HspH (Studer *et al.*, 2002). The p26 C-terminal extension influences oligomer assembly less than the N-terminal region. In comparison, pea Hsp17.7 variants lacking 3, 5, or 10 amino acid residues of the C-terminal fail to form full size oligomers (Kirschner *et al.*, 2000), while C-terminal truncated *B. japonicum* HspB and HspC without the conserved IXI motif exist as small oligomers (Narberhaus, 2002). Deletion of the last 11 or more C-terminal residues of αA-crystallin significantly decreases oligomeric mass, although removing up to 10 residues causes little change (Thampi and Abraham, 2003). High resolution crystal structures of *Ta* Hsp16.9 reveal inter-dimer interactions between hydrophobic residues around the C-terminal extension β10 strand with a hydrophobic patch on the surface of α-crystallin β4, β5 and β8 strands, indicating the involvement of

C-terminal sequence encompassing the conserved IXI motif in sHSP oligomerization (van Montfort *et al.*, 2001b; Giese and Vierling, 2002; Kim *et al.*, 2003a).

Single site mutations to the conserved α-crystallin domain of p26 resulted in generally smaller oligomers than for WT p26, with F112R oligomers exhibiting a much narrower range than WT. Intriguingly, the largest oligomers obtained for mutant R114A were 500 KDa, contrasting to R116C αA-crystallin and R120G αB-crystallin, mutants with molecular mass of >2 MDa and 1.4 MDa, respectively (Bova *et al.*, 1999a; Andley *et al.*, 2002). Clearly, modification of this highly conserved arginine residue had less effect on p26 oligomer formation than for the α-crystallins.

4.3 Chaperone activity of p26

sHSPs are effective molecular chaperones, recognizing and interacting with nonnative rather than native structures. The chaperone activity of p26 towards heat-induced citrate synthase aggregation and inactivation and DTT-induced insulin aggregation was determined. Citrate synthase, a model protein for the characterization of chaperone activity has been used extensively for studies of molecular chaperones including GroEL, HSP90 and sHSPs (Muchowski and Clark, 1998). Citrate synthase is inactivated at 43 °C, a temperature relevant to physiological heat shock conditions, and it subsequently forms aggregation-prone intermediates, thereby allowing examination of sHSP chaperone activity (Buchner *et al.*, 1998; Rajaraman *et al.*, 2001). Insulin is another ideal substrate for investigation of sHSP chaperone function. The β-chain of insulin aggregates upon reduction of the disulfide bond between the α- and β-chains, increasing solution turbidity. sHSPs bind to the unfolding β-chain and reduce aggregation (Haslbeck *et al.*, 1999). This assay allows examination of p26 substrate aggregation kinetics in the absence

of heat shock, and mimics non-thermal stressful conditions that *Artemia* cysts experience during development.

In contrast to GroEL, which accommodates one or two substrate molecules per 14 subunits (Houry *et al.*, 1999), sHSPs usually have a much higher binding capacity. A 2:1 molar ratio of chaperone to substrate (monomer to monomer) often prevents most protein aggregation (Studer and Narberhaus, 2000). Native p26 from *Artemia* and recombinant p26 from bacteria efficiently prevented thermally induced citrate synthase aggregation and chemically induced insulin aggregation, with a molar ratio of p26 to substrate of 4:1 for the former (monomer to dimer) and 0.4:1 for the latter. The former contrasts a molar ratio of 7:1 for *C. elegans* Hsp16-2 and 8:1 for *Mt* Hsp16.3 to citrate synthase (Chang *et al.*, 1996; Leroux *et al.*, 1997b), and a molar ratio of 3:1 for αA- and αB-crystallins to the same substrate (Santhoshkumar and Sharma, 2001). The relative binding capacity of sHSPs for DTT-sensitive proteins ranges from 2:1 (sHSPs to insulin or α-lactalbumin) to 10:1 (sHSPs to ovotransferrin) (Lindner *et al.*, 1998). It is reasonable to speculate that p26 binding capability in *Artemia* cysts equals values observed *in vitro*, and considerable amounts of protein can be stored by interacting with p26. Due to the abundance of p26 in encysted embryos, this provides a large reservoir of proteins for renaturation under permissive conditions as *Artemia* resumes development.

Neither BSA nor IgG significantly affected the aggregation or inactivation kinetics of target proteins, indicating that effects observed with p26 are due to its chaperone activity instead of non-specific protein interactions. However, chaperoning by modified p26 was compromised. p26 variants either composed of only the α-crystallin domain or without the N-terminal region were relatively poor chaperones in comparison with WT, and

activity decreased as truncation increased. The single site mutation R114A led to a considerable loss of p26 chaperone ability. Incubation of R114A p26 with thermally denatured citrate synthase did not inhibit aggregation as well as WT, nor did R114A p26 suppress citrate synthase aggregation effectively until its concentration was increased to 1200 nM when the molar ratio of chaperone to substrate was 8:1. Even at concentrations of R114A p26 higher than 1200 nM, substrate aggregation remained the same, indicating the mutant had reached its maximum ability to chaperone citrate synthase at this concentration. The same results were found for the inhibition of DTT-induced insulin aggregation, where R114A p26 concentrations of 1.6 μM or higher were required for effective chaperoning. That R114A lost substantial *in vitro* chaperone capability against thermal or chemical stress suggests that the substrate-binding site is impaired, preventing effective contact between the chaperone and substrates.

Among three internal deletions, "R" was most detrimental and had the lowest capability to suppress protein aggregation. Although both R114A and "R" exhibited reduced chaperone activity, they functioned as chaperones to a certain extent, in contrast to either R116C αA-crystallin whose chaperone activity is almost completely abolished, or R120G αB-crystallin which enhances the kinetics and extent of substrate aggregation (Kumar *et al.*, 1999; Chavez-Zobel *et al.*, 2003). Although α-crystallins usually function for the entire lifespan of mammalian, a single site mutation may bring highly pathological effects. By comparison, p26 seems more resistant to modification of the conserved arginine residue than its mammalian counterparts, and our data suggest p26 may be more stable than other sHSPs.

4.4 Secondary structure of p26

WT p26 from *Artemia* and bacteria possess similar secondary structure elements, while most p26 variants exhibit increased α-helical conformations and decreased β-structure. This was especially remarkable for R114A, whose α-helical percentage increased by 8%. Residue R114 of p26 is in the β7 strand which is buried in the α-crystallin domain, and it has no apparent access to aqueous environments as indicated in Fig. 37. Mutation of R114A may disrupt the organization of the β-strand-enriched α-crystallin domain and decrease β-strand amounts, as occurred when αB-crystallin was modified in the same fashion (Bova *et al.*, 1999a). Charged, buried amino acid residues are usually paired with a residue of opposite charge by forming salt bridges, this of structural importance, and addition or removal of these residues leads to protein conformational changes (Shroff *et al.*, 2000). For example, T4 lysozyme is destabilized upon positioning of an unpaired, charged residue in its hydrophobic core (Xu *et al.*, 1998). R114 of p26 is a charged, bulky residue which was replaced by the small uncharged alanine, potentially leading to destabilization of p26 structure. Although p26 oligomerization remained largely unchanged upon mutation of R114A, the secondary structure was modified and chaperone activity was compromised.

Deletion of the arginine-enriched stretch 36RPFRRRMMRR45 in the N-terminal region led to similar consequences, within the α-helical percentage increased by 7.2%. This stretch is located in a random coil of the p26 N-terminal region, and deleting the sequence may produce new α-helices, thereby altering p26 secondary structure composition.

4.5 Intrinsic p26 fluorescence and surface hydrophobicity

Fluorescence emission is observed when electrons return from the excited state to the ground state after proteins absorb light, and is sensitive to microenvironment changes of chromophores, such as side chains of aromatic residues especially tryptophans. Protein conformation perturbations may lead to large changes in fluorescence emission, with shifts in wavelength and alterations in intensity detected upon protein unfolding and refolding. Protein fluorescence is thus an excellent marker for investigation of protein conformational changes. All p26 variants had a reduction in fluorescence intensity as compared to WT, implying altered microenvironments for tryptophan residues. This indicates that mutations introduced changes to p26 tertiary structure. A significant decrease in fluorescence intensity occurred for mutants R114A and "R", suggesting aromatic residues especially tryptophans in each protein are in more flexible environments with increased mobility than for WT p26, as was reported for R116C αA-crystallin and R114A αB-crystallin (Kumar *et al.*, 1999).

Surface hydrophobicity is an important parameter for chaperone-substrate interaction, although not the sole determinant (Reddy *et al.*, 2000). ANS is a hydrophobic molecule that becomes highly fluorescent upon binding to protein hydrophobic sites or patches, providing a sensitive measure of protein hydrophobicity. ANS binding showed considerably reduced surface hydrophobicity for R114A, with changes to other α-crystallin domain mutants more moderate. This is consistent with changes in the intrinsic fluorescence spectra for mutant R114A, both indicating that this mutation caused a stronger conformational change in p26 than did other α-crystallin domain mutations. Internal deletion of multiple arginine residues had consequences similar to those caused

by the R114A mutation, although the deletion was in the N-terminal region. Arginine residues are positively charged, thus a decrease in surface hydrophobicity upon deletion of an arginine-enriched stretch, as occurred in the "R" mutant, implies reorganization of protein tertiary structure.

4.6 Nuclear migration of p26

Some sHSPs enter nuclei upon stress, although their mission within the organelle remains elusive. For instance, a subpopulation of Hsp20 migrates into the nuclei of cultured rat neonatal cardiac myocytes during heat stress, indicating a role for the protein in myocyte nuclei (van de Klundert and de Jong, 1999). αB-crystallin and Hsp27 are nuclear speckle components in unstressed, transcriptionally active cells, and Hsp27 is found in the nucleolus, implying these sHsps have similar but not completely overlapping roles in the nucleus (van den IJssel *et al.*, 2003). Mutation R120G in αB-crystallin inhibits nuclear speckle localization, potentially affecting the nuclear functions of αB-crystallin and the RNA splicing machinery, and contributing to development of cardiomyopathy and cataract phenotypes (van den IJssel *et al.*, 2003).

p26 is found in *Artemia* nuclei during diapause and upon stress including heat shock, anoxia *in vivo*, and low pH *in vitro* (Willsie and Clegg, 2001). The movement of p26 into nuclei implies association with specific nuclear components, such as protein assemblies required for DNA replication, transcription, RNA splicing and genome maintenance. The majority of nuclear p26 and a lamin share similar distributions in *Artemia* nuclei and are associated with the nuclear matrix, implying that p26 stabilizes nuclear matrix proteins (Willsie and Clegg, 2002). p26 sequence analysis failed to reveal a typical nuclear localization signal (NLS) consisting of either a short stretch of lysines (PKKKRKV) or a

bipartite signal where a spacer region of 10 to 20 amino acid residues separates a pair of basic clusters (KRPAATKKAGQAKKKK) (Liang *et al.*, 1997a). In contrast, the variable p26 N-terminal region is uniquely enriched in arginine, which potentially exists as an unusual cellular localization signal, the absence of which may disrupt p26 intracellular distribution. However, removal of these arginines resulted in the strong tendency of modified p26 to translocate into transiently transfected COS-1 nuclei, indicating the arginine residues are not required for translocation. The single site substitution R114A had similar consequences for nuclear migration. This is in contrast to mutation R116C of αA-crystallin, which is equivalent to R114A of p26, but does not modify the cytoplasmic localization of αA-crystallin (Andley *et al.*, 2002).

Interestingly, a novel R49C αA-crystallin variant is abnormally localized to the nucleus of human lens epithelial cells (HLE B-3) and fails to protect cells from staurosporine-induced apoptosis. R49C is the first dominant nuclear cataract mutation located outside the phylogenetically conserved sHSP α-crystallin domain (Mackay *et al.*, 2003).

How p26 is translocated into nuclei remains unknown. One proposal is that decreased oligomer assembly permits p26 movement through nuclear pore complexes by simple diffusion. However, modified p26 with reduced oligomer size due to C-terminal truncation remained in the cytoplasm, and mutant R114A existing as oligomers of similar size to that of WT readily entered nuclei, suggesting that simple diffusion does not occur. In addition, p26 oligomers in heat shocked and control cysts including those from nuclei were similar, even though their mass was maintained in reduced pH, a condition promoting p26 translocation into *Artemia* nuclei *in vivo* and *in vitro*. Thus, the migration of p26 from cytoplasm into nuclei depends on a mechanism other than oligomer mass

reduction, although the transient dissociation into small oligomers followed by rapid reassociation within nuclei is possible.

4.7 Comparative modeling of p26

According to the model generated in this study, the p26 monomer likely has a buried N-terminal region, a partially exposed α-crystallin domain and a solvent-accessible C-terminal extension, this a general pattern of diverse sHsps (Treweek *et al.*, 2003). Because of its hydrophobic character, the p26 N-terminal region may be involved in oligomer formation. The α-crystallin domain is an immunoglobulin-like fold as a β-sandwich, composed of eight β-strands organized into two antiparallel β-sheets. The C-terminal extension is polar, flexible and thought to maintain p26 oligomer solubility and stability, thereby minimizing protein precipitation.

There are deviations in the number and size of loops in the polypeptide backbone between *Ta* Hsp16.5 and the modeled p26. The most obvious difference is the loop, designated as 3 for p26, which connects β5 and β7 strands and is smaller for p26 than for *Ta* Hsp16.9. *Ta* Hsp16.9 monomers are stabilized at the dimer interface by interactions among residues of the long loop extending from the α-crystallin β-strands (van Montfort *et al.*, 2001b). By analogy, loop 3 of p26 may be involved in structural stability and dimer formation, an interesting possibility that deserves further study.

Small oligomers such as dimers are the main building blocks of sHsps and subunit-subunit interactions are strongest along the dimerization interface (Sobott *et al.*, 2002). *Ta* Hsp16.9 dimers form tetramers using β7 strands and the dimerization loops from two monomers with ordered N-terminal arms (van Montfort *et al.*, 2001b). In this work, the single point mutation F112R which substituted the conserved hydrophobic phenylalanine

with a positively charged arginine, interfered with oligomerization and resulted in relatively small but active p26 complexes. In a similar case, the substitution of F94 of *B. japonicum* HspH, a residue corresponding to F112 of p26 and potentially involved in subunit-subunit interactions, resulted in oligomers of dramatically reduced size (Lentze *et al.*, 2003). Thus, F112, a residue located in the β7 strand of p26 and close to loop 3, is possibly involved in inter-subunit interaction. Internal deletion "G" which lacks loop 1 did not disturb p26 oligomerization dramatically, and this variant exhibited relatively good chaperone activity. This suggests loop 1 has limited involvement in protein stability and function. The structural and functional importance of loop 2 and loop 4 in p26 remain to be determined.

4.8 Conclusions

Site-directed mutagenesis is a powerful approach to explore relationships between protein structure and function. Truncation of either the N- or C-terminus of p26 affected oligomerization and chaperone activity, although to different extents, with the N-terminal region of critical relevance for assembly of large oligomers. For single site mutations, dramatic effects were observed when the highly conserved, positively charged residue R114, located in the central α-crystallin domain of p26, was replaced by alanine. There are several possibilities for the involvement of this conserved residue in p26 structure and function. A salt bridge formed between R114 and another residue in the protein may be important for structural integrity. Disruption of such an ionic interaction within p26 explains the altered secondary structure, disturbed tertiary structures, reduced surface hydrophobicity, and compromised chaperone activity. Alternatively, interference of ionic interactions between p26 and denaturing substrates is another possibility. Even though it

seems that binding of substrates mainly depends on hydrophobic interactions, contributions of electrostatic forces cannot be excluded.

The oligomeric range of mutant F112R was narrower than for R114A, but its chaperone activity was higher, demonstrating the absence of a positively proportional relationship between oligomerization and chaperone function. As the least effective mutants in this study, R114A and "R" exhibited significantly decreased chaperone function *in vivo* and *in vitro*, but their protection capabilities remained relatively high. This indicates the robust nature of p26 and that it can effectively accommodate critical single site mutations and multiple deletions.

p26 functions as an effective sHSP not only protecting substrate against aggregation *in vitro* but conferring thermotolerance on bacteria cells *in vivo*. It is thus reasonable to speculate that in oviparously developing *Artemia* cysts p26 prevents irreversible denaturation of intracellular proteins, which may be refolded by other molecular chaperones in an ATP-dependent manner once favorable conditions are resumed. However, p26 chaperone efficiency is still low in comparison with WT α-crystallins which account for approximately one-third of the total soluble lens protein and maintain refractive power (Santhoshkumar and Sharma, 2001). Of multicellular eukaryotes, *Artemia* cysts are among the most resistant to environmental insults, surviving years of continuous anoxia, desiccation and temperature extremes. This undoubtedly necessitates molecular chaperone function and the sHSP, p26, which is produced in large amounts in oviparous embryos, is very likely an important component of this impressive stress resistance.

Appendix I. Solutions and Recipes

Solutions for SDS-Polyacrylamide Gel Electrophoresis

1A: 39 g acrylamide
1 g bis
20 ml glycerol
Add ddH_2O to 100 ml.

1B: 18.3 g Tris
2.5 ml 20% SDS stock
Add ddH_2O to 100 ml, pH 8.8.

1C: 0.1 ml TEMED
Add ddH_2O to 50 ml.

2B: 6.0 g Tris
2.5 ml 20% SDS stock
Add ddH_2O to 100 ml, pH 6.8.

2C: 0.2 ml TEMED
Add ddH_2O to 10 ml.

1D: 50 mg Ammonium persulfate
Add ddH_2O to 10 ml.

Running Buffer (4L)
12.0 g Tris
57.6 g glycine
8.0 ml 20% SDS stock
Add ddH_2O to 4L. Adjust to pH 8.1-8.3.

Coomassie Brilliant Blue Staining Solution (2L)
10 g Coomassie Brilliant Blue R-250
140 ml acetic acid
800 ml methanol
Add ddH_2O to 2L. Stir 1 h, filter through miracloth.

Destaining Solution (2L)
400 ml methanol
140 ml acetic acid
100 ml glycerol
Add ddH_2O to 2L. Filter through miracloth.

4×Treatment Buffer (20ml)
0.6 g Tris
1.6 g SDS
8.0 ml glycerol
4.0 ml 2-mercaptoethanol
Add ddH_2O to 20 ml. Adjust to pH 6.8 with HCl.

Solutions for Western Blotting and Immunodetection

Blot Electrode Buffer (4L)
12.0 g Tris
57.6 g glycine
800 ml methanol
Add ddH_2O to 4L.

TBS Buffer (1L)
1.21 g Tris
8.18 NaCl
Add ddH_2O to 1L. Adjust pH to 7.4 with HCl.

TBS-Tween Buffer (1L)
999ml TBS buffer
1ml Tween 20

HST Buffer (1L)
1.21 g Tris
58.4 g NaCl
5.0 ml Tween 20
Add ddH_2O to 1L. Adjust pH to 7.4 with HCl.

2% Ponceau S Solution
2.0 g Ponceau S
30 g Trichloroacetic acid (TCA)
Add ddH_2O to 100 ml. Dilute 1:9 in ddH_2O for staining blots.

Developer
100 ml Developer
Add ddH_2O to 500 ml.

Fixer
124.5 ml Solution A
13.7 ml Solution B
Add ddH_2O to 500 ml.

Media for Bacteria Culture
LB medium
10 g Tryptone
5 g Yeast extract
10 NaCl
Add ddH_2O to 1L, adjust pH to 7.0 with NaOH.
1.5% agar for solid broth. Autoclave at 121 °C for 15 min.

NZY^+ medium
10g NZ Amine (casein hydrolysate)
5 g Yeast extract

5 g NaCl
Add ddH_2O to 1L, adjust pH to 7.5 with NaOH. Autoclave at 121 °C for 15 min.

Solutions for DNA Gel Electrophoresis

6×DNA Loading Buffer
0.25% Bromophenol blue
0.25% Xylene cynol
15% Ficoll (type 400)
Add ddH_2O.

50×TAE
242 g Tris
57.1 ml Glacial acetic acid
100 ml 0.5 M EDTA, pH 8.0
Add ddH_2O to 1L.

DNA Storage Solution

TE Buffer
10 mM Tris
1 mM EDTA
Add ddH_2O. Adjust pH to 8.0 with HCl.

Solutions for Immunofluorescence Staining of COS-1 Cells

5×PBS
40 g NaCl
1.0 g KCl
5.75 Na_2HPO_4
1 g KH_2PO_4
Add ddH_2O to 1L, pH 7.3-7.4 as mixed.

Triton X-100 PBS
100 ml PBS
200 µl Triton X-100

Paraformaldehyde Fixative
25 ml PBS
1g paraformaldehyde.

Solutions for *Artemia* Nuclei Isolation

10×HPC Buffer (500 ml)
0.735 g $CaCl_2 \cdot 2H_2O$
0.075 g PIPES
Add ddH_2O to 500 ml. Adjust pH to 6.5 with NaOH. Autoclave.

1×HPC Solution

50 ml 10×HPC
32 ml Hexylene glycol
418 ml ddH_2O

10×NaCl/$MgCl_2$/Tris Solution (100 ml)
8.7 g NaCl
2.8 g $MgCl_2 \cdot 6H_2O$
1.9 g Tris
Add ddH_2O to 100 ml. Adjust pH to 6.5 with HCl. Autoclave.

Percoll Solution
188 ml Percoll
25 ml 10× NaCl/$MgCl_2$/Tris Solution
37 ml autoclaved ddH_2O

Solutions for Protein Purification
1×Extraction/Wash Buffer
50 mM Na_3PO_4
300 mM NaCl
Add ddH_2O. Adjust pH to 7.5.

1×Elution Buffer
50 mM Na_3PO_4
300 mM NaCl
150 mM Imidazole
Add ddH_2O. Adjust pH to 7.5.

Protease Inhibitor Cocktail
Solution A (5 ml)
5 mg Leupeptin
5 mg Soybean trypsin inhibitor
Dissolve in PIPES buffer.

Solution B (5 ml)
5 mg Pepstatin A
10 mg PMSF
Dissolve in methanol.

Appendix II. Prokaryotic Expression Vectors Applied in p26 cDNA Cloning

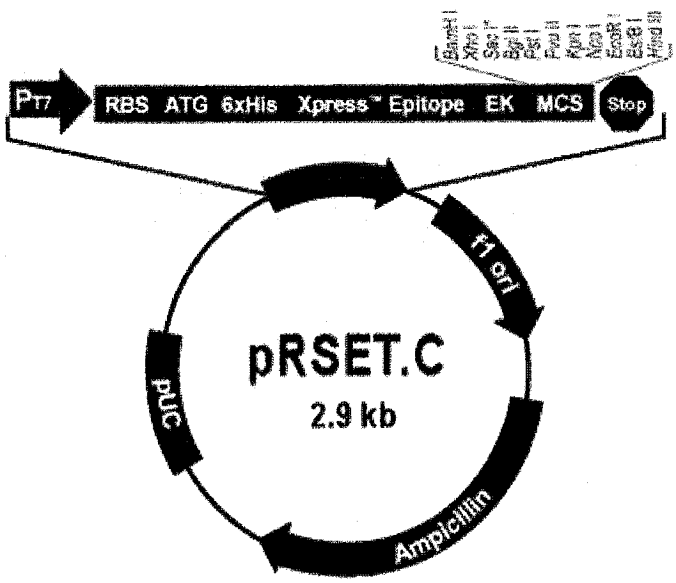

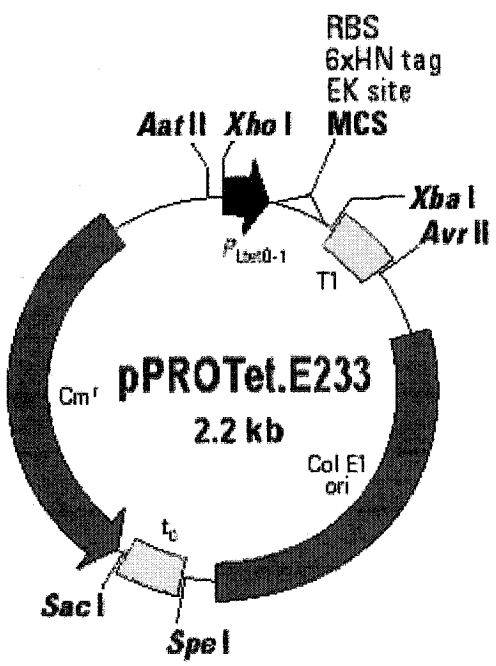

Appendix III. Eukaryotic Expression Vectors Applied in p26 cDNA Cloning

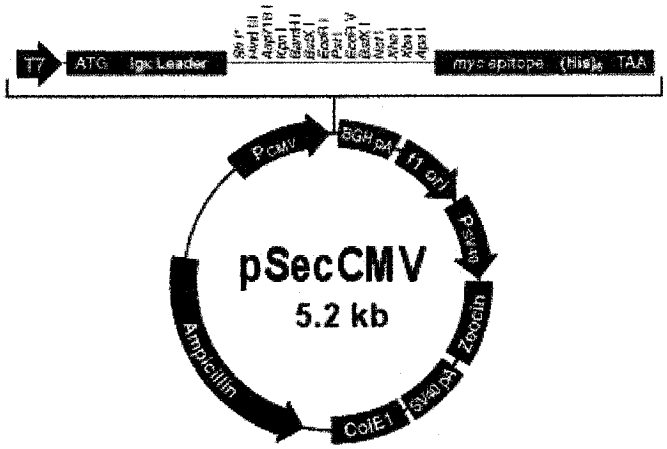

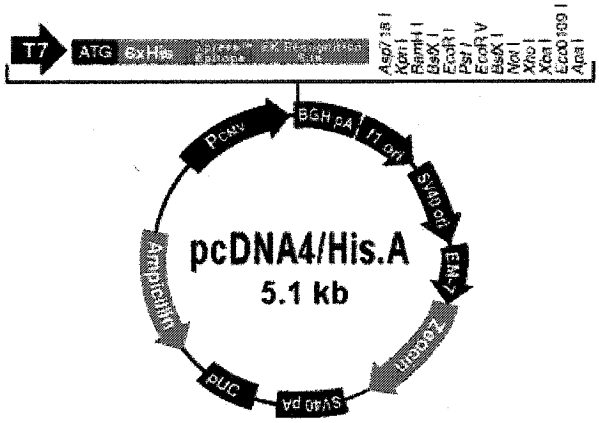

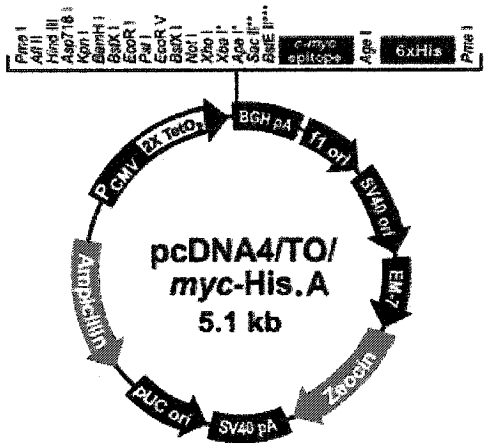

Appendix IV. Schematic Representation of Single Amino Acid Substitutions and Internal Deletions of p26

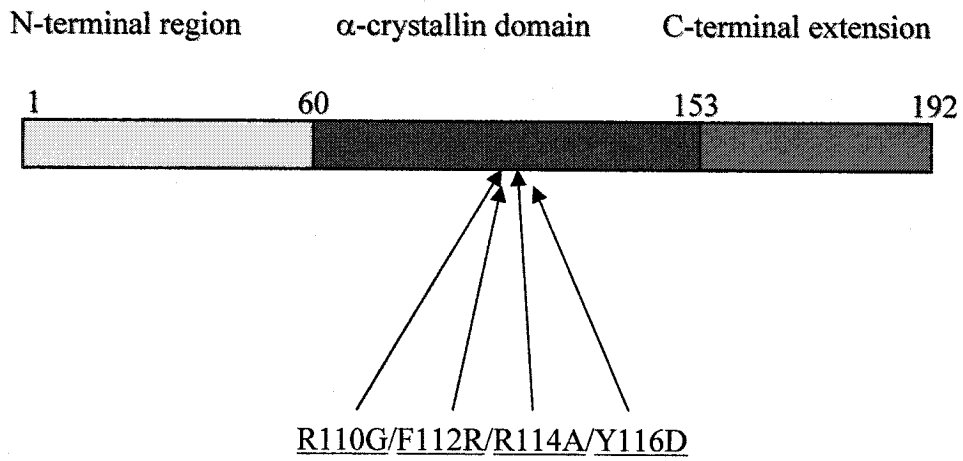

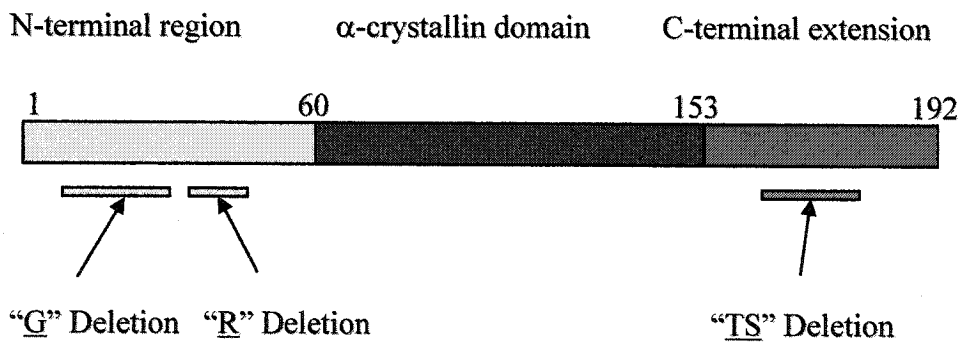

Appendix V. Sequence Alignment of *Ta* Hsp16.9 and p26

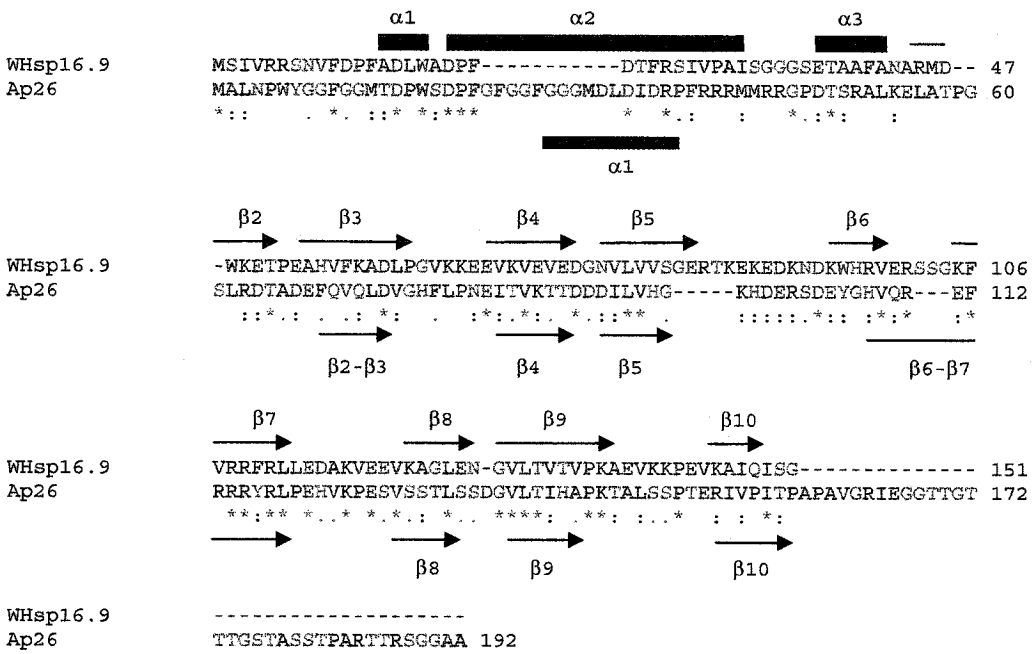

The amino acid sequences of *Ta* Hsp16.9 and p26 were analyzed by CLUSTAL W (1.82). WHsp16.9, *Triticum aestivum* Hsp16.9, 1GME_A; Ap26, *Artemia franciscana* p26, AAB87967. (-) no amino acid residue; (*) identical residues; (:) conserved substitution; (.) semi-conserved substitution. The secondary structure of *Triticum aestivum* Hsp16.9 is depicted above the alignment (van Montfort *et al.*, 2001b), while the predicted secondary structure of p26 is below the alignment. Amino acid residues in red, small and hydrophobic; blue, acidic; magenta, basic; green, residues containing a hydroxyl or amine group. Residue number is indicated on the right.

References

Abulimiti, A., Fu, X., Gu, L., Feng, X. and Chang, Z. 2003. *Mycobacterium tuberculosis* Hsp16.3 nonamers are assembled and re-assembled via trimer and hexamer intermediates. J Mol Biol. **326**: 1013-1023.

Andley, U. P., Mathur, S., Griest, T. A. and Petrash, J. M. 1996. Cloning, expression, and chaperone-like activity of human alpha A-crystallin. J. Biol. Chem. **271**: 31973-31980.

Andley, U. P., Patel, H. C. and Xi, J. H. 2002. The R116C mutation in alpha A-crystallin diminishes its protective ability against stress-induced lens epithelial cell apoptosis. J Biol Chem. **277**: 10178-10186.

Bai, F., Xi, J. H., Wawrousek, E. F., Fleming, T. P. and Andley, U. P. 2003. Hyperproliferation and p53 status of lens epithelial cells derived from alphaB-crystallin knockout mice. J Biol Chem. **278**: 36876-36886.

Basha, E., Lee, G. J., Breci, L. A., Hausrath, A. C., Buan, N. R., Giese, K. C. and Vierling, E. 2004. The identity of proteins associated with a small heat shock protein during heat stress *in vivo* indicates that these chaperones protect a wide range of cellular functions. J Biol Chem. **279**: 7566-7575.

Bera, S., Thampi, P., Cho, W. J. and Abraham, E. C. 2002. A positive charge preservation at position 116 of alpha A-crystallin is critical for its structural and functional integrity. Biochemistry. **41**: 12421-12426.

Bloemendal, M., Toumadje, A. and Johnson, W. C. 1999. Bovine lens cyrstallins do contain helical structures: a circular dichroism study. Biochim. Biophys. Acta. **1432**: 234-238.

Bova, M. P., Ding, L. L., Horwitz, J. and Fung, B. K. 1997. Subunit exchange of alphaA-crystallin. J Biol Chem. **272**: 29511-29517.

Bova, M. P., Yaron, O., Huang, Q., Ding, L., Haley, D. A., Stewart, P. L. and Horwitz, J. 1999. Mutation R120G in alphaB-crystallin, which is linked to a desmin-related myopathy, results in an irregular structure and defective chaperone-like function. Proc Natl Acad Sci U S A. **96**: 6137-6142.

Buchner, J., Grallert, H. and Jakob, U. 1998. Analysis of chaperone function using citrate synthase as nonnative substrate protein. Methods in Enzymology. **290**: 323-338.

Chang, Z., Primm, T. P., Jakana, J., Lee, I. H., Serysheva, I., Chiu, W., Gilbert, H. F. and Quiocho, F. A. 1996. *Mycobacterium tuberculosis* 16-kDa antigen

(Hsp16.3) functions as an oligomeric structure *in vitro* to suppress thermal aggregation. J Biol Chem. **271**: 7218-7223.

Chavez-Zobel, A. T., Loranger, A., Marceau, N., Theriault, J. R., Lambert, H. and Landry, J. 2003. Distinct chaperone mechanisms can delay the formation of aggresomes by the myopathy-causing R120G alphaB-crystallin mutant. Hum Mol Genet. **12**: 1609-1620.

Clegg, J. S., Jackson, S. A., Liang, P. and MacRae, T. H. 1995. Nuclear-cytoplasmic translocations of protein p26 during aerobic-anoxic transitions in embryos of *Artemia franciscana*. Exp. Cell Res. **219**: 1-7.

Clegg, J. S., Jackson, S. A. and Popov, V. I. 2000. Long-term anoxia in encysted embryos of the crustacean, *Artemia franciscana*: viability, ultrastructure, and stress proteins. Cell Tissue Res. **301**: 433-446.

Clegg, J. S., Jackson, S. A. and Warner, A. H. 1994. Extensive intracellular translocations of a major protein accompany anoxia in embryos of *Artemia franciscana*. Exp. Cell Res. **212**: 77-83.

Clegg, J. S., Willsie, J. K. and Jackson, S. A. 1999. Adaptive significance of a small heat shock/alpha-crystallin protein (p26) in encysted embryos of the brine shrimp, *Artemia franciscana*. Amer. Zool. **39**: 836-847.

Cobb, B. A. and Petrash, J. M. 2000a. Characterization of alpha-crystallin-plasma membrane binding. J. Biol Chem. **275.**: 6664-6672.

Cobb, B. A. and Petrash, J. M. 2000b. Structural and functional changes in the alpha A-crystallin R116C mutant in hereditary cataracts. Biochemistry. **39**: 15791-15798.

Crack, J. A., Mansour, M., Sun, Y. and MacRae, T. H. 2002. Functional analysis of a small heat shock/alpha-crystallin protein from *Artemia franciscana*. Oligomerization and thermotolerance. Eur J Biochem. **269**: 933-942.

Day, R. M., Gupta, J. S. and MacRae, T. H. 2003. A small heat shock/alpha-crystallin protein from encysted *Artemia* embryos suppresses tubulin denaturation. Cell Stress Chaperones. **8**: 183-193.

de Jong, W. W., Caspers, G. J. and Leunissen, J. A. 1998. Genealogy of the alpha-crystallin--small heat-shock protein superfamily. Int J Biol Macromol. **22**: 151-162.

Derham, B. K. and Harding, J. J. 1999. Alpha-crystallin as a molecular chaperone. Prog Retin Eye Res. **18**: 463-509.

Diamant, S., Eliahu, N., Rosenthal, D. and Goloubinoff, P. 2001. Chemical chaperones regulate molecular chaperones *in vitro* and in cells under combined salt and heat stresses. J Biol Chem. **276**: 39586-39591.

Drinkwater, L. E. and Clegg, J. S. (1991). Experimental biology of cyst diapause. *Artemia* biology. Browne, R. A., Sorgeloos, P. and Trotman, C. N. A. Boca Raton, Florida, CRC Press: 93-117.

Ehrnsperger, M., Lilie, H., Gaestel, M. and Buchner, J. 1999. The dynamics of Hsp25 quaternary structure. Structure and function of different oligomeric species. J Biol Chem. **274**: 14867-14874.

Ellis, R. J. 1990. The molecular chaperone concept. Semin Cell Biol. **1**: 1-9.

Feil, I. K., Malfois, M., Hendle, J., van Der Zandt, H. and Svergun, D. I. 2001. A novel quaternary structure of the dimeric alpha-crystallin domain with chaperone-like activity. J Biol Chem. **276**: 12024-12029.

Fernando, P., Megeney, L. A. and Heikkila, J. J. 2003. Phosphorylation-dependent structural alterations in the small hsp30 chaperone are associated with cellular recovery. Exp Cell Res. **286**: 175-185.

Friedrich, K. L., Giese, K. C., Buan, N. R. and Vierling, E. 2004. Interactions between small heat shock protein subunits and substrate in small heat shock protein-substrate complexes. J Biol Chem. **279**: 1080-1089.

Giese, K. C. and Vierling, E. 2002. Changes in oligomerization are essential for the chaperone activity of a small heat shock protein *in vivo* and *in vitro*. J Biol Chem. **277**: 46310-46318.

Goldfarb, L. G., Vicart, P., Goebel, H. H. and Dalakas, M. C. 2004. Desmin myopathy. Brain. **127**: 723-734.

Graf, P. C. F., Martinez-Yamout, M., VanHaerents, S., Lilie, H., Dyson, H. J. and Jakob, U. 2004. Activation of the redox-regulated chaperone Hsp33 by domain unfolding. J. Biol. Chem. **279**: 20529-20538.

Guex, N., Diemand, A. and Peitsch, M. C. 1999. Protein modeling for all. Trends Biochem Sci. **24**: 364-367.

Guex, N. and Peitsch, M. C. 1997. SWISS-MODEL and the Swiss-PdbViewer: an environment for comparative protein modelling. Electrophoresis. **18**: 2714-2723.

Haley, D. A., Bova, M. P., Huang, Q. L., McHaourab, H. S. and Stewart, P. L. 2000. Small heat-shock protein structures reveal a continuum from symmetric to variable assemblies. J Mol Biol. **298**: 261-272.

Hand, S. C. 1998. Quiescence in Artemia franciscana embryos: reversible arrest of metabolism and gene expression at low oxygen levels. J Exp Biol. **201**: 1233-1242.

Haslbeck, M. 2002. sHsps and their role in the chaperone network. Cell Mol Life Sci. **59**: 1649-1657.

Haslbeck, M., Braun, N., Stromer, T., Richter, B., Model, N., Weinkauf, S. and Buchner, J. 2004. Hsp42 is the general small heat shock protein in the cytosol of *Saccharomyces cerevisiae*. Embo J. **23**: 638-649.

Haslbeck, M., Walke, S., Stromer, T., Ehrnsperger, M., White, H. E., Chen, S., Saibil, H. R. and Buchner, J. 1999. Hsp26: a temperature-regulated chaperone. Embo J. **18**: 6744-6751.

Hendrick, J. P. and Hartl, F. U. 1993. Molecular chaperone functions of heat-shock proteins. Annu Rev Biochem. **62**: 349-384.

Horúath, I., Glatz, A., Varvasovszki, V., Török, Z., Páli, T., Balogh, G., Kovács, E., Nádasdi, L., Benkö, S., Joó, F. and Vigh, L. 1998. Membrane physical state controls the signaling mechanism of the heat shock response in *Synechocystis* PCC 6803: identification of hsp27 as a "fluidity gene". Proc. Natl. Acad. Sci. USA. **95**: 3513-3518.

Houry, W. A., Frishman, D., Eckerskorn, C., Lottspeich, F. and Hartl, F. U. 1999. Identification of in vivo substrates of the chaperonin GroEL. Nature. **402**: 147-154.

Hsu, A. L., Murphy, C. T. and kenyon, C. 2003. Regulation of aging and age-related disease by DAF-16 and heat shock factor. Science. **300**: 1142-1145.

Irobi, J., Van Impe, K., Seeman, P., Jordanova, A., Dierick, I., Verpoorten, N., Michalik, A., De Vriendt, E., Jacobs, A., Van Gerwen, V., Vennekens, K., Mazanec, R., Tournev, I., Hilton-Jones, D., Talbot, K., Kremensky, I., Van Den Bosch, L., Robberecht, W., Van Vandekerckhove, J., Broeckhoven, C., Gettemans, J., De Jonghe, P. and Timmerman, V. 2004. Hot-spot residue in small heat-shock protein 22 causes distal motor neuropathy. Nat Genet. **36**: 597-601.

Jackson, S. A. and Clegg, J. S. 1996. The ontology of low molecular weight stress protein p26 during early development of the brine shrimp, *Artemia franciscana*. Develop. Growth Different. **38**: 153-160.

Kamradt, M. C., Chen, F. and Cryns, V. L. 2001. The small heat shock protein alpha B-crystallin negatively regulates cytochrome c- and caspase-8-dependent activation of caspase-3 by inhibiting its autoproteolytic maturation. J Biol Chem. **276**: 16059-16063.

Kamradt, M. C., Chen, F., Sam, S. and Cryns, V. L. 2002. The small heat shock protein alpha B-crystallin negatively regulates apoptosis during myogenic differentiation by inhibiting caspase-3 activation. J Biol Chem. **277**: 38731-38736.

Kedersha, N. L., Gupta, M., Li, W., Miller, I. and Anderson, P. 1999. RNA-binding proteins TIA-1 and TIAR link the phophorylation of eIF-2alpha to the assembly of mammalian stress granules. J. Cell Biol. **147**: 1431-1442.

Kim, K. K., Kim, R. and Kim, S. H. 1998. Crystal structure of a small heat-shock protein. Nature. **394**: 595-599.

Kim, R., Lai, L., Lee, H. H., Cheong, G. W., Kim, K. K., Wu, Z., Yokota, H., Marqusee, S. and Kim, S. H. 2003. On the mechanism of chaperone activity of the small heat-shock protein of *Methanococcus jannaschii*. Proc Natl Acad Sci U S A. **100**: 8151-8155.

Kirschner, M., Winkelhaus, S., Thierfelder, J. M. and Nover, L. 2000. Transient expression and heat-stress-induced co-aggregation of endogenous and heterologous small heat-stress proteins in tobacco protoplasts. Plant J. **24**: 397-411.

Koteiche, H. A. and McHaourab, H. S. 2002. The determinants of the oligomeric structure in Hsp16.5 are encoded in the alpha-crystallin domain. FEBS Lett. **519**: 16-22.

Koteiche, H. A. and McHaourab, H. S. 2003. Mechanism of chaperone function in small heat-shock proteins. Phosphorylation-induced activation of two-mode binding in alphaB-crystallin. J Biol Chem. **278**: 10361-10367.

Kumar, L. V., Ramakrishna, T. and Rao, C. M. 1999. Structural and functional consequences of the mutation of a conserved arginine residue in alphaA and alphaB crystallins. J Biol Chem. **274**: 24137-24141.

Laskey, R. A., Honda, B. M., Mills, A. D. and Finch, J. T. 1978. Nucleosomes are assemblied by an acidic protein which binds histones and transfers them to DNA. Nature. **275**: 416-420.

Lee, G. J. and Vierling, E. 2000. A small heat shock protein cooperates with heat shock protein 70 systems to reactivate a heat-denatured protein. Plant Physiol. **122**: 189-198.

Lee, S., Owen, H. A., Prochaska, D. J. and Barnum, S. R. 2000. HSP16.6 is involved in the development of thermotolerance and thylakoid stability in the

unicellular cyanobacterium, *Synechocystis sp.* PCC 6803. Curr. Microbiol. **40**: 283-287.

Lentze, N., Studer, S. and Narberhaus, F. 2003. Structural and functional defects caused by point mutations in the alpha-crystallin domain of a bacterial alpha-heat shock protein. J Mol Biol. **328**: 927-937.

Leroux, M. R., Ma, B. J., Batelier, G., Melki, R. and Candido, E. P. 1997a. Unique structural features of a novel class of small heat shock proteins. J Biol Chem. **272**: 12847-12853.

Leroux, M. R., Melki, R., Gordon, B., Batelier, G. and Candido, E. P. 1997b. Structure-function studies on small heat shock protein oligomeric assembly and interaction with unfolded polypeptides. J Biol Chem. **272**: 24646-24656.

Liang, P., Amons, R., Clegg, J. S. and MacRae, T. H. 1997a. Molecular characterization of a small heat shock/alpha-crystallin protein in encysted *Artemia* embryos. J Biol Chem. **272**: 19051-19058.

Liang, P., Amons, R., Macrae, T. H. and Clegg, J. S. 1997b. Purification, structure and *in vitro* molecular-chaperone activity of *Artemia* p26, a small heat-shock/alpha-crystallin protein. Eur J Biochem. **243**: 225-232.

Liang, P. and MacRae, T. H. 1997. Molecular chaperone and the cytoskeleton. J. Cell Sci. **110**: 1431-1440.

Liang, P. and MacRae, T. H. 1999. The synthesis of a small heat shock/alpha-crystallin protein in *Artemia* and its relationship to stress tolerance during development. Dev Biol. **207**: 445-456.

Lindner, R. A., Carver, J. A., Ehrnsperger, M., Buchner, J., Esposito, G., Behlke, J., Lutsch, G., Kotlyarov, A. and Gaestel, M. 2000. Mouse Hsp25, a small shock protein. The role of its C-terminal extension in oligomerization and chaperone action. Eur J Biochem. **267**: 1923-1932.

Lindner, R. A., Kapur, A., Mariani, M., Titmuss, S. J. and Carver, J. A. 1998. Structural alterations of alpha-crystallin during its chaperone action. Eur J Biochem. **258**: 170-183.

Litt, M., Kramer, P., LaMorticella, D. M., Murphey, W., Lovrien, E. W. and Weleber, R. G. 1998. Autosomal dominant congenital cataract associated with a missense mutation in the human alpha crystallin gene CRYAA. Hum Mol Genet. **7**: 471-474.

Mackay, D. S., Andley, U. P. and Shiels, A. 2003. Cell death triggered by a novel mutation in the alphaA-crystallin gene underlies autosomal dominant cataract linked to chromosome 21q. Eur J Hum Genet. **11**: 784-793.

MacRae, T. H. 2000. Structure and function of small heat shock/alpha-crystallin proteins: established concepts and emerging ideas. Cell Mol Life Sci. **57**: 899-913.

MacRae, T. H. 2003. Molecular chaperones, stress resistance and development in *Artemia franciscana*. Semin Cell Dev Biol. **14**: 251-258.

Malaviarachchi, K. (2002). Production and characterization of transgenic *Drosophila* synthesizing a small heat shock/alpha-crystallin protein from *Artemia*. Halifax, Biology Department, Dalhousie University.

Mogk, A., Deuerling, E., Vorderwulbecke, S., Vierling, E. and Bukau, B. 2003. Small heat shock proteins, ClpB and the DnaK system form a functional triade in reversing protein aggregation. Mol Microbiol. **50**: 585-595.

Morimoto, R. I. and Santoro, M. G. 1998. Stress-inducible responses and heat shock proteins: new pharmacological targets for cytoprotection. Nat. Biotechnol. **16**: 833-838.

Morrow, G., Inaguma, Y., Kato, K. and Tanguay, R. M. 2000. The small heat shock protein Hsp22 of *Drosophila melanogaster* is a mitochondrial protein displaying oligomeric organization. J Biol Chem. **275**: 31204-31210.

Morrow, G., Samson, M., Michaud, S. and Tanguay, R. M. 2004. Overexpression of the small mitochondrial Hsp22 extends *Drosophila* life span and increases resistance to oxidative stress. Faseb J. **18**: 598-599.

Muchowski, P. J., Bassuk, J. A., Lubsen, N. H. and Clark, J. I. 1997. Human alphaB-crystallin. Small heat shock protein and molecular chaperone. J Biol Chem. **272**: 2578-2582.

Muchowski, P. J. and Clark, J. I. 1998. ATP-enhanced molecular chaperone functions of the small heat shock protein human alphaB crystallin. Proc Natl Acad Sci U S A. **95**: 1004-1009.

Muchowski, P. J., Hays, L. G., Yates, J. R., 3rd and Clark, J. I. 1999. ATP and the core "alpha-Crystallin" domain of the small heat-shock protein alphaB-crystallin. J Biol Chem. **274**: 30190-30195.

Narberhaus, F. 2002. Alpha-crystallin-type heat shock proteins: socializing minichaperones in the context of a multichaperone network. Microbiology and Molecular Biology Reviews. **66**: 64-93.

Nover, L. and Scharf, K. D. 1997. Heat shock proteins and transcription factors. Cell Mol. Life Sci. **53**: 80-103.

Ohtsuka, K. and Hata, M. 2000. Molecular chaperone function of mammalian Hsp70 and Hsp40--a review. Int J Hyperthermia. **16**: 231-245.

Pasta, S. Y., Raman, B., Ramakrishna, T. and Rao Ch, M. 2003. Role of the conserved SRLFDQFFG region of alpha-crystallin, a small heat shock protein. Effect on oligomeric size, subunit exchange, and chaperone-like activity. J Biol Chem. **278**: 51159-51166.

Pasta, S. Y., Raman, B., Ramakrishna, T. and Rao, C. M. 2004. The IXI/V motif in the C-terminal extension of alpha-crystallins: alternative interactions and oligomeric assemblies. Molecular Vision. **10**: 655-662.

Perng, M. D., Cairns, L., van den, I. P., Prescott, A., Hutcheson, A. M. and Quinlan, R. A. 1999. Intermediate filament interactions can be altered by HSP27 and alphaB-crystallin. J Cell Sci. **112 (Pt 13)**: 2099-2112.

Pockley, A. G. 2003. Heat shock proteins as regulators of the immune response. The Lancet. **362**: 469-476.

Rajaraman, K., Raman, B., Ramakrishna, T. and Rao, C. M. 2001. Interaction of human recombinant alphaA- and alphaB-crystallins with early and late unfolding intermediates of citrate synthase on its thermal denaturation. FEBS Lett. **497**: 118-123.

Reddy, G. B., Das, K. P., Petrash, J. M. and Surewicz, W. K. 2000. Temperature-dependent chaperone activity and structural properties of human alphaA- and alphaB-crystallins. J Biol Chem. **275**: 4565-4570.

Rekas, A., Adda, C. G., Aquilina, J. A., Barnham, K. J., Sunde, M., Galatis, D., Williamson, N. A., Masters, C. L., Anders, R. F., Robinson, C. V., Cappai, R. and Carver, J. A. 2004. Interaction of the molecular chaperone alphaB-crystallin with alpha-synuclein: effects on amyloid fibril formation and chaperone activity. J. Mol. Biol. **340**: 1167-1183.

Ritossa, F. A. 1962. A new puffing pattern induced by temperature shock DNP in *Drosophila*. Experientia. **18**: 571-573.

Rogalla, T., Ehrnsperger, M., Preville, X., Kotlyarov, A., Lutsch, G., Ducasse, C., Paul, C., Wieske, M., Arrigo, A. P., Buchner, J. and Gaestel, M. 1999. Regulation of Hsp27 oligomerization, chaperone function, and protective activity against oxidative stress/tumor necrosis factor alpha by phosphorylation. J Biol Chem. **274**: 18947-18956.

Santhoshkumar, P. and Sharma, K. K. 2001. Analysis of alpha-crystallin chaperone function using restriction enzymes and citrate synthase. Mol Vis. **7**: 172-177.

Scharf, K. D., Heider, H., Höhfeld, I., Lyck, R., Schmidt, E. and Nover, L. 1998. The tomato Hsf system: HsfA2 needs interaction with HsfA1 for efficient nuclear import and may be located in cytoplasmic heat stress granules. Mol. Cell. Biol. **18**: 2240-2251.

Schwede, T., Kopp, J., Guex, N. and Peitsch, M. C. 2003. Swiss-Model: an automated protein homology-modeling server. Nucleic Acids Res. **31**: 3381-3385.

Shroff, N. P., Cherian-Shaw, M., Bera, S. and Abraham, E. C. 2000. Mutation of R116C results in highly oligomerized alphaA-crystallin with modified structure and defective chaperone-like function. Biochemistry. **39**: 1420-1426.

Singh, K., Groth Vasselli, B. and Farnsworth, P. N. 1998. Interaction of DNA with bovine lens alpha-crystallin: its function implications. Int. J. Biol. Macromol. **22**: 315-320.

Sobott, F., Benesch, J. L., Vierling, E. and Robinson, C. V. 2002. Subunit exchange of multimeric protein complexes. Real-time monitoring of subunit exchange between small heat shock proteins by using electrospray mass spectrometry. J Biol Chem. **277**: 38921-38929.

Stromer, T., Fischer, E., Richter, K., Haslbeck, M. and Buchner, J. 2004. Analysis of the regulation of the molecular chaperone Hsp26 by temperature-induced dissociation: the N-terminal domail is important for oligomer assembly and the binding of unfolding proteins. J Biol Chem. **279**: 11222-11228.

Studer, S. and Narberhaus, F. 2000. Chaperone activity and homo- and hetero-oligomer formation of bacterial small heat shock proteins. J Biol Chem. **275**: 37212-37218.

Studer, S., Obrist, M., Lentze, N. and Narberhaus, F. 2002. A critical motif for oligomerization and chaperone activity of bacterial alpha-heat shock proteins. Eur J Biochem. **269**: 3578-3586.

Takemoto, L., Emmons, T. and Horwitz, J. 1993. The C-terminal region of alpha-crystallin: involvement in protection against heat-induced denaturation. Biochem. J. **294**: 435-438.

Takeuchi, N., Ouchida, A. and Kamei, A. 2004. C-terminal truncation of alpha-crystallin in hereditary cataractous rat lens. Biol Pharm Bull. **27**: 308-314.

Thampi, P. and Abraham, E. C. 2003. Influence of the C-terminal residues on oligomerization of alpha A-crystallin. Biochemistry. **42**: 11857-11863.

Theriault, J. R., Lambert, H., Chavez-Zobel, A. T., Charest, G., Lavigne, P. and Landry, J. 2004. Essential role of the NH2-terminal WD/EPF motif in the phosphorylation-activated protective function of mammalian Hsp27. J Biol Chem. **279**: 23463-23471.

Tissières, A., Mitchell, H. K. and Tracy, U. M. 1974. Protein synthesis in salivary glands of *Drosophila melanogaster*: relation to chromosome puffs. J. Mol. Biol. **84**: 389-398.

Treweek, T. M., Morris, A. M. and Carver, J. A. 2003. Intracellular protein unfolding and aggregation: the role of small heat-shock chaperone proteins. Aust. J. Chem. **56**: 357-367.

Tsan, M.-F. and Gao, B. 2004. Cytokine function of heat shock proteins. Am. J. Physiol. Cell Physiol. **286**: C739-C744.

Ullian, M. E., Gantt, B. J., Ford, A. K., Tholanikunnel, B. G., Spicer, E. K. and Fitzgibbon, W. R. 2003. Potential importance of glomerular citrate synthase activity in remnant nephropathy. Kidney International. **63**: 156-164.

Usui, K., Hatipoglu, O. F., Ishii, N. and Yohda, M. 2004. Role of the N-terminal region of the crenarchaeal sHsp, StHsp14.0, in thermal-induced disassembly of the complex and molecular chaperone activity. Biochem Biophys Res Commun. **315**: 113-118.

van Breukelen, F., Maier, R. and Hand, S. C. 2000. Depression of nuclear transcription and extension of mRNA half-life under anoxia in *Artemia franciscana* embryos. J Exp Biol. **203 Pt 7**: 1123-1130.

van de Klundert, F. A. and de Jong, W. W. 1999. The small heat shock proteins Hsp20 and alphaB-crystallin in cultured cardiac myocytes: differences in cellular localization and solubilization after heat stress. Eur J Cell Biol. **78**: 567-572.

van den IJssel, P., Wheelock, R., Prescott, A., Russell, P. and Quinlan, R. A. 2003. Nuclear speckle localisation of the small heat shock protein alpha B-crystallin and its inhibition by the R120G cardiomyopathy-linked mutation. Exp Cell Res. **287**: 249-261.

van Montfort, R., Slingsby, C. and Vierling, E. 2001a. Structure and function of the small heat shock protein/alpha-crystallin family of molecular chaperones. Adv Protein Chem. **59**: 105-156.

van Montfort, R. L., Basha, E., Friedrich, K. L., Slingsby, C. and Vierling, E. 2001b. Crystal structure and assembly of a eukaryotic small heat shock protein. Nat Struct Biol. **8**: 1025-1030.

Vicart, P., Caron, A., Guicheney, P., Li, Z., Prevost, M. C., Faure, A., Chateau, D., Chapon, F., Tome, F., Dupret, J. M., Paulin, D. and Fardeau, M. 1998. A missense mutation in the alphaB-crystallin chaperone gene causes a desmin-related myopathy. Nat Genet. **20**: 92-95.

Viner, R. I. and Clegg, J. S. 2001. Influence of trehalose on the molecular chaperone activity of p26, a small heat shock/alpha-crystallin protein. Cell Stress Chaperones. **6**: 126-135.

Warner, A. H. and Clegg, J. S. 2001. Diguanosine nucleotide metabolism and the survival of artemia embryos during years of continuous anoxia. Eur. J. Biochem. **268**: 1568-1576.

Willsie, J. K. and Clegg, J. S. 2001. Nuclear p26, a small heat shock/alpha-crystallin protein, and its relationship to stress resistance in *Artemia franciscana* embryos. J Exp Biol. **204**: 2339-2350.

Willsie, J. K. and Clegg, J. S. 2002. Small heat shock protein p26 associates with nuclear lamins and HSP70 in nuclei and nuclear matrix fractions from stressed cells. J Cell Biochem. **84**: 601-614.

Wintrode, P. L., Friedrich, K. L., Vierling, E., Smith, J. B. and Smith, D. L. 2003. Solution structure and dynamics of a heat shock protein assembly probed by hydrogen exchange and mass spectrometry. Biochemistry. **42**: 10667-10673.

Xu, J., Baase, W. A., Baldwin, E. and Matthews, B. W. 1998. The response of T4 lysozyme to large-to-small substitutions within the core and its relation to the hydrophobic effect. Protein Science. **7**: 158-177.